(12)

AFAMRL-TR-81-5

AD A114887

A DYNAMIC MODEL OF THE CERVICAL SPINE AND HEAD

J. WILLIAMS
T. BELYTSCHKO

NORTHWESTERN UNIVERSITY
EVANSTON, ILLINOIS 60201

NOVEMBER 1981

AIR FORCE AEROSPACE MEDICAL RESEARCH LABORATORY
AEROSPACE MEDICAL DIVISION
AIR FORCE SYSTEMS COMMAND
WRIGHT-PATTERSON AIR FORCE BASE, OHIO 45433

NOTICES

When US Government drawings, specifications, or other data are used for any purpose other than a definitely related Government procurement operation, the Government thereby incurs no responsibility nor any obligation whatsoever, and the fact that the Government may have formulated, furnished, or in any way supplied the said drawings, specifications, or other data, is not to be regarded by implication or otherwise, as in any manner licensing the holder or any other person or corporation, or conveying any rights or permission to manufacture, use, or sell any patented invention that may in any way be related thereto.

Please do not request copies of this report from Air Force Aerospace Medical Research Laboratory. Additional copies may be purchased from:

National Technical Information Service
5285 Port Royal Road
Springfield, Virginia 22161

Federal Government agencies and their contractors registered with Defense Documentation Center should direct requests for copies of this report to:

Defense Documentation Center
Cameron Station
Alexandria, Virginia 22314

TECHNICAL REVIEW AND APPROVAL

AFAMRL-TR-81-5

This report has been reviewed by the Office of Public Affairs (PA) and is releasable to the National Technical Information Service (NTIS). At NTIS, it will be available to the general public, including foreign nations.

This technical report has been reviewed and is approved for publication.

FOR THE COMMANDER

HENNING E. VON GIERKE
Director
Biodynamics and Bioengineering Division
Air Force Aerospace Medical Research Laboratory

AIR FORCE/56780/22 December 1981 — 150

SECURITY CLASSIFICATION OF THIS PAGE *(When Data Entered)*

REPORT DOCUMENTATION PAGE	READ INSTRUCTIONS BEFORE COMPLETING FORM
1. REPORT NUMBER: AFAMRL-TR-81-5	2. GOVT ACCESSION NO.: AD-A124 887
3. RECIPIENT'S CATALOG NUMBER	
4. TITLE *(and Subtitle)*: A DYNAMIC MODEL OF THE CERVICAL SPINE AND HEAD	5. TYPE OF REPORT & PERIOD COVERED: Final Technical Report May 1978 - August 1980
	6. PERFORMING ORG. REPORT NUMBER
7. AUTHOR(s): J. Williams and T. Belytschko	8. CONTRACT OR GRANT NUMBER(s): F33615-78-C-0523
9. PERFORMING ORGANIZATION NAME AND ADDRESS: Northwestern University, Evanston, Illinois 60201	10. PROGRAM ELEMENT, PROJECT, TASK AREA & WORK UNIT NUMBERS: 62202F; 7231-15-06
11. CONTROLLING OFFICE NAME AND ADDRESS: Air Force Aerospace Medical Research Laboratory, Aerospace Medical Div, Air Force Systems Command, Wright-Patterson Air Force Base, OH 45433	12. REPORT DATE: November 1981
	13. NUMBER OF PAGES: 159
14. MONITORING AGENCY NAME & ADDRESS *(if different from Controlling Office)*	15. SECURITY CLASS. *(of this report)*: UNCLASSIFIED
	15a. DECLASSIFICATION/DOWNGRADING SCHEDULE

16. DISTRIBUTION STATEMENT *(of this Report)*

Approved for public release, distribution unlimited.

17. DISTRIBUTION STATEMENT *(of the abstract entered in Block 20, if different from Report)*

18. SUPPLEMENTARY NOTES

19. KEY WORDS *(Continue on reverse side if necessary and identify by block number)*

Biomechanics
Spine Impact
Intervertebral Disc
Stress Analysis

20. ABSTRACT *(Continue on reverse side if necessary and identify by block number)*

A data base of the head and cervical spine structure for a three-dimensional mathematical model of the human head-spine system has been developed on the basis of recently obtained geometric and stiffness data. The model was developed for predicting detailed head-spine system responses and injury probabilities during, for example, retraction/ejection and ground

[continued on reverse]

DD FORM 1 JAN 73 1473 EDITION OF 1 NOV 65 IS OBSOLETE

SECURITY CLASSIFICATION OF THIS PAGE *(When Data Entered)*

20. ABSTRACT (Continued)

impact. This model of the head and cervical spine structure treats the cervical spine and head as a collection of rigid bodies and deformable elements; the rigid bodies represent the vertebral bodies and head and the deformable elements represent the intervertebral discs, ligaments, facet joints and muscles. The model is completely three dimensional and can treat nonlinearities due to large displacements and material properties.

The geometric data consist of the initial configuration of the vertebrae and the points of attachments of the muscles, discs and ligaments to the vertebrae. Particular attention was devoted to reproducing the orientations of the articular facets. Stiffness data for the intervertebral discs, ligaments and facet joints were developed. A muscle model which includes reflex and voluntary activation was included for the major muscles. Inertial data was developed by estimating the height and cross-sectional area of the sections of the neck associated with each motion segment and multiplying by a uniform density.

Preliminary simulations have been made of G_x (frontal) and G_y (lateral) impact accelerations. Computed results were compared to experiments. Agreement is quite good for the first 150 msec, which indicates that the properties of the ligamentous cervical spine are well represented. After 150 msec, significant discrepancies develop; those are attributed to incorrect lines of action for the major muscles caused by the simplifying assumption that the muscles act along straight lines connecting the origin to the insertion. This problem is being addressed in a follow-on contract, with a curved, multinode muscle element having been developed, and currently being validated.

This detailed, discrete parameter head-cervical spine model will serve as the most useful tool developed to date for the study of head-cervical spine system responses in military impact environments.

PREFACE

Research in this final report was performed under Air Force contract F33615-78-C-0523 awarded to Northwestern University for the period May 1978 to August 1980. The Air Force program monitors were Ints Kaleps and Eberhardt Privitzer of the Mathematics and Analysis Branch, Biodynamics and Bioengineering Division, Air Force Aerospace Medical Research Laboratory, Aerospace Medical Division, Air Force Systems Command, Wright-Patterson Air Force Base, Ohio. We wish to acknowledge their many contributions to this work through their suggestions and critical evaluation of the work.

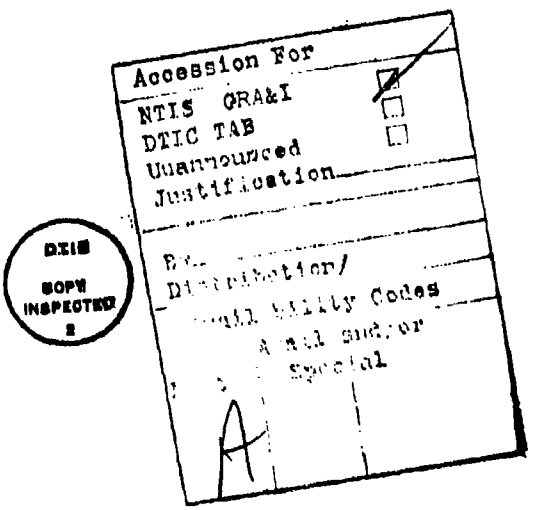

TABLE OF CONTENTS

Table of Contents (cont.)

Figure

LIST OF ILLUSTRATIONS

Page

LIST OF ILLUSTRATIONS, continued

LIST OF TABLES

Section I

INTRODUCTION

Recent technological developments in helmet design and devices for enhancing performance and protection of the head have added additional mass to the helment and resulted in asymmetric mass distributions. Ejection from the aircraft or other crewmember emergency procedures associated with high acceleration environments may lead to high forces on the crewmember's neck. For example, during ejection, the entire force required to accelerate the head and helmet passes through the cervical spine. If the helmet is asymmetric, this may result in bending and twisting of the cervical spine. Thus, there is considerable concern with the possiblity of injuries in the cervical spine. For this reason, it is desirable in the design and evaluation of helmet-mounted devices that procedures be available for predicting stresses and the likelihood of injury in high acceleration environments.

This predictive capability is also useful in other fields. It has been said that about two-thirds of all traffic fatalities are a result of injuries to the head and neck. Of the nonfatal injuries that are vehicle related, whiplash certainly remains a puzzling problem. Another related area that might benefit from such models is the design and use of helmets for motorcyclists and parachutists.

The objective of this study was to develop a model of the head and cervical spine based on data obtained by Liu et al. (1981) under AMRL sponsorship, data available in the literature, and the mathematical model for biodynamic response developed by Belytschko and Privitzer (1978). The bio-

dynamic model is based on a large-deflection finite element program for transient analysis described in Belytschko et al. (1977) and Belytschko et al. (1978). Elements which represent ligaments and muscles were added to model the passive response as well as the active response due to the stretch-reflex or voluntary pre-tensing of the muscles. The validity of the resulting spine model was examined by simulating $-G_x$ and G_y impact and comparing the response to the studies of Ewing and Thomas (1972) and Ewing et al. (1978).

Orne and Liu (1969), Von Gierke (1971) and King and Chou (1976), reported early models for the dynamic response of the spine. The first comprehensive discrete-parameter model of the spine was that of Orne and Liu (1969). This two-dimensional model represented the axial, shear, and bending stiffness of the discs, the variable size and mass of the vertebrae, the eccentricity of the head and trunk inertia as well as the natural shape of the spine. Prasad and King (1974) extended this model by including the facets as an additional load path between the vertebrae. McKenzie and Williams (1971) used the basic equations of Orne and Liu to model the dynamic behavior of the head and neck during whiplash. Belytschko et al. (1976, 1978) developed a three-dimensional model of the spine and head for evaluating pilot ejection. It included some soft tissue elements in addition to the discs, such as ligaments and the viscera. This model included the cervical spine with vertebrae C7 through C2. The cervical spine facets were modeled by hydrodynamic elements and the stabilizing effects of the ligaments and passive musculature were modeled by adding beam elements to the neck.

Simpler models have also been developed to study the effects of particular components in the head-neck-restraint system. These models are of limited

usefulness since they do not predict the force distribution within the neck. Martinez and Garcia (1968) developed a nonlinear lumped parameter model for studying whiplash. This model considers the head and neck as separate elements of a mechanical linkage which allows the neck to rotate at the base and the head to rotate and translate with respect to the top of the neck. Becker (1972) proposed a two-dimensional mechanical linkage model for the head and neck to study $-G_x$ impact response. The model consists of springs and dashpots and two links, one of constant length, the other of variable length. The mass is concentrated at the mass centroid of the head. A two-dimensional head-neck-torso model was developed by Bowman et al. (1974, 1975) for use in simulating $-G_x$ and G_y impact. This model has a two-joint neck element and the musculature is represented by two muscle elements (Maxwell-type elements) to restrict angulation at the two neck joints. Both the stiffness and damping coefficients are functions of the degree of muscle activation, which in turn is a function of time. A similar model of the neck with musculature is that of Frisch et al. (1977) in which the neck is a link with two ball-and-socket joints: a so-called neck pivot and a head pivot. In all joints, rotation is almost unresisted up to the joint-limiting angle, where quadratic and cubic springs prevent further motion. Ligaments and muscles were represented by two spring dampers connecting the base of the skull and T1.

Two discrete parameter models of much greater sophistication have recently been reported. Huston et al. (1978) developed a three-dimensional model of the head and neck including nine rigid bodies, discs, muscles and nonlinear ligaments with joint restraints modeled by one-way dampers. Reber and Goldsmith (1979) developed a two-dimensional model of the head-neck

system. The discs, muscles, ligaments and facets are modeled by various arrangements of springs and dashpots, which can be either linear or non-linear. The muscles in both of these models act as passive elements. These models seem to match the kinematic response of the Ewing et al. (1972) experiments well, although the Reber and Goldsmith model has problems with the facets, which introduce large spikes in the acceleration response. Neither of these two models was developed as part of a general analytical model that would easily permit variations of the complexity of the model, such as would be necessary to represent the thoraco-lumbar spine or the head encumbrances, and they were not validated for lateral accelerations.

In this investigation, a cervical spine and head model was developed within the framework of the program SAM (Structural Analysis of Man). The SAM model represents the anatomy by a collection of rigid bodies interconnected by deformable elements. The rigid bodies are used for the modeling of bones, while deformable elements are used to model ligaments and muscles.

For purposes of describing the model it is worthwhile to distinguish between the following:

1. The computer-based method of solution, or mathematical model, which is a rather general system for the treatment of the dynamics of collections of rigid bodies interconnected by deformable elements; and
2. The specific model of the cervical spine, which constitutes a data base for the mathematical model.

This approach to biodynamics, which separates the mathematical formulation from the anatomical data, has several advantages. For example, this model of the cervical spine employs the same mathematical framework used in the

thoraco-lumbar spine in Belytschko and Privitzer (1978). Therefore the two can be combined when necessary.

This report is primarily concerned with the development of the data base and its exercise in some simulations for which experimental data are available. The anatomy of the spine is described in Section II. Section III gives an overview of the mathematical model and the cervical spine data base; details of the latter are given in the Appendices. Section IV gives some results of preliminary simulations of $-G_x$ and G_y accelerations and compares them to experimental data.

SECTION II

ANATOMY OF THE CERVICAL SPINE

Spine as a Whole

General Configuration

The human spine is made up of 33 vertebrae joined by ligaments, cartilage and intervertebral discs. There are seven cervical, twelve thoracic, five lumbar, five sacral vertebrae and one coccygeal vertebra. The coccygeal vertebra is a fusion of four small vertebrae. The five sacral vertebrae are also fused as one so that the spine is often said to consist of 26 separate bones. The inter-vertebral discs make up about one-fifth of the length of the spine, excluding the first two vertebrae in the neck, which have no intervertebral discs. When the entire spine is viewed from the side, one can distinguish four separate curves: (1) the cervical curve, which is convex forward; (2) the thoracic curve, which is convex backward; (3) the lumbar curve which is convex forward again; and (4) the sacral bones and coccyx, making up the pelvic curve which is concave downward.

Vertebrae

Each vertebra consists of an anterior part called the body and a posterior vertebral arch which encloses the vertebral foramen, housing the spinal cord. Connecting each pair of vertebrae is an intervertebral disc of fibrocartilage, strongly bound to each vertebral body, and two

apophyseal joints linking the arches. The bodies and discs form a continuous, flexible rod that transmits most of the body load. In addition to the weight of the body even greater loads are placed on this structure by the muscles either directly or indirectly. The vertebral bodies are approximately cylindrical. Their width gradually increases from the second cervical vertebra to the first thoracic. From then on they decrease in width for about three vertebrae before gradually increasing their width again. The lumbar vertebrae are the most heavily built, reflecting the loads they carry. Between the arches of adjacent vertebrae, on each side, are the intervertebral foramina which allow passage of the spinal nerves and vessels. These foramina are smallest in the cervical region and steadily increase in size as they approach the lowest lumbar vertebrae.

The vertebral canal, which extends all along the spinal column, conforms to the various curvatures in the spine and to the changes in the spinal cord's shape and size. It is triangular and large in the cervical region, small and circular in the thoracic and returns to a triangular shape in the lumbar region.

The vertebral arch is bilaterally symmetric. It leaves the vertebral body on either side as short, thick, rounded bars, called pedicles. These become vertically broad and plate-like in the posterior part of the arch and are then called laminae. The arch supports two lateral articular processes and one spinous process. The articular processes can carry a significant part of the total spinal load and meet to form small synovial joints between adjacent vertebrae. The orientation of these articulating processes controls much of the movement in the spine. The

transverse processes extend laterally from the junction of the pedicles and laminae. They serve as levers for the muscles and ligaments engaged in rotation and lateral bending. The spinous process extends posteriorly from the arch. It serves as attachment sites for muscles and ligaments involved in extension of the spine.

Intervertebral Discs

The joints between adjacent vertebrae give the spinal column its flexibility. Although most of the load is transmitted through the discs and vertebral bodies, the articular processes and the disc must be thought of as an integrated unit. Movement in the disc implies movement in the articular joints as well. The disc consists of a central core, the nucleus pulposus surrounded by an outer laminated part, the tough collagenous annulus fibrosus. Within the annulus the collagen fibers lie in sheets, which run obliquely and concentrically and spiral from one vertebral body to the next adjacent one. They also form a complex network with one another, thereby providing effective resistance to pressures. The alternating laminae lie at about 30° to the horizontal plane, one layer oriented 30° one way and the next 30° the other. This arrangement allows flexion to take place without damage to the disc. But, torsion necessarily lengthens the laminae in one direction while shortening those in the other so that damage is more likely to occur. The nucleus pulposus is a soft, gelatinous structure consisting of randomly oriented collagen fibers implanted in a matrix of water and polysaccharides. It is better developed in the cervical and lumbar part of the spine than in the thoracic region. In the young the nucleus is like a gel, it is deformable but not compressible. Pressures placed upon the

nucleus therefore result in an isotropic stress distribution. This has the desirable result of redistributing vertical forces in a radial direction to be taken up by the tough annulus. As the disc ages, however, the nucleus loses much of its gel-like properties. Loads are then distributed in an anisotropic manner so that localized high stress states develop in the annular wall.

The shape of the intervertebral discs corresponds to that of the vertebral bodies between which they are placed. Their thickness varies in different parts of the column and in different parts of the same disc. The discs are thin in the cervical region; larger in surface area, but thinner in the thoracic region; and thick and large in the lumbar region. They are thicker in front than in behind in the cervical and lumbar spine, thereby contributing to the spinal curvatures in those segments. In the thoracic region they are almost uniform in thickness; and the anterior concavity of the spine in this region is formed by the shape of the vertebral bodies. The cervical and lumbar segments of the spine have, in proportion to their length, a larger amount of intervertebral disc material than the thoracic region.

The vertebral bodies are convex in the transverse plane except in the dorsal sections where they become concave in order to complete the vertebral foramen. Vertically the vertebral bodies are concave except on the dorsal side where they are flat. Inside, the vertebral body consists of trabecular bone throughout, covered by a layer of compact bone which is thin in the vertebral bodies but much thicker in the arch and its processes. The trabecular interiors of the bodies are traversed by blood vessels. The discs, on the other hand, are avascular and are supported by diffusion through the trabecular bone of the vertebrae.

Ligaments

The ligaments are strong fibrous bands varying in width and strength which bind together and strengthen the units of the backbone and thereby also limit its movement. They also function in protecting the spinal cord.

The vertebral bodies are joined together by the intervertebral discs and by two ligaments:

The anterior longitudinal ligament, which is a strong band starting at the second cervical vertebra; is a continuation of the anterior atlanto-axial ligament and continues down the entire front end of the vertebral bodies until it reaches the sacrum. This ligament is tightly attached to the discs but loosely connected to the vertebral bodies. It consists of several layers of fibers, the shortest being on the inside and extending from one vertebrae to the next. The intermediate length fibers cover three or four vertebrae and the longest fibers, which lie on the external surface, extend over more than four vertebrae. In the cervical region this ligament is thin and narrow and covers only the middle portion of the anterior aspects of the vertebral bodies.

The posterior longitudinal ligament, which starts at the posterior margin of the second cervical vertebra, continues down inside the vertebral canal along the central part of the posterior wall of the bodies. It attaches to the margins of the vertebral bodies where it branches out for reinforcement. Both of these ligaments are thinnest in the cervical and lumbar segments. In the cervical spine the posterior longitudinal ligament is always thicker than its anterior counterpart and measures about 2 to 3 mm in its thickest anterior-posterior part. It is widest from side to side in the upper cervical region and becomes thicker and

narrower in the lower cervical spine. It appears to limit flexion as well as distraction of the vertebrae (Johnson et al., 1975).

The vertebral arches are held together by several different ligaments:

The interspinous ligaments are thin and almost membranous and connect the adjoining spinous processes from their tips to their roots. They are only slightly developed in the neck, narrow and long in the thoracic region, and thick in the lumbar region. In the neck, they consistently limit flexion and anterior horizontal displacement (Johnson et al., 1975).

The supraspinous ligament is a strong fibrous cord that joins the tips of the spinous processes from the seventh cervical vertebra to the sacrum. Between the spine of the seventh cervical vertebra and the external occipital protuberance, this ligament continues as the ligamentum nuchae. The ligamentum nuchae forms a septum in the midline between the muscles on both sides of the neck. It is a strong fan-shaped structure, which stretches in between all seven cervical vertebrae, joining their spinous processes from root to apex. It is the cervical counterpart of the supraspinous and interspinous ligaments of the rest of the spinal column.

The ligamentum flavum connects the laminae of adjacent vertebrae. It is found on either side of the spinous process and extends laterally to the articular facets. The main component of this ligament is yellow elastic tissue and the fibers extend from the lower part of the anterior surface of the lamina, above, to the posterior surface and upper part of the lamina, below. These ligaments are thinnest in the cervical region, where they are broad and long, and increase in thickness as

they approach the lower lumbar area. These ligaments are said to limit the amount of forward flexion that can be achieved; they are also said to help in returning the vertebral column to an upright position and may protect the disc from injury.

The intertransverse ligaments connect the transverse processes. In the cervical region they consist of only a few fibers and their place is taken by intertransversarius muscles.

Movements in the Vertebral Column

The amount and type of movement that can occur in the vertebral column is determined by the discs and ligaments and, to a significant extent, by the shape and orientation of the articular facets. The orientation of the articular facets is shown diagrammatically in Fig. 1, as adapted from White et al. (1978). The anatomical planes, used in Fig. 1 to illustrate the facet joint orientation, are defined in Fig. 2 The orientation of the facets varies with the location in the spine and is different for each of the three major regions, i.e. the cervical, thoracic and lumbar regions.

In the cervical region the plane of the facet can be visualized by rotating a surface, lying initially in the transverse plane, about the y-axis by 45° (Fig. 1). This position is maintained with some variation for both the left and right facets of C2-C3 to C7-T1.

In the thoracic region (T1-T2 to T11-T12) the plane of the facet joint lies in a position that is best described by imagining two consecutive rotations of a surface, initially in the transverse plane. First rotate about the y-axis by 60°, then rotate about the z-axis by 20°. The second rotation is positive for the right facet and negative for

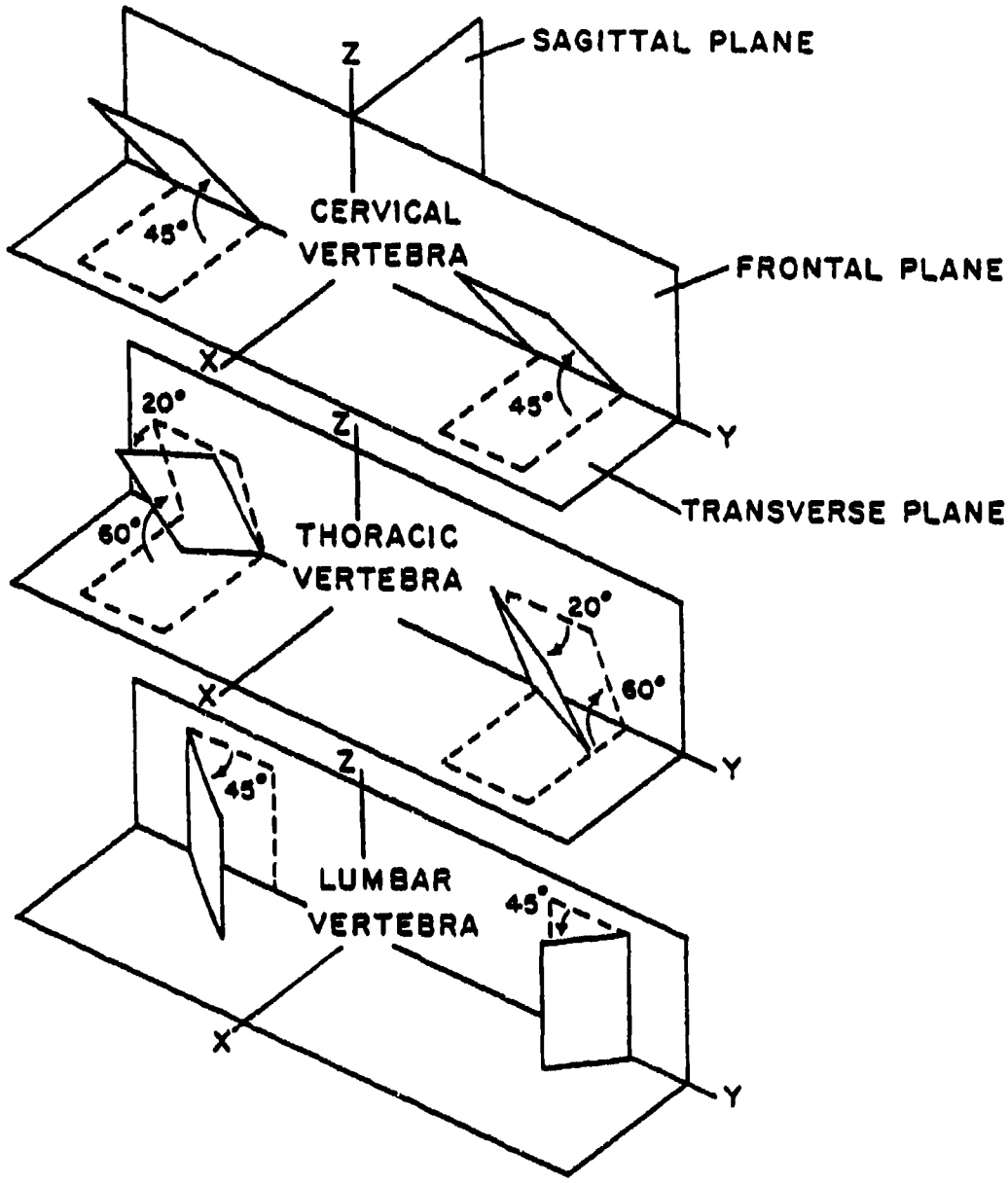

FIGURE 1. Approximate orientation of the facet joints as a function of position. (Adapted from White III, A. A. and Panjabi, M. M., Clinical Biomechanics of the Spine, 1978.)

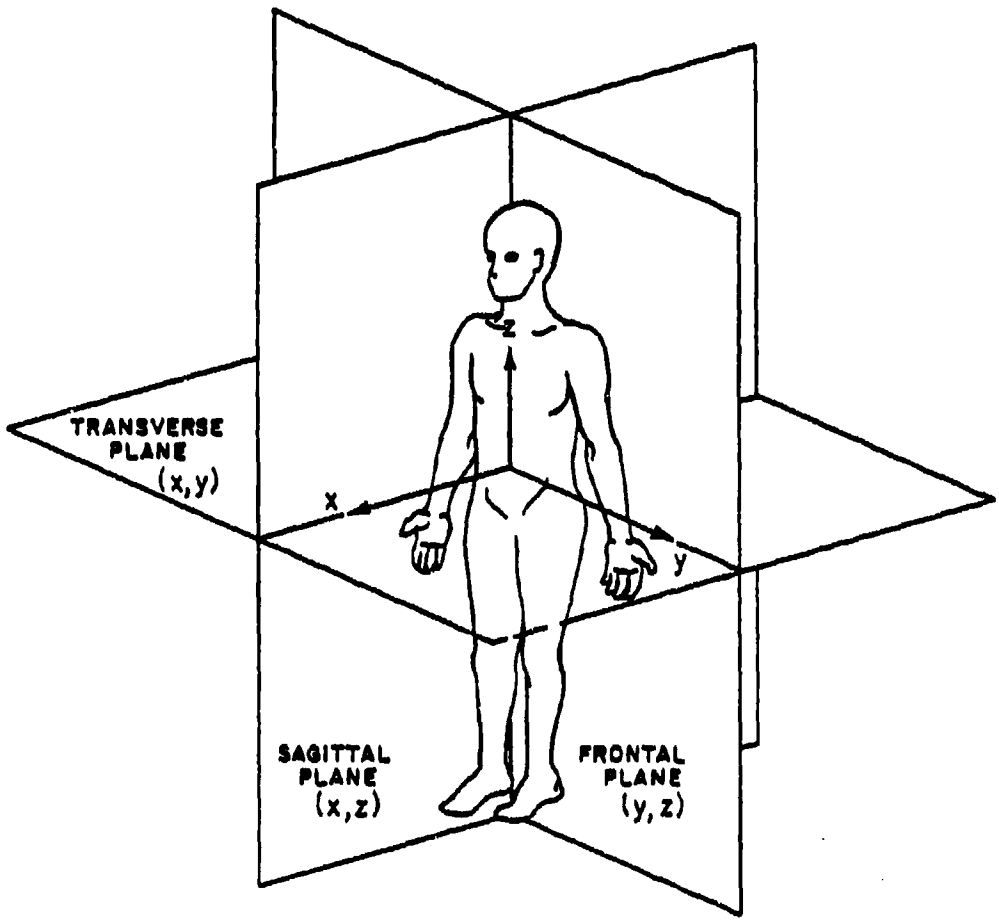

FIGURE 2. Anatomical planes and coordinate system used in text.

the left facet.

The orientation of the facet joints in the lumbar spine (T12-L1 to L5-S1) may be visualized by rotating a surface, that lies initially in the frontal plane, about the z-axis by 45°. This rotation is negative for the right facet and positive for the left facet.

Possible motions in the vertebral column are flexion (or forward bending), extension (backward bending), lateral flexion (bending to one side), and axial rotation. The range of motion for different levels of the spine is listed in Table 1, which is taken from the results of White et al. (1978).

Flexion is most extensive in the cervical and lumbar regions. During this movement the anterior longitudinal ligament is relaxed and the front parts of the discs are compressed. When maximum flexion has taken place the posterior longitudinal ligament, the ligamenta flava and the interspinous and supraspinous ligaments are stretched. Tension in the extensor muscles is an additional important restraint to further motion. In the cervical region the approximately upward and downward directions of the articular facets permits free flexion and extension. Flexion in this region occurs until the cervical convexity is straightened. It is limited by the approximation of the lower lips of the vertebra above and the upper rim of the vertebra below. In the thoracic region the anteriorly and posteriorly directed facets limit the extent of flexion possible. In the lumbar region flexion is quite extensive, probably because of the relative thickness of the discs.

In extension it is the stretching in the anterior longitudinal ligament and the apposition of the spinous processes which limit further movement. The articular processes also play an important role in

TABLE 1

RANGE OF MOTION AT DIFFERENT LEVELS IN THE SPINE

Level	Flexion-Extension	Lateral Flexion	Axial Rotation
	Total Range (degrees)	Total Range (degrees)	Total Range (degrees)
C1-head	13	8	0
C1-C2	10	0	47
C2-C3	8	10	9
C3-C4	13	11	11
C4-C5	12	11	12
C5-C6	17	8	10
C6-C7	16	7	9
C7-T1	9	4	8
T1-T2	4	6	9
T2-T3	4	6	8
T3-T4	4	6	8
T4-T5	4	6	8
T5-T6	4	6	8
T6-T7	5	6	8
T7-T8	6	6	8
T8-T9	6	6	7
T9-T10	6	6	4
T10-T11	9	7	2
T11-T12	12	9	2
T12-L1	12	8	2
L1-L2	12	6	2
L2-L3	14	6	2
L3-L4	15	8	2
L4-L5	17	6	2
L5-S1	20	3	5

Source: A. A. White III and M. M. Panjabi, Clinical Biomechanics of the Spine (Philadelphia: J. B. Lippincott, 1978), pp. 65, 71, 75, 79.

limiting the amount of extension that can take place.

Lateral flexion may take place in any part of the column but is most free in the cervical and lumbar regions. The amount of movement is limited by the resistance offered by ligaments and antagonistic muscles. Lateral flexion is always accompanied by a certain degree of axial rotation.

Axial rotation between individual pairs of vertebrae is slight, but has an additive effect, so that a large amount of rotation can take place along the entire column. This occurs to a slight extent in the cervical area, more so in the upper thoracic, and least in the lumbar. In the cervical section, lateral flexion is always combined with rotation. This is due to the upward and medial direction of the superior articular facets. Rotation is nearly impossible in the lumbar region because of the medial and lateral inclination of the articular facets.

Cervical Spine

Vertebrae

A typical cervical vertebra is shown in Fig. 3. The characteristic feature of the cervical vertebrae is a foramen in the transverse processes for the passage of the vertebral artery, vein and sympathetic nerves. The first, second and, to some extent, the seventh cervical vertebrae are special and will be described later. The other four conform to a standard format. They have small vertebral bodies that are broader from side to side than from front to back. The upper surface of the body of the vertebra is concave with prominently raised edges on each side. The lower surface of the body is concave from front to back, but slightly convex from side to side. It is saddle-shaped. The

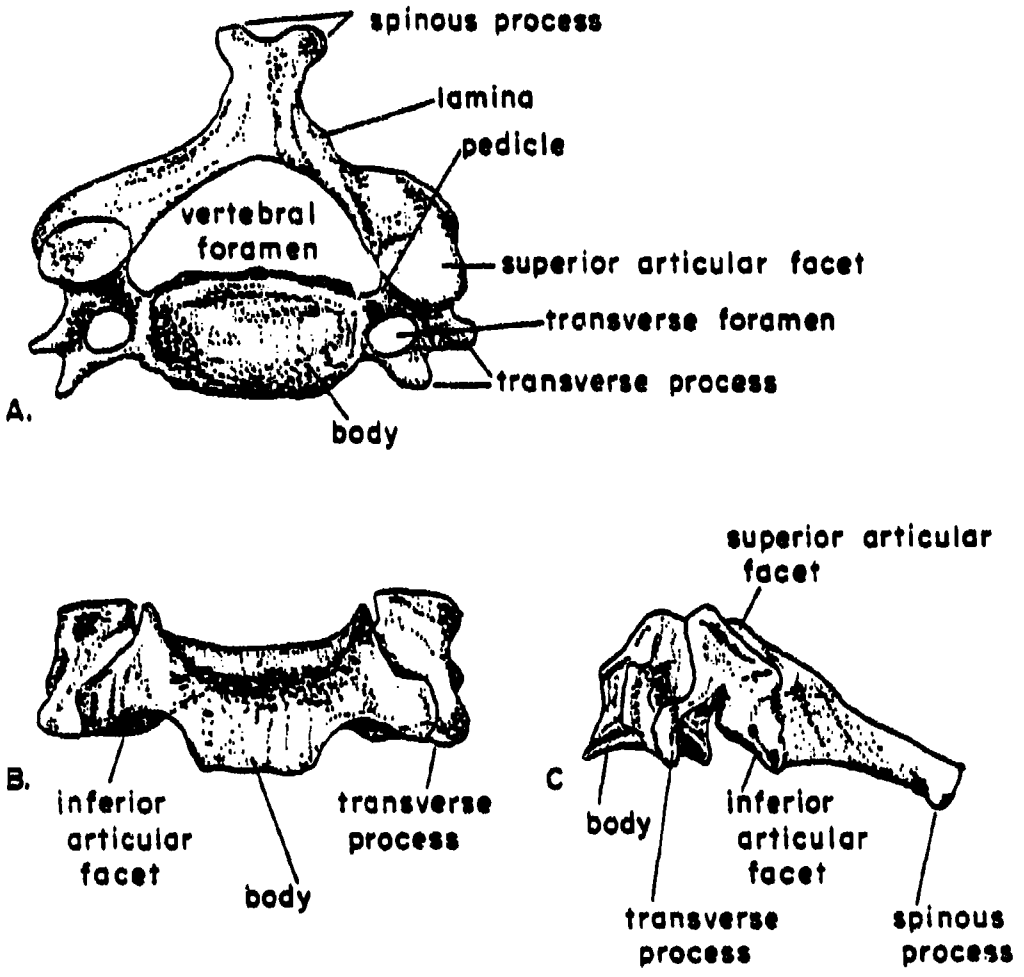

FIGURE 3. Typical Cervical Vertebra

A. Top view
B. Front view
C. Side view

anterior rim of the lower surface projects down and overlaps the front part of the disc below and the upper portion of the vertebra below.

The vertebral foramen is relatively large and triangular in shape rather than round. The laminae are relatively long and narrow and meet in the posterior midline to form short bifid spinous processes. Projecting laterally from the junction of the pedicles and the laminae are the superior and inferior articular processes which form an articular pillar. The superior articulating facet is oriented upward, backward and medially. The inferior facet is oriented forward, downward and laterally. Two cervical vertebrae in an articulated position are shown in Fig. 4.

The first cervical vertebra, known as the atlas (Fig. 5), supports the skull. It has no vertebral body and no spinous process, but is made up of two lateral masses and two arches. The anterior arch is convex and has a tubercle at its midpoint to which is attached the anterior longitudinal ligament and on each side of this the longus colli muscle. Medially placed on the posterior surface of this arch is a small oval facet for articulation with the odontoid process. The posterior arch is convex backward.

The two lateral masses have a superior and inferior facet whose long axes run forward and medially. The superior facet is large and elongated, constricted in its middle and concave. It is directed upward and medially and supports the condyles of the occipital bone. This is where the nodding, or "yes" movement of the head occurs. The inferior facet is slightly convex to flat and is circular. It is directed downward, medially and somewhat backwards, and articulates with the vertebra below. Another unusual feature is the large size of the transverse

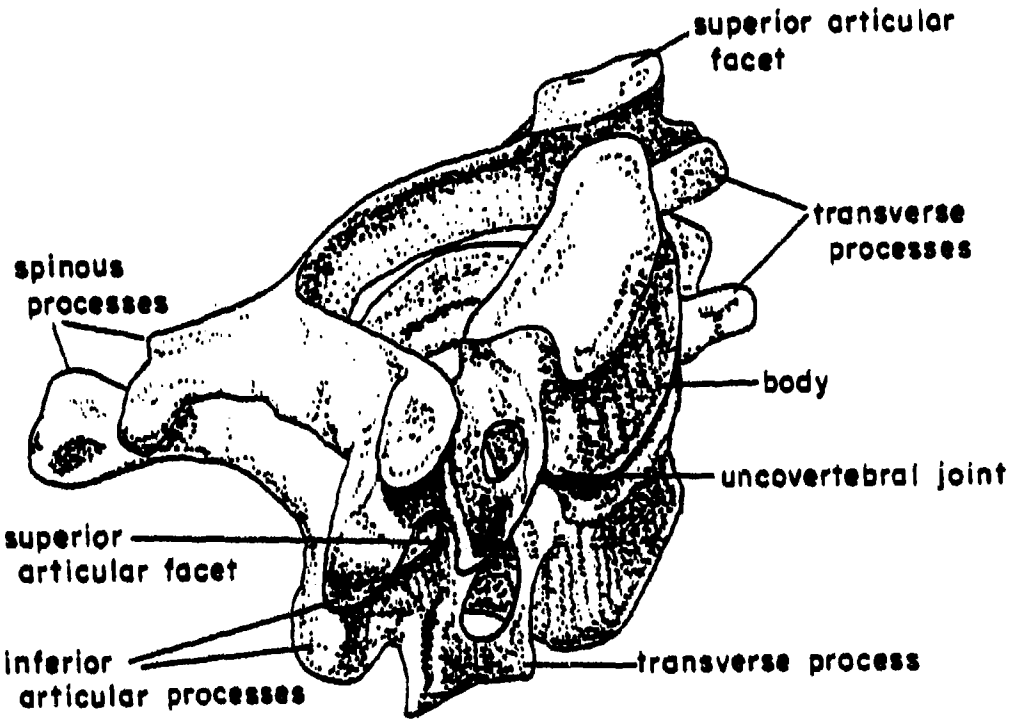

FIGURE 4. Two cervical vertebrae in articulated position

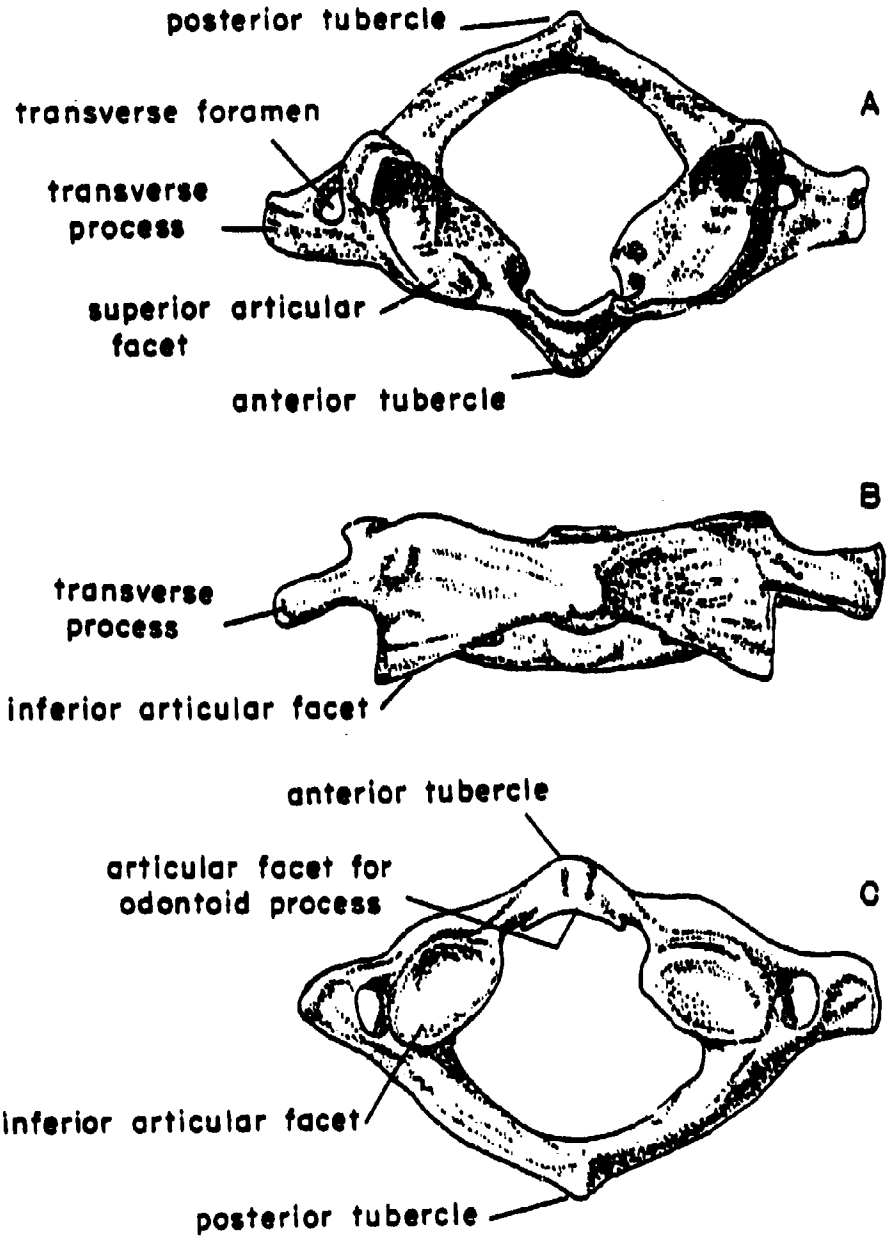

A. Atlas viewed from above

B. Atlas viewed from in front

C. Atlas viewed from below

FIGURE 5. First cervical vertebra.

processes making the width of this vertebra exceed that of all other cervical vertebrae except the seventh. These processes serve as levers for muscles that rotate the head.

The second cervical vertebra, the axis or epistropheus (Fig. 6), has a remarkable feature called the odontoid process. This toothlike process, conical in shape, rises perpendicularly for 1.5 cm from the midpoint of the upper surface of the body of the axis. There is a slight constriction at the base of the odontoid process, which serves as a groove for the transverse ligament of the atlas. The odontoid process fits into the anterior compartment of the vertebral foramen of the atlas, where it is held by the transverse ligament, thereby serving as a pivot around which the atlas turns, as shown in Fig. 7. This mechanism serves as the basis for the rotation or "no" movement of the head. On the anterior surface of the odontoid process is an oval facet for articulation with a similar facet on the back of the anterior arch of the atlas. The body of the axis is prolonged downward anteriorly, where it overlaps the superior part of the body of the third cervical vertebra.

On each side of the body of this vertebra is a superior and inferior facet. The superior facets face upward and laterally and articulate with the atlas. Unlike the superior facets in the other cervical vertebrae, they are not lined up with the inferior facets to form an articular pillar. The inferior facets are considerably posterior to the superior facets, and face downward and medially. The pedicles are relatively short and thick. The laminae are thicker than anywhere else in the cervical region. The spinous process is large, strong, and bifid. It serves as an attachment point for many of the muscles that

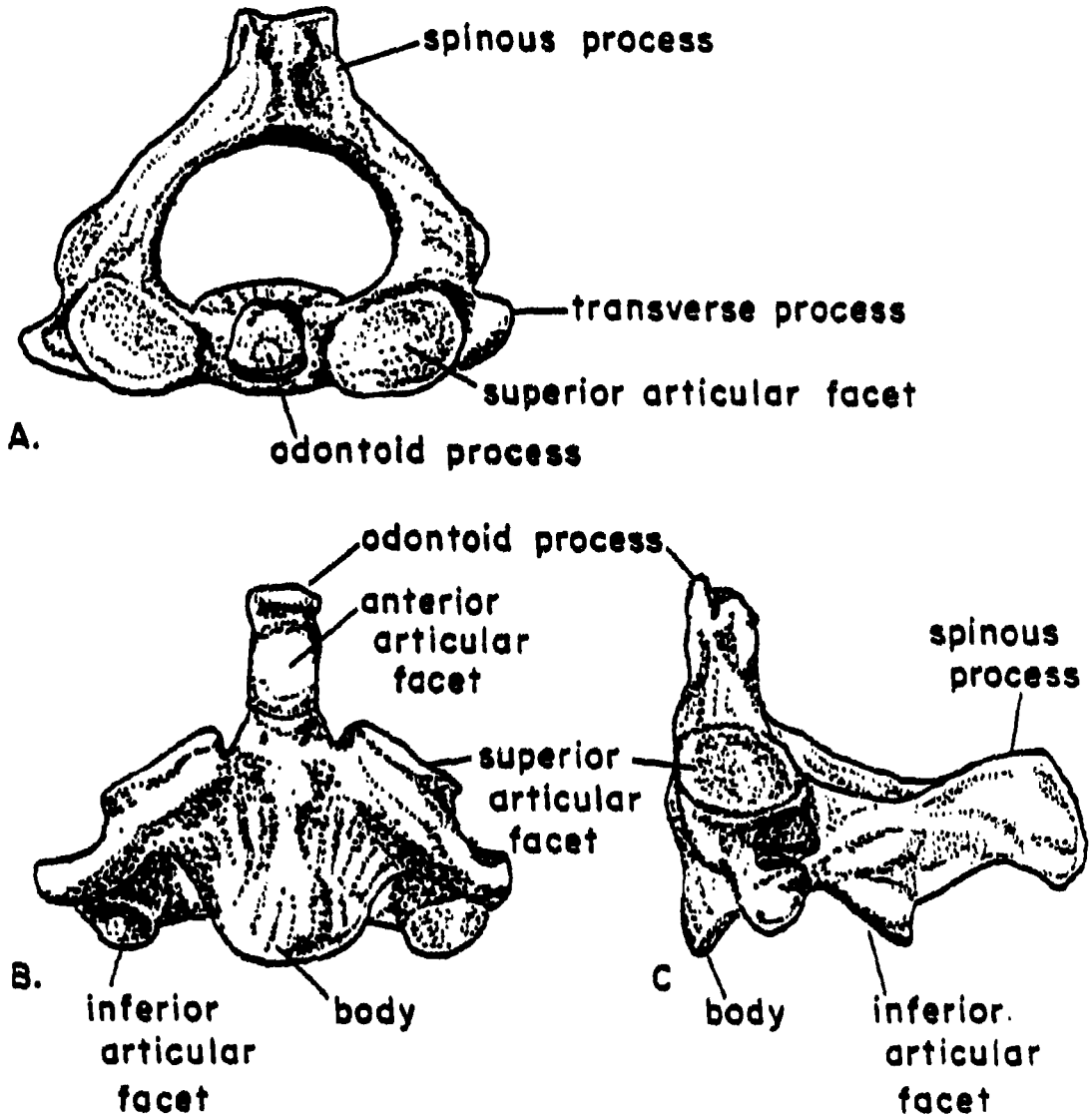

A. The axis viewed from the top
B. The axis viewed from in front
C. The axis viewed from the side

FIGURE 6. Second cervical vertebra.

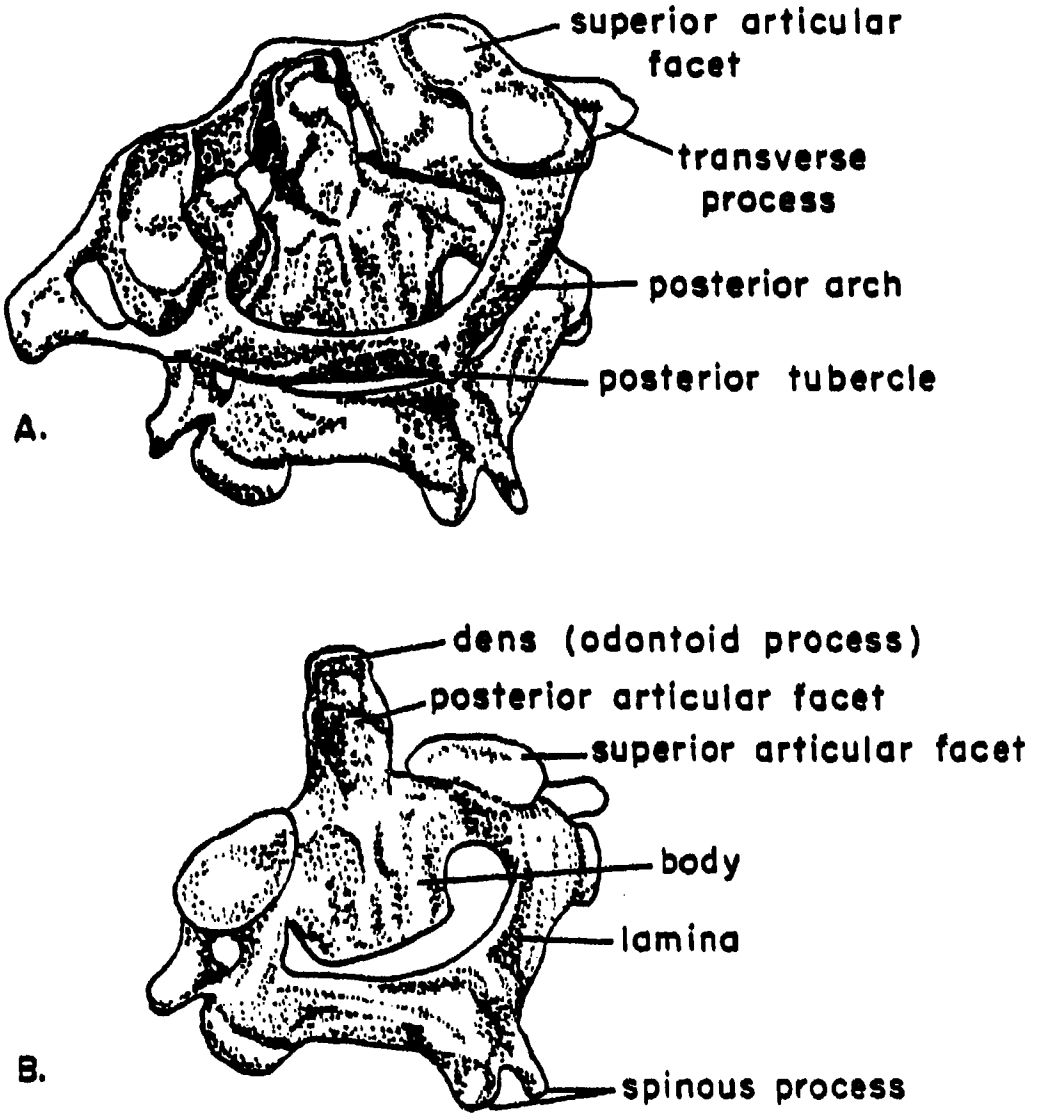

A. The atlas and axis in articulated position Viewed from above and behind

B. The axis viewed from above and behind

FIGURE 7. First and second cervical vertebrae.

extend, retract, and rotate the head. The transverse processes are small. The vertebral foramen is relatively large.

The seventh cervical vertebra or vertebra prominens is distinctive because of its long, nearly horizontal spinous process at the end of which is attached the ligamentum nuchae. It also serves as an attachment point for many neck muscles. The transverse processes are large and have foramina which vary in size and are sometimes absent. Most often the vertebral arteries and veins pass in front of, rather than through, the foramina of this vertebra.

Ligaments of the Cervical Spine

The ligaments of the cervical spine bind the vertebrae together as they do in the rest of the spine and together with the paracervical muscles prevent any motion that would injure the spinal cord and nerve roots. In addition to the basic ligaments already described, which are found in the lower cervical spine, there are specialized ligamentous structures connecting the vertebrae with the head to allow for coarse and fine movements of the head. The largest and most rigid ligaments in the cervical spine are the longitudinal ligament, the annulus fibrosus, if it can be considered a ligament, and the capsular ligaments (Johnson et al., 1975). These ligaments stabilize the cervical spine, whereas the others play a more specialized but secondary role (Johnson, 1975). The capsular ligaments are thick and dense in the cervical region. They are attached just peripheral to the margins of the articular facets of adjacent articular processes. They permit considerable sliding motion but not more than 2 to 3 mm from the neutral position.

The specialized ligaments connecting the head to the spine are associated with the first two cervical vertebrae and the occipital bone of the skull. These ligaments are best described in relation to the joints they support.

1. atlas-axis bones

Most of the rotation of the head on the neck occurs between the atlas and the axis. The ligamentous structures joining the atlas with the axis are the anterior and posterior longitudinal ligaments, the ligamentum flavum, and the articular capsules, as in the other joints. However, there are two major differences between this joint and the others: there is no intervertebral disc and the atlas has no vertebral body. Instead there is a pivot joint between the odontoid process of the axis and the ring formed by the arch of the atlas and the so-called transverse ligament of the atlas. This transverse ligament arises from a small tubercle on either side of the anterior arch of the atlas and stretches across the ring of the atlas to retain the odontoid process in contact with the arch. As it crosses the odontoid process, a small band stretches upward and another downward from its upper and lower fibers; the upper band, called the apical odontoid ligament, stretches from the tip of the odontoid process to the midpoint of the anterior margin of the foramen magnum. The lower band, if present, is attached to the posterior side of the body of the axis. The whole structure forms what is known as the cruciform ligament.

2. atlas-occipital bones

These bones are united by the articular capsules and the anterior and posterior atlanto-occipital ligaments.

The anterior atlanto-occipital ligament is a wide, dense band of fibers connecting the anterior margin of the foramen magnum and the upper border of the anterior arch of the atlas. It is continuous laterally with the capsular ligaments. The continuation of the anterior longitudinal ligament strengthens this ligament in the middle as it stretches from the anterior tubercle of the atlas to the basilar part of the occipital bone.

The posterior atlanto-occipital ligament is a wide, thin band of fibers stretching from the margins of the foramen magnum to the upper border of the posterior arch of the atlas.

The tectorial ligament (membrane) is the upward continuation of the posterior longitudinal ligament. It is broad and strong and fans out to attach to the basilar groove of the occipital bone. It covers the odontoid process giving extra strength to the transverse ligament of the atlas. There are also deep fibers that form two bands stretching from the lateral borders of the anterior foramen magnum to the posterior surface of the body of the axis.

3. axis-occipital bones

The tectorial membrane, already described, the paired alar ligaments, and the apical ligament extend between the occipital bone and the axis.

The alar (check) ligaments are very strong rounded bands connecting the upper lateral parts of the odontoid process with the inner aspects of the occipital condyles. They check rotation of the skull.

The apical ligament of the odontoid process stretches from the apex of the odontoid process to the anterior border of the foramen magnum.

Finally, the ligamentum nuchae connects all seven cervical vertebrae to the cranium.

Movements of the Cervical Spine

As mentioned, most of the axial rotation of the head on the neck occurs between the atlas and the axis. This joint comprises three synovial joints so that movement must occur at all three at the same time. This movement consists entirely of the rotation of the atlas along with the skull on the axis. The two lateral joints support the weight of the head, while the pivot joint guides the rotatory movement. Flexion and extension also occur at this joint, but lateral flexion is negligible.

In the atlanto-occipital joints the long axes of the facets are obliquely arranged and run medially from back to front. The two joints act as one and allow flexion, extension and slight lateral bending, but no axial rotation.

Extension in the cervical spine is limited at the upper end by the superior facets of the atlas whose posterior edges lock into the occipital condylar fossae; at the lower end it is checked by the inferior articular processes of the seventh cervical vertebra which slip into grooves behind and underneath the superior articular processes of the subjacent vertebra.

Flexion is stopped just after the cervical convexity is straightened; the limiting factor is the contacting of the overhanging lips of the bodies of the vertebrae with the walls of the subjacent vertebral bodies. When the head and neck are flexed, the inferior articular facets slide forward on the superior facets of the vertebra below. The maximum amount of sliding occurs at the C5-C6 joint.

Lateral flexion in the lower cervical spine (C2-C7) is always coupled with a certain amount of axial rotation. This coupling is such that during lateral bending to the left the spinous processes go to the right, and during lateral bending to the right they go to the left. (Using our coordinate system shown in Fig. 2, $-\theta_x$ is coupled with $+\theta_z$, and $+\theta_x$ is coupled with $-\theta_z$.) These coupling characteristics are important because they play a vital role in understanding dislocation injuries in the cervical spine (White et al., 1978).

Lysell (1969) studied this coupling phenomenon quantitatively using a radiographic technique. At C2 every 3° of lateral bending is coupled with 2° of axial torsion. The amount of coupling decreases as one goes down the spine, until at C7 there is, for every 7.5° of lateral bending, only 1° of coupled axial torsion. The cephalocaudal decrease in the amount of coupling may be related to gradual decrease in the angle the facet planes make with the transverse plane.

The orientation of the superior articular facet joints in the cervical region is for the most part upward and backward. According to Veleanu (1971) the normal vector to the superior facet joint makes an angle of 50° with the horizontal plane in vertebrae C3 through C5. This angle changes to 35° at C6 and becomes 23° at C7, thus approaching the angle of the normal to the thoracic facet of zero degrees. Liu et al. (1981) provided data on the facet orientations for two cervical spines. The results of one of these are plotted, after averaging the left and right sides in Fig. 8. These results are reasonably close to Veleanu's results.

The relative load-carrying importance of the facets in the cervical region has not yet been studied. Nevertheless, one can speculate,

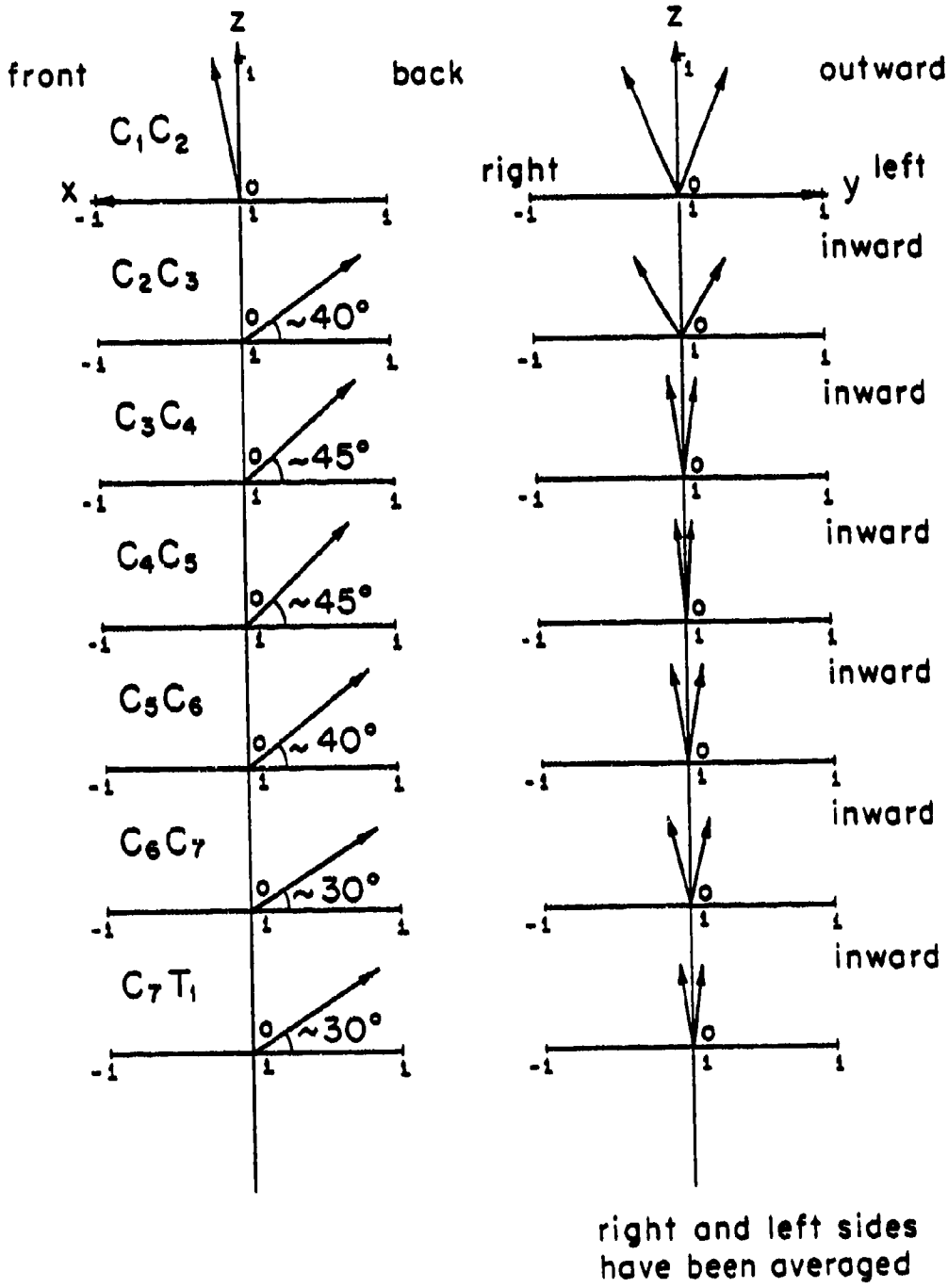

FIGURE 8. Lines of action of articular facets.

on the basis of the orientation of the facets, their relative bearing surface areas, and the mechanical properties of the motion segments, that they support a significant proportion of the total load. The cervical articular facet areas are relatively large compared to those of the other parts of the spine. At C3 the sum of the articular surface areas is 181 mm^2, at C6 it is 184 mm^2, whereas at T6 it is 128 mm^2 and at T12, 140 mm^2 (Veleanu, 1971). The vertebral-disc-to-articular-facet area ratio ranges from 1.1 to 1.4 between C3 and C6; at C7 it is 1.8, at T6 it is 3.6 and at T12 it is 5.6 (Veleanu, 1971). The surface areas of the facets between C1 and C2 are even larger; and since C1 has no vertebral body, these facets transmit most of the load placed on the vertebrae.

Finally, an important mechanism of protection described by Veleanu (1975) is the cervical-locking mechanism. During extension, lateral flexion, and rotation of the neck, the transverse processes of the vertebra engage the top of the upper articular processes of the vertebra immediately below. This locking mechanism takes place before vascular or nerve damage can occur (Fig. 9). That is, narrowing of the spinal canal is arrested by the locking mechanism so that damage to the spinal cord is prevented. Muscular relaxation, along with rotation of the neck with tensile forces, could induce or worsen a vertebral subluxation by having the transverse process jump over the articular process of the vertebra below. This prevents the locking mechanism from taking place and the result is compression of the vertebral artery. On the other hand, contraction of the deep muscles of the neck increases the efficiency of the locking mechanism (Veleanu, 1975) so that one might expect less injuries when the muscles are contracted. Unfortunately, this

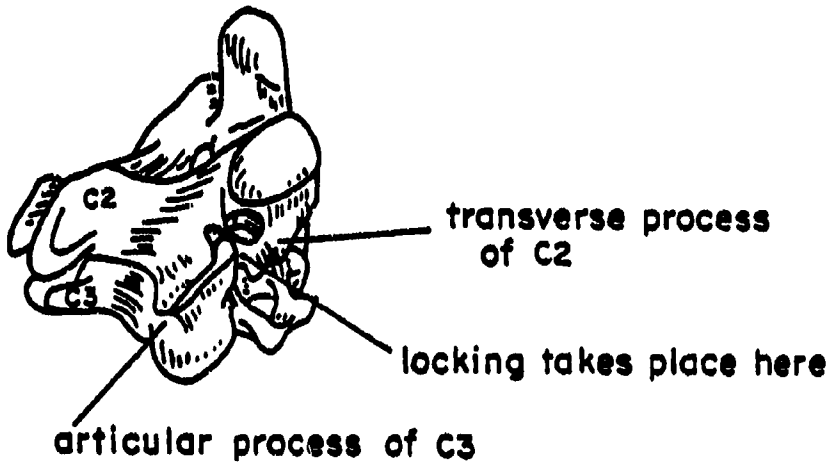

FIGURE 9. Locking mechanism.

[from C. Veleanu, Acta. Anat. Vol. 92, p. 475, 1975]

simple theory is contradicted by clinical findings that show that contraction of the muscles of the neck may actually increase the chances of injury in accidents involving the neck (Feuer, 1976). For example, in diving injuries, where the muscles are tensed, spine dislocations result from low impact forces. Opposed to this is the case of the intoxicated driver, whose muscles are usually relaxed and whose spinal injuries are usually minor in spite of the high impact forces.

Muscles of the Neck

Vertebral balance is maintained by a continuous adjustment of ligamentous and muscular forces in the spine. The short muscles of the back function, for the most part, as postural muscles, which steady adjoining vertebrae and control the movements of the vertebrae, with respect to each other, and of the column as a whole. Lucas and Bresler (1961) showed that the isolated ligamentous spine, devoid of muscles, is incapable of supporting more than 2 kg without buckling. This indicates the importance of the musculature of the trunk in providing stability to the spine. The term "stability" here is used in the engineering sense. "Clinical stability" is a term used to denote the ability of the spine to limit its extent of motion under physiological loads, so as to avoid damage to the spinal cord and nerve roots. In the clinical sense of the word Panjabi (1975) stated that the role of the muscles in providing stability to the cervical region is secondary to that of the ligaments under ordinary circumstances. Support for this view comes from the finding of Perrey and Nickel (1959) who found no clinical instability in patients with total paralysis of the cervical muscles. These two definitions of the term stability are not synonymous and so

the different statements found in the literature regarding the relative importance of the muscles and ligaments are not necessarily contradictory.

For the purpose of this study the muscles of the neck can be classified as either flexors or extensors. The primary neck flexor is the sternomastoid, which is a single muscle. The neck extensors, which prevent flexion of the neck and forward rotation of the head, are located posteriorly of the vertebral bodies. They are the trapezius, levator scapulae, splenius capitis, longissimus capitis, splenius cervicis, semispinalis capitis, semispinalis cervicis, obliquus capitis inferior, obliquus capitis superior, rectus capitis posterior major, and rectus capitis posterior minor, multifidus, and the interspinales. The muscles which restrain lateral flexion are the intertransversarius, scalenus and sternocleidomastoideus. The location and specific function of these muscles can be found in standard anatomy texts (e.g. Crouch, 1972). The neck extensor muscles can exert a stronger force than the flexor muscles, probably because of a more favorable mechanical advantage (Foust, 1973).

Stretch reflex times of the neck muscles were measured by Foust et al. (1973). The stretch reflex time is the time between the onset of the acceleration and the beginning of muscle activity, as measured by electromyography. The extensor muscles were consistently slower than the flexor muscles. Average neck muscles reflex times ranged from 56 msec to 92 msec for flexors and 54 to 87 msec for extensors. The stretch reflex is evoked at head acceleration of about 0.4 G (Foust, 1973). The average time needed for the muscles to activate fully has been estimated to be 54 msec to 66 msec for flexors and 64 msec to 86

msec for extensors in the 18-44 year old male (Foust, 1973).

Neck muscle strength was also estimated by Foust et al. (1973). For males, aged 18-44 years, the neck flexors could exert a total force of about 123-162 N and the extensors a force of 149-206 N.

Muscles can act as active or as passive elements. In unanticipated car accidents it may be assumed that a person's muscles are relaxed at the time of impact and that they act as passive elements during the first 60-200 msec. However, in the pilot ejection situation, especially in a pilot with ejection training, many of the neck muscles needed to resist neck flexion are probably tensed from the start of acceleration. On the other hand, the forces of the ejection are impossible to resist so far as forward rotation of the head is concerned; volunteers have been unable to prevent chin-chest contact.

Section III

MODELING PROCEDURE

Mathematical Model

The mathematical model used for this study is described in detail elsewhere (Belytschko et al. 1976). It is a structural analysis program for analyzing completely nonlinear response; both large displacement and material nonlinearities can be treated. It is thus ideally suited for modeling the neck, which undergoes much larger deflection than the rest of the spine in high acceleration environments.

The model consists essentially of a system of rigid bodies in three-dimensions interconnected by deformable elements. Each rigid body is associated with a node called a master (primary) node which has six degrees of freedom: three translations and three rotations. For each degree of freedom an equation of motion is integrated in time by the central difference method. In addition to master nodes, the system has provisions for slave (secondary) nodes, which provide a means of attaching deformable elements to points other than master nodes.

The rigid bodies are used to represent bones, since the deformation of bones is small compared to that of soft tissues. The deformable elements are used to represent ligaments, muscles, and other soft tissues.

Three types of deformable elements are used:

- Spring elements, which have stiffness along the axis joining the two nodes which they connect; this is called axial stiffness;
- Beam elements, which are elements that, in addition to axial stiffness, have bending stiffness in two planes and torsional stiffness;

- Muscle elements, which are similar to spring elements except that the axial force in the spring may be activated independently of the elongation to replicate activation of the muscle.

The data for the mathematical model then consist of the following:

- Geometric data, which include:
  a. coordinates of all master nodes (in the global coordinate system these define the configuration of the spine);
  b. coordinates of all slave nodes in the body coordinates of the master nodes with which they are associated (these define the shapes of the rigid bodies and the connection points for ligaments and muscles);
  c. connectivity data for each deformable element (the nodes which are connected by the elements must be specified).
- Stiffness data: for each deformable element, stiffness data must be given.

Cervical Spine Data

The present model developed for the head-neck system consists of vertebrae T1 though C1 and the head; each is represented by a rigid body. These rigid bodies are interconnected by

- intervertebral discs which are represented by beam elements with linear torsional, flexural and axial stiffnesses. The axial stiffness is bilinear with a different stiffness in compression and tension. The beam elements connect the centers of the end plates of the vertebral bodies to each other.

- articular facets, which are represented by a structural arrangement of springs to model both the line of action of the facets as well as the resistance to sliding, compression and distraction. Some of the springs act only in compression, some only in tension and others in both compression and tension.
- ligaments, which stretch from vertebra to vertebra and to the head, are modeled by linear springs and have stiffness only in tension.
- muscles, which are modeled by viscoelastic muscle elements especially developed for this study and based on the mathematical model of Apter and Graessley (1970) with the ability to mimic voluntary contractions as well as the stretch-reflex response.

The anatomical details and material properties of these elements are given in Appendices A, B and C. The structural arrangement of these interconnections is the same for all levels from T1 to C2. Due to the anatomical peculiarity of the C1-C2 and C1 - head joints, the interconnecting elements were arranged somewhat differently in these joints. The C1-C2 rigid bodies are connected by a beam element as the other joints, in spite of the absence of an intervertebral disc in this motion segment. This serves to model the resistance to shear offered by the odontoid process of the axis (C2) when the atlas (C1) is moved laterally or antero-poteriorly. The ability of the C1 ring to rotate around this odontoid process is modeled by using a low torsional stiffness for this beam element.

The lateral orientation of the C1-C2 facets is also included. The C1 - head joint is modeled by using two disc beam elements to represent the joints between the occipital condyles and C1. Further details of these joints are

provided in Appendix A. The T1 rigid body is presently the lowest point of the model and is constrained from rotation. This will be changed later when a simplified representation of the lower spine will be added.

Data for the coordinates of the anatomical points were based on the work of Liu et al. (1981), Francis (1955), and Lanier (1939). These data are presented in Appendices A and C. Stiffness data for the discs, facets, ligaments and muscles are more difficult to obtain and are quite fragmented. As a result, some simple biomechanical reasoning has to be applied to provide reasonable estimates of the missing stiffness data. Liu et al. (1981) tested cervical motion segments for two spines and provided stiffness data for complete motion segments (discs, facets and ligaments) comprising two vertebrae at a time. These tests are no doubt difficult to carry out; the results show many inconsistencies between the two spines and large variations from level to level. Therefore, the data were smoothed before use in the model.

Furthermore, the model requires stiffness data for individual discs, facets and ligaments in order to represent a motion segment. Because these data are not available from Liu et al. (1981), estimates were made of the relative contributions of the discs, the facets and the ligaments to the total stiffness (see Appendix B for the calculations and results). Disc compressive stiffnesses vary from 1.05×10^9 to 2.00×10^9 dynes/cm and tensile stiffnesses from 3.50×10^8 to 6.67×10^8 dynes/cm. An axial damping of 0.2% stiffness proportional damping is used for the discs. Ligament stiffnesses range from 5.0×10^6 dynes/cm for the intertransverse ligaments to 5.0×10^7 dynes/cm for the longitudinal ligaments. The facets, which are oriented at about a 45° angle in the posterior direction, have a total compressive stiffness of

about 1.0×10^9 dynes/cm and a total tensile stiffness of about 5.0×10^7 dynes/cm. No damping is employed in the ligaments and facets.

The muscle constants were obtained by approximating the results of Inman and Ralston (1964) who reported in vivo studies on human amputees. The various constants were adjusted until the stress-time curve and the velocity of contraction approached the results of Inman and Ralston and others (Fick, 1910; Haxton, 1944; Hill, 1970; Yamada, 1970). Appendix B gives further details of the muscle model. Cross-sectional areas of the muscles were obtained from Eycleshymer and Shoemaker (1911) and vary from 0.25 cm^2 to 10 cm^2. Attachment sites for the muscles were obtained from anatomy texts, such as Crouch (1973), Quiring (1949) and Warwick et al. (1973). Twenty-two different neck and head-neck muscle groups are included in the model, most of which are extensors and lateral flexors.

Section IV

SIMULATION RESULTS

To examine the validity of the model, several preliminary simulations of $-G_x$ and G_y impact acceleration were made. The predicted kinematic responses are compared to the experimental results of Ewing and Thomas (1972), who conducted vehicular acceleration tests on fully instrumented volunteers for $-G_x$ impact acceleration, and Ewing et al. (1978) who did similar tests for the G_y impact response. The purpose of both of these experimental studies was to measure not only the dynamic response of the head and neck but also the complete input acceleration to the head and neck at the first thoracic vertebra. So far, simulations with the model have been limited to the cervical spine alone. Three runs are reported here: $-G_x$ and G_y runs of the cervical spine and head including representations of discs, facets and all the ligaments, and a $-G_x$ run with 21 different muscles. The muscles in the last simulation are passive throughout the 200 msec of the simulation. The ability to permit the muscles to contract has been built into the model and the effect of muscle contraction on the kinematics of the head and neck is being investigated. The model does not yet include the viscous effect of soft tissues other than the muscles and the inertia of the muscles has been neglected.

$-G_x$ Impact Simulation

The test used for comparison with our $-G_x$ simulation is one in which

a maximum acceleration of 7.4 G was attained. The acceleration increases linearly from 0 to its maximum at 14.2 msec, followed by a linear decay to zero acceleration at 340 msec. No chin-chest impact was reported for any of the $-G_x$ tests conducted by Thomas and Ewing and the head and neck were unrestrained in all experiments. This triangular acceleration profile was prescribed in the program by using the following displacement function for the T1 primary node in the model:

$$u_x(t) = \begin{cases} -85680.75\ t^3 & 0 \leq t < 0.0142 \text{ sec} \\ 11203.19\ [\frac{t^3}{3} - 0.34t^2 + 0.004828t - 2.2853 \times 10^{-5}] & \\ & 0.0142 \leq t \leq 0.034 \end{cases}$$

The T1 vertebra was fixed in the y and z directions and no rotations were permitted. This unnatural condition will be corrected later when the cervical spine is combined with a simplified representation of the rest of the spine. The initial position of the spine and head is shown in Figure 10.

The computed kinematic data are compared with the experimental results of Ewing and Thomas, in Figures 11 to 13.

The linear acceleration of the head in the global x direction is portrayed in Figure 11a. The experimental curve shows two characteristic peaks, the first of which occurs at 55 msec. Our model exhibits one well-defined peak at about 82 msec and a less obvious peak at around 120 msec. The magnitude of the first peak matches the experimental value quite well. The agreement between computational results and experiment is seen to be good

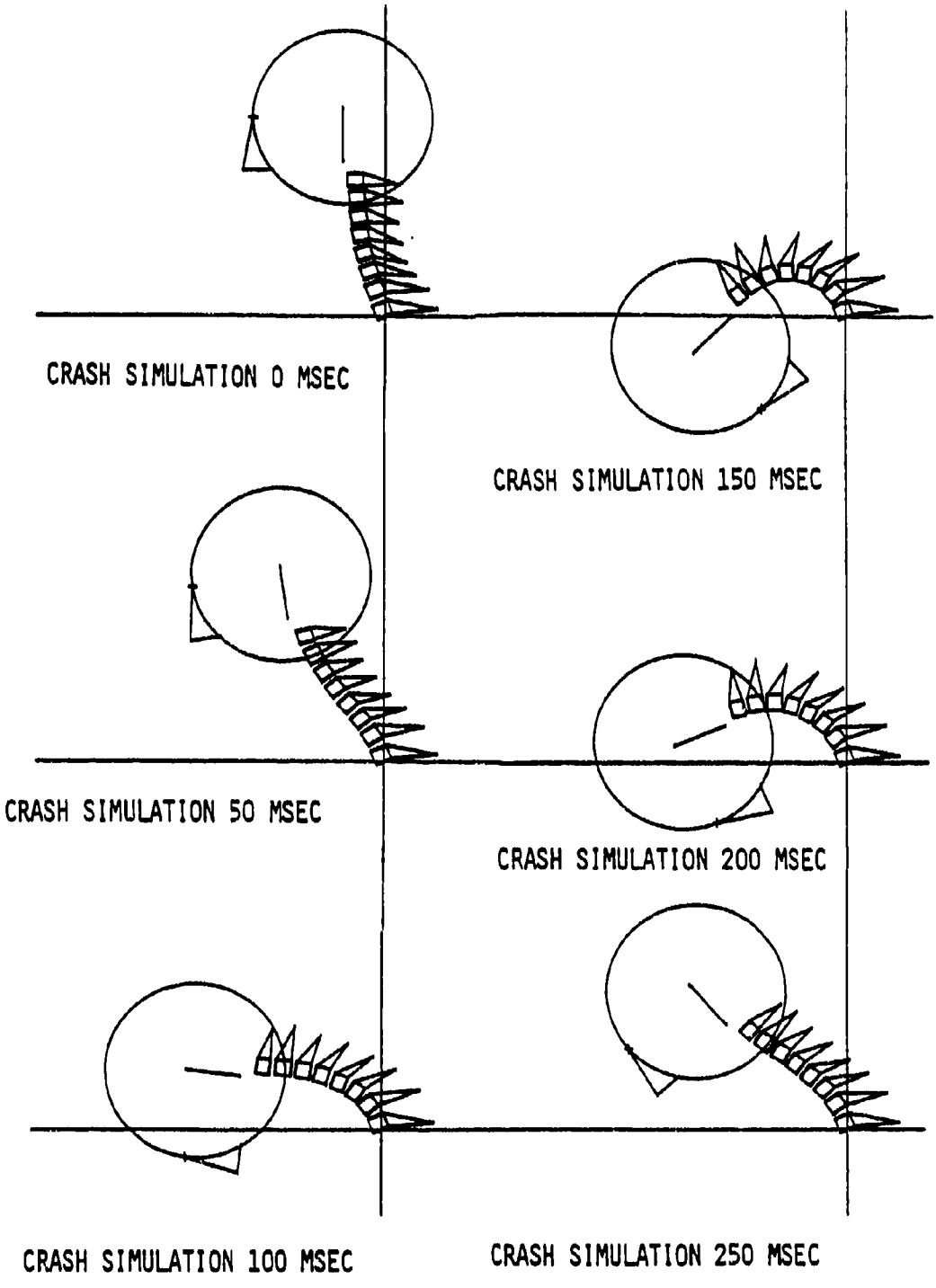

FIGURE 10. Response of ligamentous neck model to $-G_x$ impact acceleration.

a.

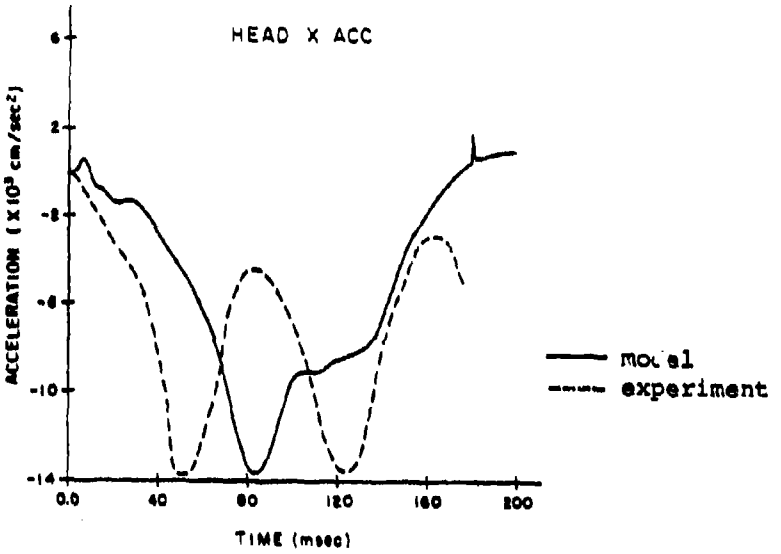

b.

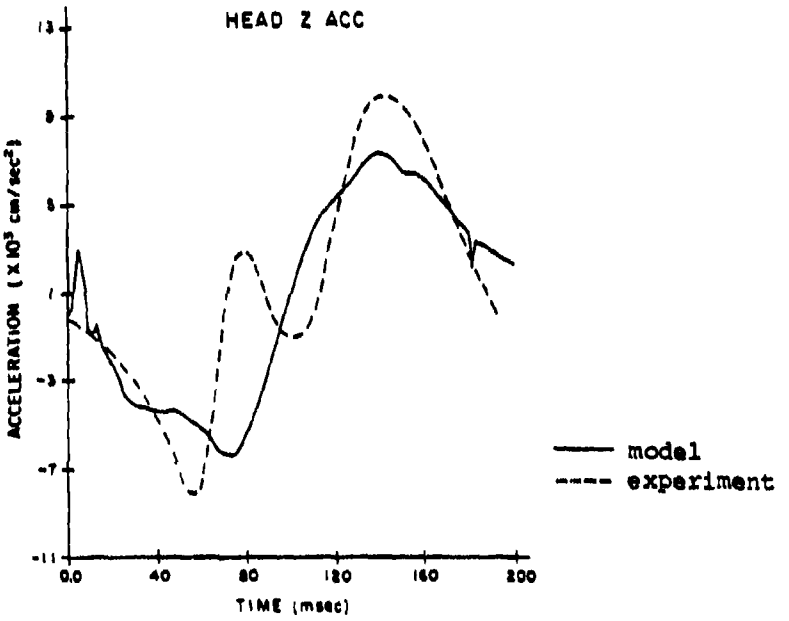

FIGURE 11 a. Head X acceleration time history for $-G_x$ impact acceleration.
b. Head Z acceleration time history for $-G_x$ impact acceleration.

until about 100 msec. A plot of the deformed spine in Figure 10 shows that at 150 msec the neck has almost reached a maximum in flexion. Figure 11b shows the linear acceleration of the head center of gravity in the global z-direction. Again, the first peak in the experiment occurs at 55 msec. The model gives similar results except for the intermediate peaks at about 100 msec.

Figures 12a, 12b and 13a show the angular displacement, velocity and acceleration of the center of gravity of the head, respectively. The experimental angular variables are reported with respect to the head anatomical coordinate system defined in the report. Figure 13a shows the angular acceleration, which for the experiment is a triphasic response lasting from 40 msec to 250 msec. The model predicts an almost identical result until around 160 msec, after which the model differs substantially from the experiment. The angular velocity (Fig. 12b) and angular displacement (Fig. 12a) are qualitatively similar to the experiment but show greater discrepancies in the magnitudes. The angular displacement is about twice the value reported by Ewing and Thomas. This difference is most likely due to action of the muscles, which were not included in this simulation.

Figure 13b shows the moment computed at the occipital condyle. Figures 14a and 14b show the time histories of axial and shear forces in the C6-C5 intervertebral disc, respectively.

a.

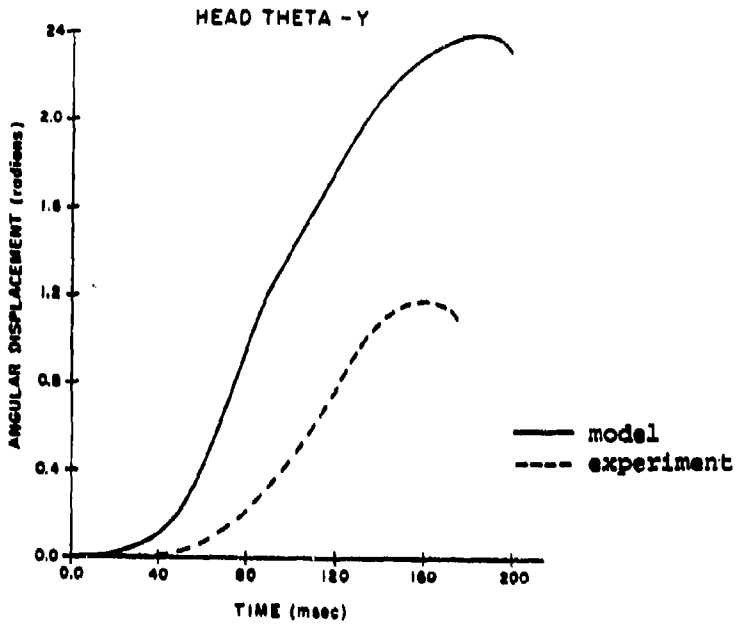

b.

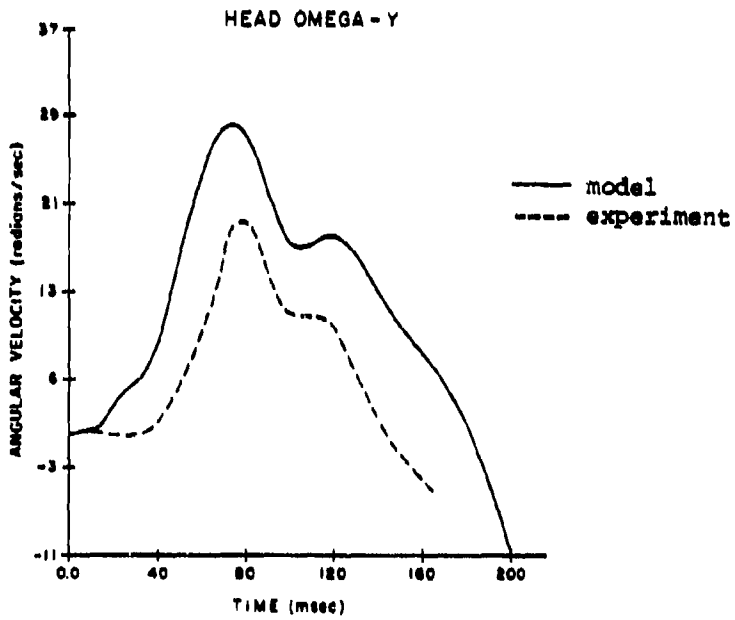

FIGURE 12 a. Head angular displacement time history for $-G_x$ impact acceleration.
b. Head angular velocity time history for $-G_x$ impact acceleration.

a.

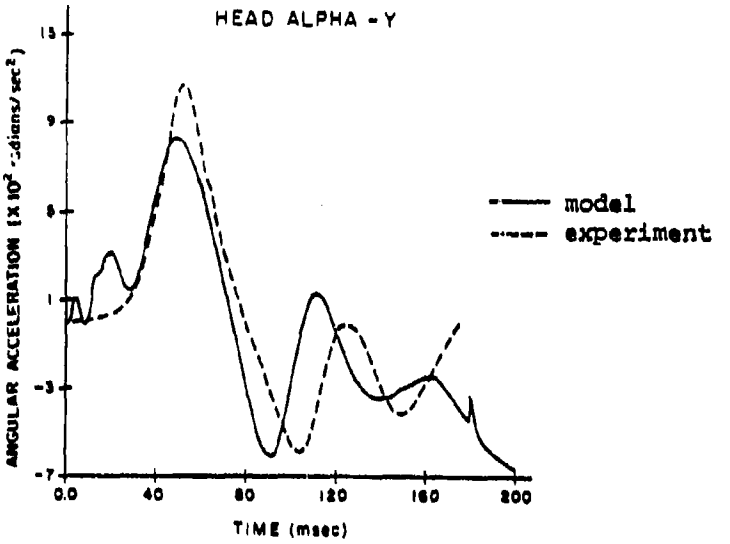

b.

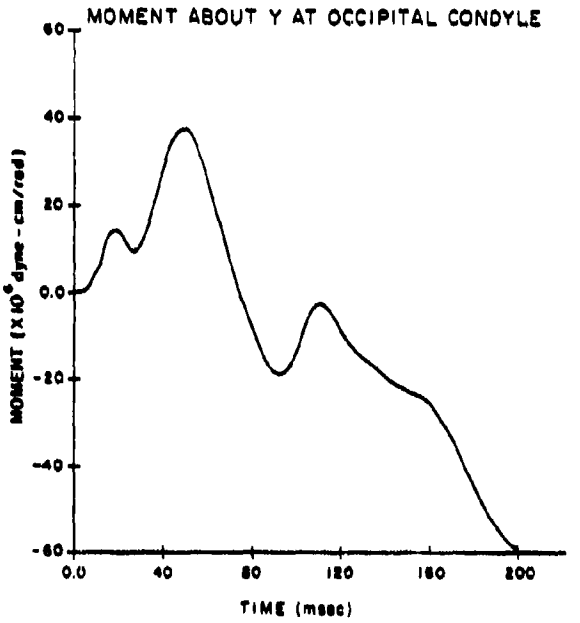

FIGURE 13 a. Head angular acceleration time history for $-G_x$ impact acceleration.
b. Moment at occipital condyles for $-G_x$ impact acceleration.

When the muscles are included in the model, as passive elements, the resulting kinematic response is virtually identical to the ligamentous spine and neck runs (see Fig. 10). The only difference is that the muscles cause the model to become unstable at about 175 msec due to large rotations of the disc beam elements. Some of the ligament forces are reduced since part of the load is taken up by the muscles (Fig. 15). The peak muscle stress in the first 150 msec varies from 0.1×10^6 dynes/cm^2 in the obliquus capitis superior muscle to 1.2×10^6 dynes/cm^2 for the spinalis cervicis and interspinales muscles. The maximum estimated strength of skeletal muscle under passive testing is about 3.2×10^6 dynes/cm^2 for the 20-39 age group (Katake, 1961). Thus, the muscles are not stressed to their ultimate strength.

The explanation for the lack of effect of the muscles on the kinematics of the head and neck as follows. The muscle elements, unlike the spring elements representing the ligaments, connect bony reference points which are usually more than two or three vertebrae apart, indeed sometimes as many as seven vertebrae apart. In the deformed cervical spine at 100 msec, (see Fig. 10) the posterior extensor muscles, which connect the lower cervical spine to the back of the skull, must pass over the vertebrae lying between the origin and insertion of the muscle. In the model, however, the insertion and origin of the muscle are connected by a straight line throughout the simulation. This not only results in an incorrect line of action, which eventually causes the model to become unstable, but it also results in the muscles being stretched much less in the model than in reality. By forcing

a.

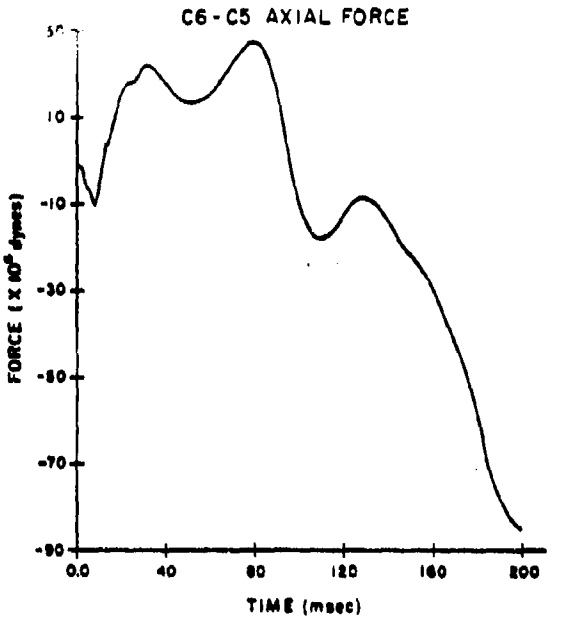

b.

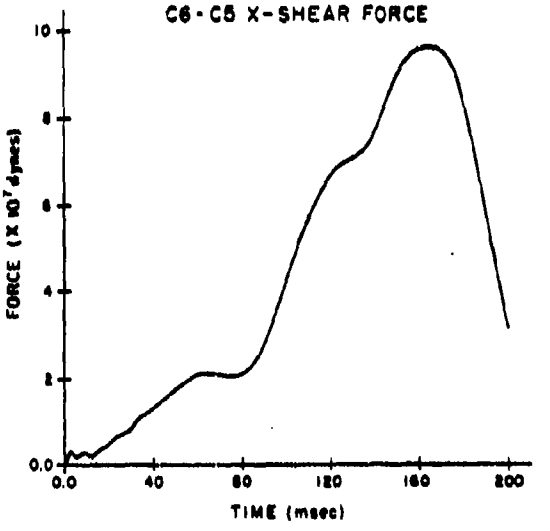

FIGURE 14 a. C6-C5 axial force time history for $-G_x$ impact acceleration.
b. C6-C5 X-shear force time history for $-G_x$ impact acceleration.

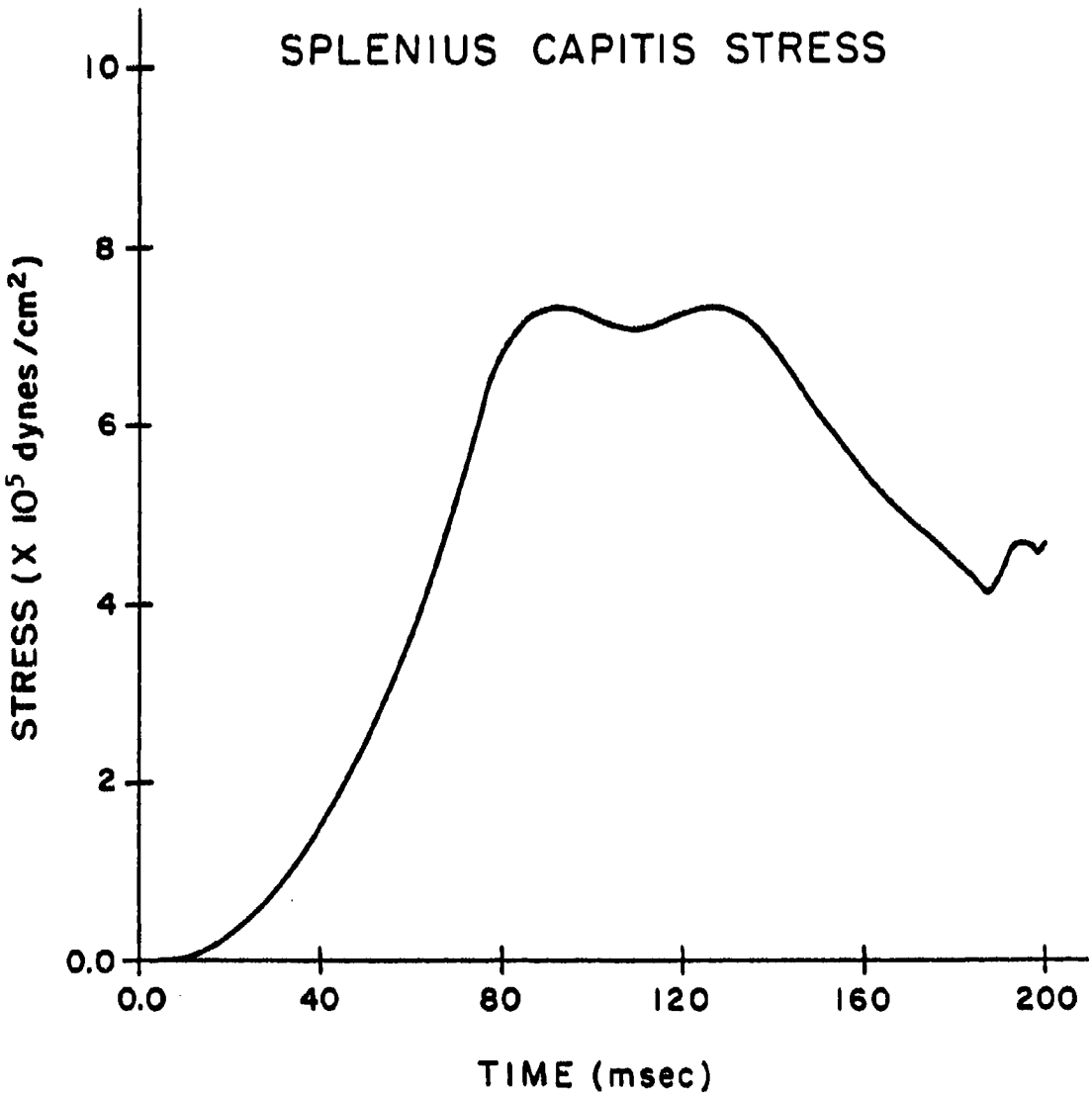

FIGURE 15. Time history of stress in splenius capitis muscle for $-G_x$ impact acceleration.

the muscle elements around the curvature of the deforming spine, more realistic lines of action could be attained and the muscles may contribute more to resisting the flexion of the spine by being stretched more.

G_y Impact Simulation

To test the lateral behavior of the model, comparisons were made with the G_y impact tests of Ewing et al. (1978). These experiments ranged from 2 to 7.5 G in peak sled accelerations. At 7.5 G, the head comes very close to impact with the right shoulder, so higher accelerations were not attempted. As in the $-G_x$ test, the head and neck were unrestrained in all experiments. Input to the neck was again measured at the T1 level.

The lateral response is quite different from the $-G_x$ response. For the same magnitude of sled acceleration the acceleration of the head is much greater for G_y than for $-G_x$. Also, the acceleration measured at T1 indicates that in the G_y tests the T1 motion can be significant, whereas in the $-G_x$ tests the motion of T1 is very small. Ewing et al. (1978) concluded from their experience with these $-G_x$ and G_y tests that the higher head acceleration in the G_y tests relative to the $-G_x$ tests is due to a higher acceleration at T1 for the same sled acceleration. They suggested that the difference is due to the manner in which the torso is restrained in the x and y directions. There is a possibility that the measured acceleration at T1 for the G_y test is an artifact, because the instrumentation mount at T1 is not rigidly connected to the bone. The accelerometer is mounted under pressure at the T1 level but, because of the intervening soft tissue between the bone and the instrument,

relative motion between the mount and the bone is possible. Ewing et al. (1977) do not believe that their T1 measurements are due to motion between the bone and the mount, but this possiblity cannot be excluded.

In the experiments of Ewing et al. the sled acceleration profile is a rise from zero to -70 m/sec^2 (7 G) in 40 msec, followed by a slow decay to zero at 140 msec. The acceleration profile measured at T1 for this sled acceleration is a sharp rise from zero to -160 m/sec^2, followed by a drop to zero at 140 msec. Thus the measured input to the neck is about twice the sled acceleration.

To simulate the G_y test of Ewing et al. a run was made with the ligamentous neck model using the experimentally measured T1 acceleration as input, by prescribing the y component of the displacement at T1 as:

$$u_y(t) \begin{cases} 66666.67\ t^3 & 0 \leq t < 0.04 \text{ sec} \\ -160000.\left(\frac{t^3}{6} - 0.07\ t^2 + 0.0028\ t - 3.7333 \times 10^{-5}\right) & 0.04 \leq t < 0.14 \text{ sec} \end{cases}$$

Figure 16 shows the deformed configuration of the cervical spine and head. The ligamentous neck model becomes unstable beyond 100 msec. This is due to a posterior displacement of the head which reaches 5 cm at 100 msec in the model; in the human tests, a posterior displacement of only 1 cm was recorded at 100 msec. The posterior displacement of the head in the model is believed to be caused by inadequate modeling of the articular facet joints. These joints are modeled by an arrangement of springs, as described in Appendix B, which lie in a saggital plane. Although this arrangement was tested in a motion segment

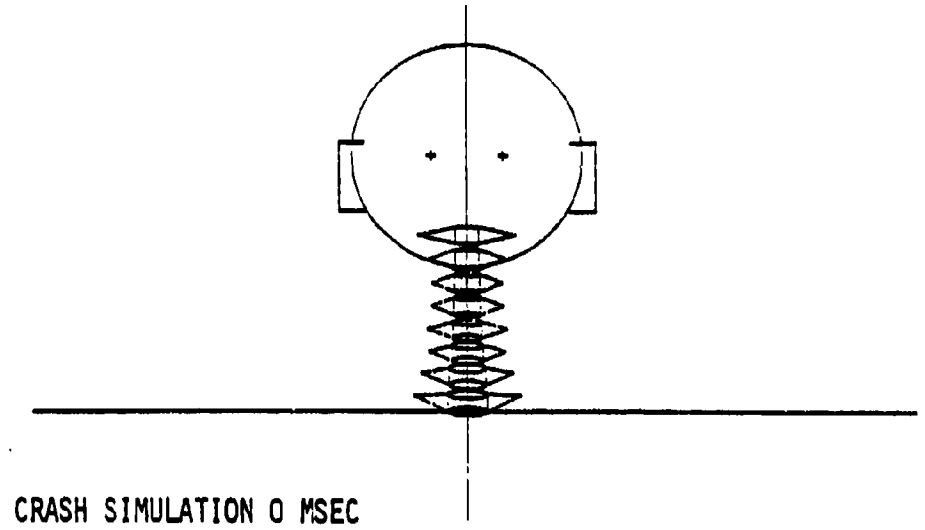

CRASH SIMULATION 0 MSEC

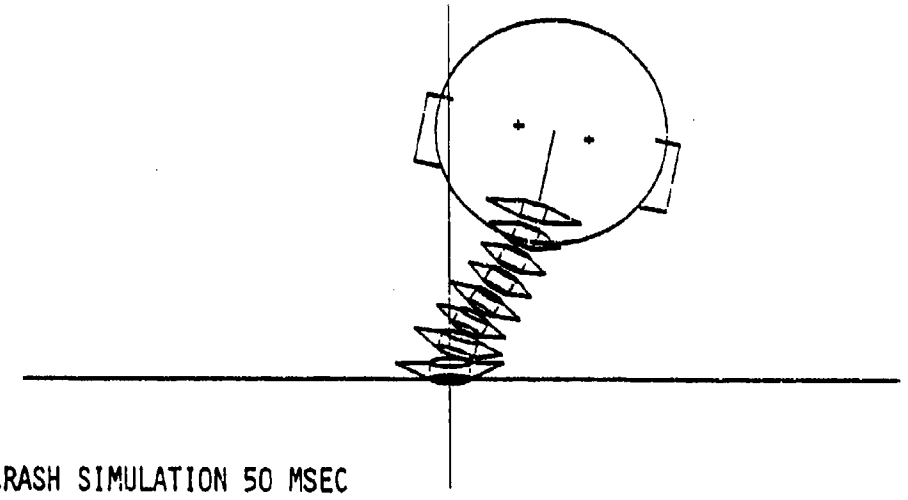

CRASH SIMULATION 50 MSEC

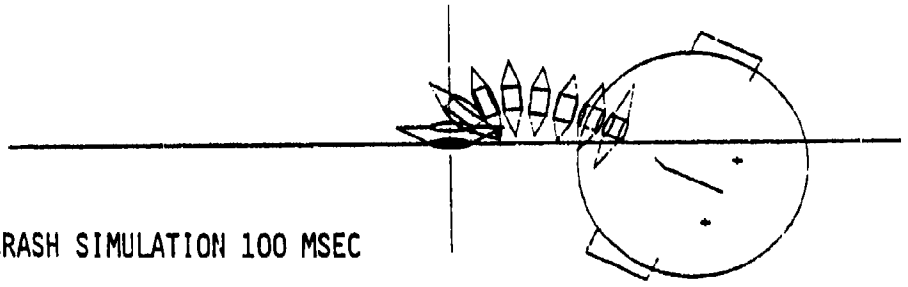

CRASH SIMULATION 100 MSEC

FIGURE 16. Response of ligamentous neck model to $+G_y$ impact acceleration.

model, as described in Appendix B, and was found to be quite adequate for motion segment modeling, the arrangement fails to perform satisfactorily in the G_y test of the overall neck model. Three-dimensional structural arrangements of the facet springs were also found to be of no use in preventing the backward movement of the head and spine. The facet model works very well for $-G_x$ impact simulation, because the $-G_x$ test involves only two-dimensional motion.

The y and z components of the head acceleration in the G_y simulation are compared in Figures 17a and 17b. The shapes of these two curves are similar to the experimental curves, but the model predicts accelerations twice the corresponding experimental accelerations.

These differences between the results predicted by the model and the results of Ewing et al. are being investigated. In addition to the role of the facets, the effects of the musculature, the lower spine, and the restraint system could all contribute to the discrepancies.

a.

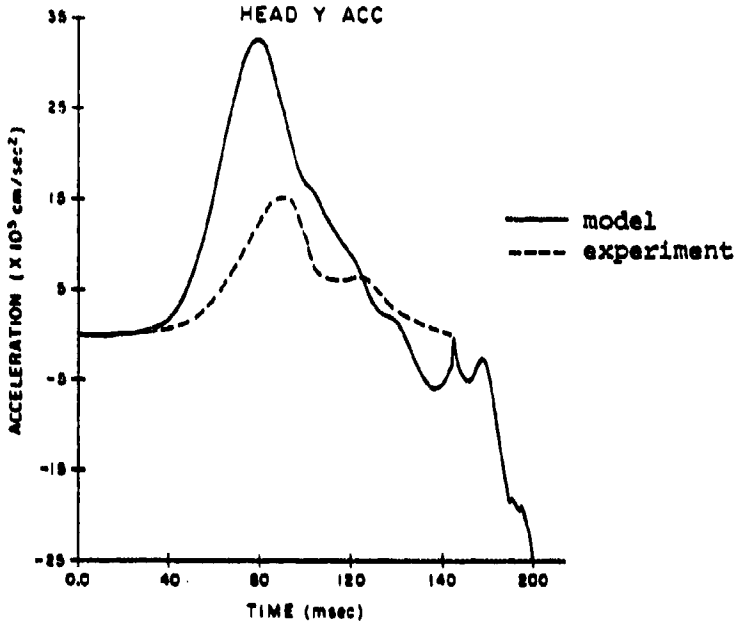

b.

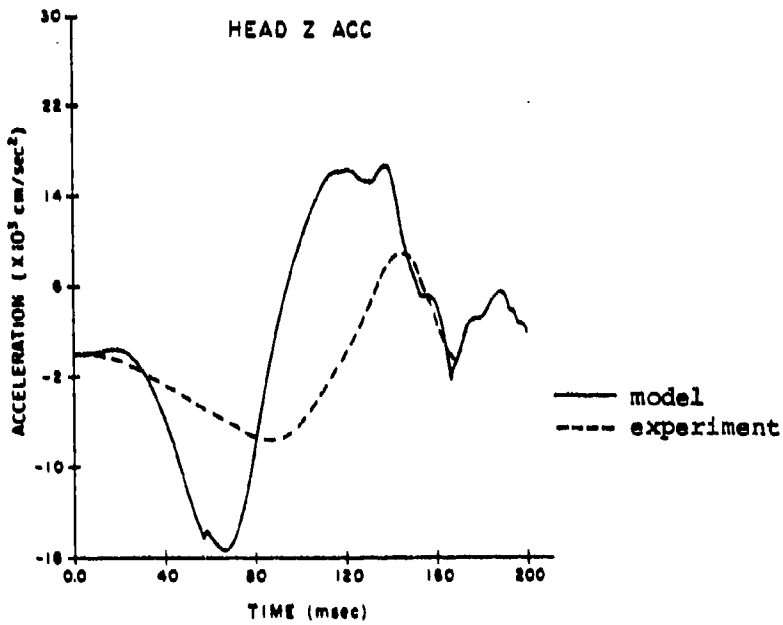

FIGURE 17 a. Head Y acceleration time history for $+G_y$ impact acceleration.
b. Head Z acceleration time history for $+G_y$ impact acceleration.

APPENDIX A

GEOMETRIC DATA

Vertebral Local and Global Data

The geometric data for the cervical spine consist of two parts: (1) geometric data of the vertebrae, which consist of the sizes and shapes of the vertebral bodies and discs and the locations of points which serve as attachment sites for ligaments or muscles; (2) global data, which consist of the locations and orientations of the vertebral bodies in space. The data for individual vertebrae are based on information provided by Liu et al. (1981), the anatomical studies of Francis (1955) and Lanier (1939), and various anatomy texts. The global data are based on radiographs and drawings from texts, such as Gray's Anatomy (1973) and, indirectly, from data provided in the Liu et al. study (1981).

The development of a consistent set of local and global data presents particular difficulties since both the articular facets and discs as defined by the global and local data must coincide.

The anatomical information given by Liu et al (1981) provides the coordinates of bony reference points on vertebrae C1 through C7 and T1 for two cervical spines. They also include computer-drawn plots of these reference points.

Since Liu et al. do not give the global data for these spines, development of these data would entail the problem of finding the positions and orientations so that end plates and synovial joints are properly aligned and

the overall curvature and shape of the spine is appropriate. We found it very difficult to carry out this procedure mathematically so that all of these conditions are met and, in addition, found it unjustified to expend such considerable effort to match a particular spine. For this reason a simpler approach was used. The computer-drawn plots of the vertebral reference points for one set of cervical vertebrae (PW-35) were cut out and arranged on graph paper. By connecting the vertebrae at the articular facets and vertebral end plates and by referring to radiographs, reasonable orientations and positions were obtained (see Fig. 18). The drawing is only diagrammatic - the transverse processes, for example, have been omitted. Superimposed on the traced vertebrae are the rigid bodies (represented as cylinders, with the triangular portions representing the spinous processes) used in plotting the neck with the plotting program.

The centers of the vertebral bodies, as defined by Liu and Krieger for their coordinate origins, are reasonably close to the centers of the rigid bodies. The rigid body heights and widths are those reported by Francis (1955) and Lanier (1939). The rigid bodies are arranged in such a manner as to obtain a smooth transition of the cervical curvature from level to level.

The intervertebral discs are modeled by disc-beam elements, which are chosen to fall along lines connecting the centers of the rigid bodies. Except for the vertebral body dimensions, all coordinates of bony reference points were obtained from the Liu et al. report. The intervertebral disc heights reported by Liu et al. range from 0.5 cm in the anterior region of the disc to 0.65 cm in the center of the disc. In the

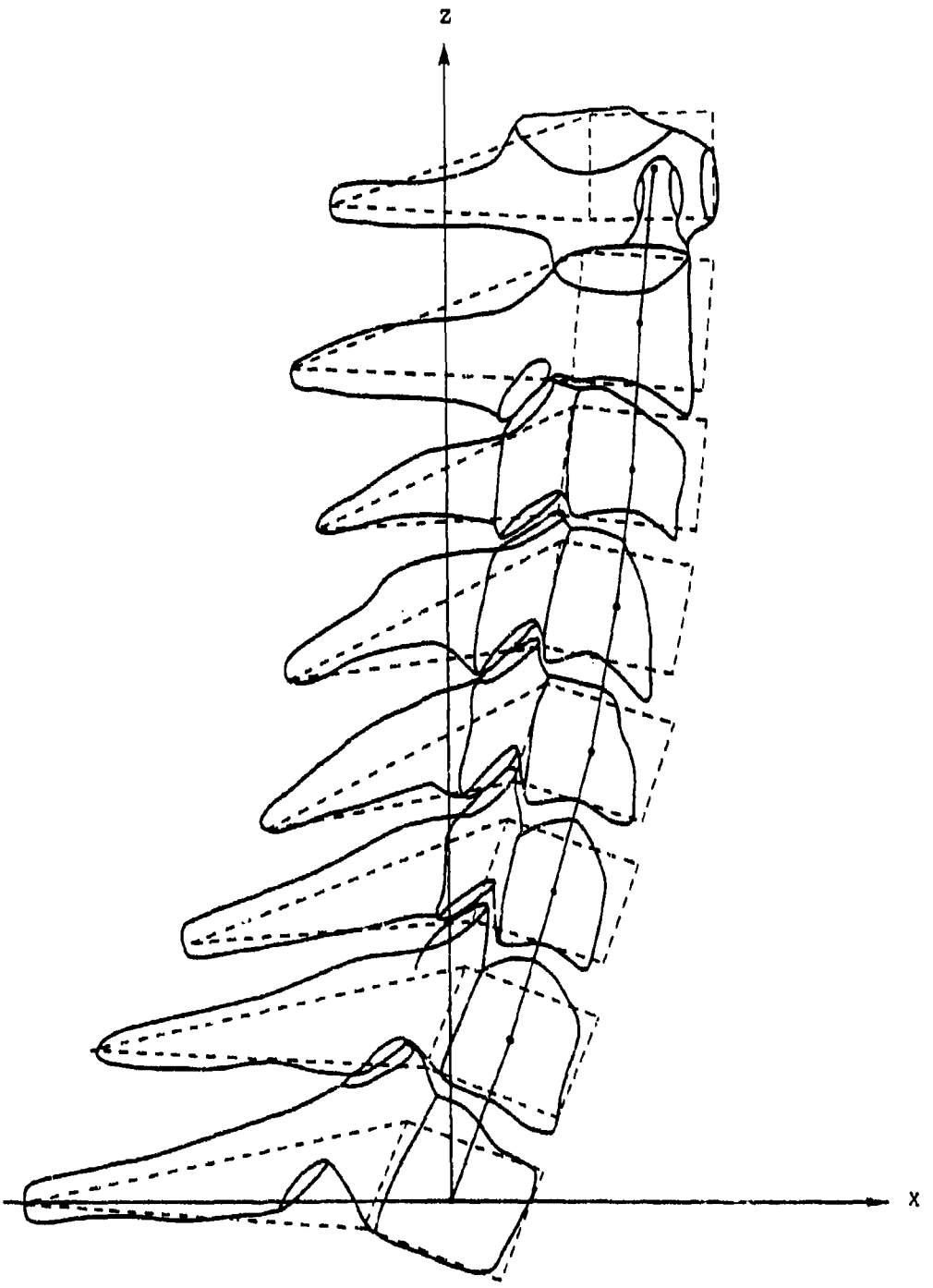

FIGURE 18. Comparison of geometry of cervical vertebrae with rigid bodies in model.

model the disc beam elements are 0.6 cm in length. The articular facets are modeled with springs and the coordinates for each of these springs were obtained by drawing two lines on the scaled drawing, one along the contact surfaces of the facets and another at 90° to the first line and through its center (Fig. 19). These joints are described further in Appendix B.

Of special concern is the upper cervical region, where the first two cervical vertebrae form unusual joints. The C1-C2 joint is modeled like the other joints by interposing a beam element between the rigid bodies, in spite of the absence of such a disc in the spine. In the model, the rigid body for vertebra C2 is not nearly as long as the real vertebra because the odontoid process is modeled in part by the disc beam element. The height of the rigid body was taken to be equivalent to the distance between the lower end plate and the superior facet planes. The center of the rigid body representing C1 coincides with the instantaneous axis of rotation of the C1 vertebra; this instantaneous axis of rotation of C1 is located in the middle of the odontoid process of C2 (White et al. 1978). The head is centered 1.8 cm anterior and 5.8 cm superior to the superior articular facets of the atlas (C1). This corresponds roughly with the measurements reported by Culver et al. (1972) for the 50th percentile male.

The articular facets in the model were chosen to approximate the same antero-posterior orientation of the spine for which radiographs were available. Since the lateral orientation of the normals to the facets is neglible until the C2-C3 and C1-C2 joints are reached, no lateral orientation is included in the lower cervical region. In the spine the normals to the C2-C3 facets are inclined at an inward angle of 30° to the vertical, but in

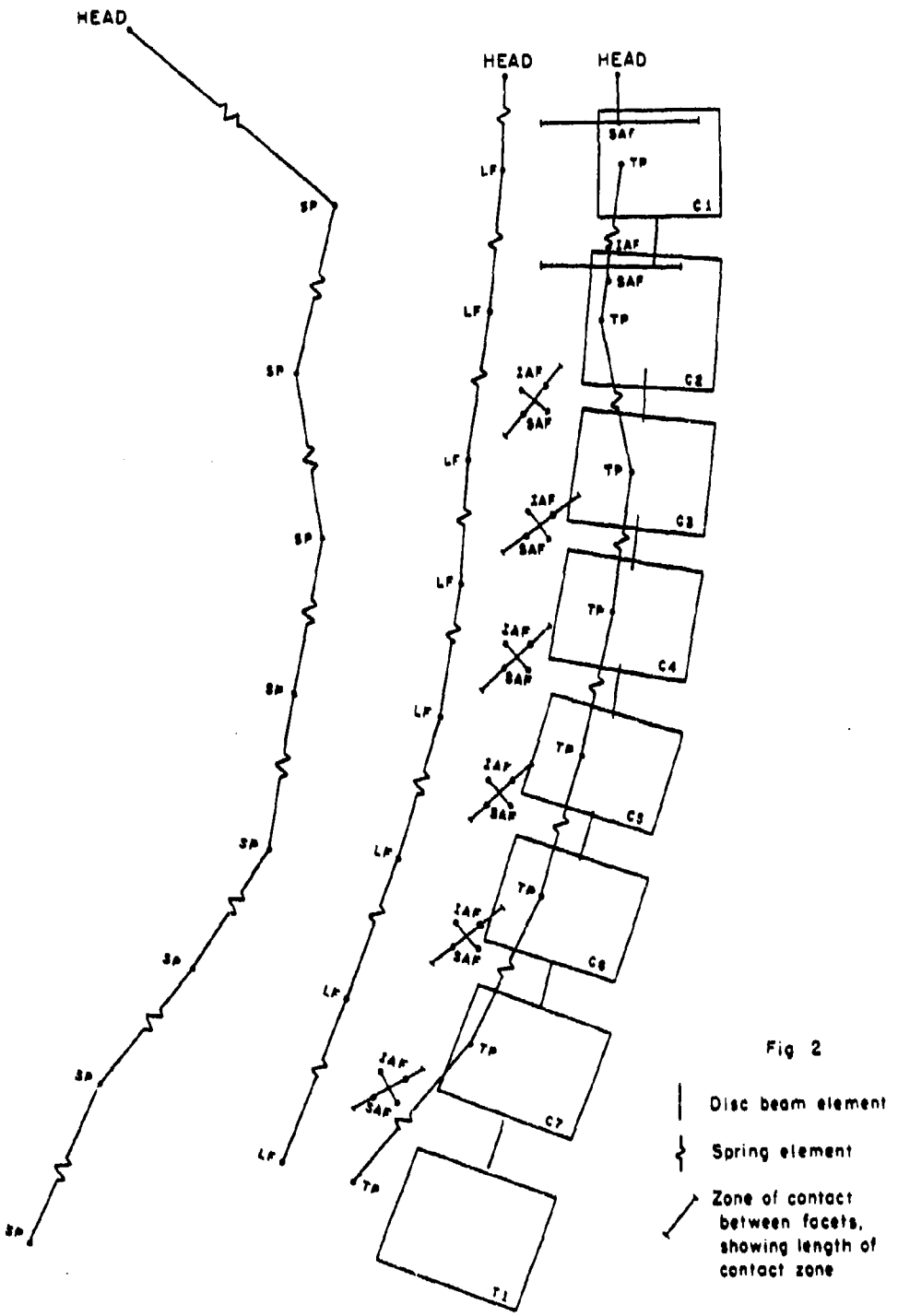

FIGURE 19. Diagram of cervical spine model.

the model the facet springs have no lateral orientation. The C1-C2 joint is the only joint in the model where the facet springs are laterally inclined. In this case the normals to the facet surfaces are inclined at an outward angle of about 20° to the vertical. In the spine the normals to the superior facets of the atlas are medially inclined but in the model the facet springs for this joint have no lateral orientation. Further details of these joints are discussed in Appendix B.

Bone reference points used as attachment points for disc beam elements, ligaments and muscles are indicated in Figure 19. These points are the spinous process tips (SP), the right and left transverse process tips (RTP, LTP), the right and left inferior articular facets (RIAF, LIAF) the right and left superior articular facets (RSAF, LSAF), and the right and left ligamentum flavum attachment sites (RLF, LLF). The ligaments pass in a straight line from one point to another. The muscle attachment sites include the same reference points as the ligaments and, in addition, midside nodes on the front and back of the vertebral bodies. The muscle elements also pass in a straight line from one node to another. This may create two possible problems: the line of action will not be correct if large deformation of the spine occurs, because the curvature of the spine will be ignored; and in reality the muscles are attached to the bones by slender tendons. Thus, many muscles have their points of attachment near each other and can function without interfering with one another. Many muscles in the neck are stacked side by side and the muscles furthest away from the bone are connected to it by longer tendons. This distance between the body of the muscle and its attachment sites creates a different line of action for the force as compared to that obtained by a straight-line connection between the attach-

ment sites, which is presently used in the model. This discrepancy is now being investigated.

The coordinates of some of the bone reference points are listed in Table 2 in a local coordinate system with the origin at the center of the lower end plate. These are the coordinates used in the model where the bodies of the vertebrae are represented by cylinders. The lower end plate is thus actually the lower face of the cylinder. Dimensions for the cylinders were estimated from vertebral body dimensions reported in the literature by Francis (1955) and Lanier (1939) and from the report by Liu et al. (1981). These data are summarized in Table 3.

The data in this table show some discrepancies between the measurement of the heights of the vertebral bodies. It is evident that Francis measured the height from rim to rim, whereas Lanier probably measured the height from the center of one end plate to the other. Because of the concavity of the end plate regions, the results are quite different. For plotting purposes Francis' heights are used because this is how the vertebrae appear to the eye when seen from the side. The data extracted from data points reported by Liu et al. are only approximate due to the location of the reference points. The estimated heights are taken from the center of one end plate to the other. These are reasonably close to Lanier's heights. Therefore the Liu et al. specimen is assumed to be of normal dimensions. Dimensions of the cylinders used in the model are listed in Table 4. The data of Liu et al. are used for the vertical heights and the data of Lanier for the diameters.

TABLE 2

COORDINATES OF VERTEBRAL REFERENCE POINTS WITH RESPECT TO LOWER ENDPLATE CENTER

Vertebral Reference Point	$\bar{x}$-coordinate (cm)	$\bar{y}$-coordinate (cm)	$\bar{z}$-coordinate (cm)
	C1 Vertebra		
SP	-4.13	0.0	0.2
RTP	-0.5	-3.80	0.4
LTP	-0.5	3.80	0.4
RIAF	-0.71	-1.80	-1.26
LIAF	-0.71	1.80	-1.26
RSAF	-0.52	-2.00	1.26
LSAF	-0.52	2.00	1.26
RLF	-2.00	-0.75	0.4
LLF	-2.00	0.75	0.4
	C2 Vertebra		
SP	-4.41	0.0	0.0
RTP	-0.6	-2.90	0.9
LTP	-0.6	2.90	0.9
RIAF	-1.62	-1.90	-0.28
LIAF	-1.62	1.90	-0.28
RSAF	-0.53	-1.75	1.57
LSAF	-0.53	1.75	1.57
RLF	-2.00	-0.73	0.9
LLF	-2.00	0.73	0.9
	C3 Vertebra		
SP	-3.86	0.0	-0.55
RTP	-0.1	-2.74	0.55
LTP	-0.1	2.74	0.55
RIAF	-1.24	-1.97	-0.12
LIAF	-1.24	1.97	-0.12
RSAF	-1.36	-1.87	1.46
LSAF	-1.36	1.87	1.46
RLF	-2.16	-0.70	0.55
LLF	-2.16	0.70	0.55

TABLE 2 - continued

Vertebral Reference Point	$\bar{x}$-coordinate (cm)	$\bar{y}$-coordinate (cm)	$\bar{z}$-coordinate (cm)
		C4 Vertebra	
SP	-3.94	0.0	-0.98
RTP	-0.17	-2.80	0.60
LTP	-0.17	2.80	0.60
RIAF	-1.18	-1.99	-0.08
LIAF	-1.18	1.99	-0.08
RSAF	-1.19	-1.88	1.65
LSAF	-1.19	1.88	1.65
RLF	-2.14	-0.72	0.60
LLF	-2.14	0.72	0.60
		C5 Vertebra	
SP	-3.74	0.0	-1.57
RTP	-0.32	-3.10	0.45
LTP	-0.32	3.10	0.45
RIAF	-1.28	-2.07	-0.04
LIAF	-1.28	2.07	-0.04
RSAF	-1.18	-1.86	1.65
LSAF	-1.18	1.86	1.65
RLF	-2.16	-0.74	0.45
LLF	-2.16	0.74	0.45
		C6 Vertebra	
SP	-4.21	0.0	-2.24
RTP	-0.38	-3.00	0.55
LTP	-0.38	3.00	0.55
RIAF	-1.22	-2.12	0.0
LIAF	-1.22	2.12	0.0
RSAF	-1.19	-2.02	1.65
LSAF	-1.19	2.02	1.65
RLF	-2.18	-0.70	0.55
LLF	-2.18	0.70	0.55

TABLE 2 - continued

Vertebral Reference Point	$\bar{x}$-coordinate (cm)	$\bar{y}$-coordinate (cm)	$\bar{z}$-coordinate (cm)
	C7 Vertebra		
SP	-4.92	0.0	-1.38
RTP	-0.70	-3.60	0.65
LTP	-0.70	3.60	0.65
RIAF	-1.63	-1.88	-0.20
LIAF	-1.63	1.88	-0.20
RSAF	-1.33	-2.16	1.97
LSAF	-1.33	2.16	1.97
RLF	-2.38	-0.64	0.65
LLF	-2.38	0.64	0.65
	T1 Vertebra		
SP	-5.12	0.0	-1.38
RTP	-1.60	-4.20	0.75
LTP	-1.60	4.20	0.75
RIAF	-2.02	-1.74	---
LIAF	-2.02	1.74	---
RSAF	-1.37	-1.92	2.09
LSAF	-1.37	1.92	2.09
RLF	-2.50	-0.58	0.75
LLF	-2.50	0.58	0.75

TABLE 3

VERTEBRAL BODY DIMENSIONS

	Francis' Data (1955)[1]			Lanier's Data (1939)[2]			Liu et al. Data (1978)[3]		
	Vertical Height (cm)	Antero-Posterior Diameter (cm)	Lateral Diameter (cm)	Vertical Height (cm)	Antero-Posterior Diameter (cm)	Lateral Diameter (cm)	Vertical Height (cm)	Antero-Posterior Diameter (cm)	Lateral Diameter (cm)
Odontoid Process	1.75	1.22	1.07	---	---	---	---	0.76	0.76
C2	3.99	1.61	1.95	3.46	1.27	1.90	2.8	1.2	1.7
C3	1.43	1.64	2.05	1.15	1.53	2.03	1.1	1.3	1.9
C4	1.38	1.65	2.15	1.11	1.56	2.12	1.2	1.3	2.1
C5	1.33	1.68	2.25	1.09	1.55	2.24	0.9	1.3	2.2
C6	1.30	1.73	2.48	1.08	1.61	2.49	1.1	1.3	2.4
C7	1.46	1.67	2.93	1.24	1.69	2.89	1.3	1.5	2.7
T1	---	---	---	1.47	1.66	3.16	1.5	1.6	2.8

[1]Measured 100 white male specimens (ages 25-36). Also measured 100 male negro specimens with no significantly different results.

[2]Measured 96 white male specimens (ages 40-55). Also measured 88 negro male specimens with no significant difference in results.

[3]From one specimen (PW-35) as estimated from the data points provided by the Liu et al. study.

TABLE 4

VERTEBRAL BODY DIMENSIONS

USED IN MODEL

Vertebral Level	Vertical Height (cm)	Antero-Posterior Half-Diameter (cm)	Lateral Half-Diameter (cm)
C1	0.80	0.78	0.925
C2	1.80	0.785	0.95
C3	1.10	0.79	1.015
C4	1.20	0.80	1.06
C5	0.90	0.805	1.12
C6	1.10	0.835	1.245
C7	1.30	0.85	1.445
T1	1.50	0.855	1.58

Ligaments - Geometry

The ligaments included in the model are the anterior and posterior longitudinal ligaments, the ligamenta flava, the capsular ligaments, the intertransverse ligaments, and the interspinous ligaments. Of those ligaments joining the head to the spine the cruciform ligament, alar ligament and deep portion of the tectorial membrane are included, as well as the extensions of the interspinous, longitudinal and flaval ligaments. The anterior and posterior longitudinal ligaments are attached to anterior and posterior points on the rigid body cylinders at midheight. The coordinates for the ligamenta flava attachment points were estimated from Liu's report, except that the z-coordinates were taken to be at the midheight level of the rigid body cylinders. The ligamenta flava are divided into two springs per motion segment, one each for the left and right sides. As with the other broad ligaments, which have broad attachment areas, the ligament spring elements are connected to the bone at the center of the area of attachment. The interspinous ligaments, the ligamentum nuchae and the supraspinous ligaments are represented by single springs connecting the spinous process tips. This ignores the connections between nonadjacent vertebrae and the long fan-like structure connecting the lower cervical vertebrae to the head. Also ignored are the unusual arrangements of the supraspinous ligaments which cross over one-another as they connect from one of the bifid tips of one spinous process to the other bifid tip on the next spinous process. The intertransverse ligaments are included because Johnson et al. (1975), observed their well-defined presence in dissections and postulated that they may limit motion in lateral flexion and rotation.

Although there is no disc between C1 and C2, in the model a disc beam element is used between C1 and C2, because the joint is extremely complex and it would be difficult to include all separate motion restraining elements and still maintain overall motion segment behavior. Furthermore, the material properties of the various restraining elements in this joint are not known. Therefore, the transverse ligament and articular joint formed by the odoncoid process with the anterior part of the C1 ring are not included, instead, the stiffness of the anterior part of C1 and the odontoid process is represented by a beam element. The articular facet joints, the cruciform ligaments and the tectorial membrane are included except for that portion of the cruciform ligament which runs horizontally and is otherwise known as the transverse ligament.

The C1 - head or atlanto-occipital joint is modeled with two disc beam elements and a number of ligament spring elements. Again this is a joint without a disc and the disc beam elements are used to model the left and right synovial joints between the occipital condyles and the facets of the atlas. The beam lengths are taken to be 0.6 cm as for the other disc beam elements. The ligaments passing around this joint are the continuation of the longitudinal, interspinous, flaval and intertransverse ligaments except that they are given different names in this region. Also crossing this joint are the deep portions of the tectoral membrane, which are attached to the posterior midheight node of the C2 rigid body cylinder and to the left and right occipital condyles. The vertical portion of the cruciform ligament spring element stretches from the tip of the odontoid process to the anterior margin of the foramen magnum. The lateral alar odontoid ligaments are modeled as two springs stretching from the odontoid tip to the left and

right occipital condyles.

Geometry of Muscles

Since this model is intended for use in pilot ejection studies and in impact studies, where the head is subjected to a forward or sideways acceleration, the muscles included are mostly extensors and lateral flexors. Out of a total of 22 different muscles four are flexors; their only function is the passive resistance of possible backward motion of the head during sideways (G_y) impact. The muscles are listed in Table 5 along with their attachment points and functions. Some muscles are represented by more than one muscle element to account for different points of attachment of the same muscle group. Attachment points for the muscles were obtained from various anatomy books, including Quiring (1949), Crouch (1973), and Warwick and Williams (1973). In the model these natural attachment sites are not always strictly adhered to. Muscles which in reality connect to thoracic vertebrae below T1 are instead connected to T1 because the present model does not include the lower thoracic vertebrae. Another approximation in the model is the absence of any connections to the ligamentum nuchae. Muscles such as the spinalis cervicis and spinalis capitis which in reality are attached to the ligamentum nuchae, a broad fan shaped ligament, are in the model attached directly to the bones. This ignores the diffusing action of the ligamentum nuchae. A further approximation in the model is the elimination of some attachment sites for muscles such as the longus colli and longissimus capitis muscles.

The muscle attachment areas on the occipital and temporal bones of the skull were obtained from drawings. The point of attachment for a muscle

TABLE 5

ATTACHMENT SITES AND PRIMARY FUNCTIONS OF MUSCLES USED IN MODEL

Muscle Group	From	To	Action
Rectus capitis posterior major	C1 spinous process	Occipital bone	Extension
Rectus capitis posterior minor	C2 spinous process	Occipital bone	Extension
Spinalis cervicis	Spinous process of T1 and C7	C2 spinous process	Extension
Spinalis capitis	Transverse processes of T1 and C7	Occipital bone	Extension
Semispinalis cervicis	Transverse processes of T1 and C7	Spinous process of C2, C3, C4 and C5	Extension
Semispinalis capitis	Transverse processes of T1 and C7	Occipital bone	Extension
Multifidus	Transverse processes of T1, C7, C6, C5, C4	Spinous process of next higher vertebra: C7, C6, C5, C4, C3	Extension Lateral flexion
Interspinales	Spinous process of T1, C7, C6, C5, C4, C3	Spinous process of C7, C6, C5, C4, C3, C2	Extension
Obliquus capitis superior	C1 transverse processes	Occipital bone	Extension
Splenius capitis	Spinous process of T1 and C7	Occipital bone and temporal bone	Extension Lateral flexion
Splenius cervicis	T1 spinous process	Transverse processes of C1, C2 C3	Extension Lateral flexion
Longissimus cervicis	T1 transverse processes	Transverse processes of C2, C3, C4, C5, C6	Extension

TABLE 5 - continued

Muscle Group	From	To	Action
Longissimus capitis	Transverse processes of T1, C6, C4	Temporal bone	Extension Lateral flexion
Trapezius	Heads of clavicles and spines of scapulae	Occipital bone	Extension Lateral flexion
Sternocleidomastoideus	Head of sternum, medial sections and heads of clavicles	Occipital bone and temporal bone	Lateral flexion Flexion
Rectus capitis lateralis	C1 transverse processes	Occipital bone	Lateral flexion
Intertransversarii	Transverse processes T1, C7, C6, C5, C4, C3, C2	Transverse processes C7, C6, C5, C4, C3, C2, C1	Lateral flexion
Levator scapulae	Medial sections of scapulae	Transverse processes of C1, C3	Extension Lateral flexion
Longus colli	Anterior side of body of C5 Anterior side of body of C6 Anterior side of body of T1	Anterior side of body of C4 Anterior side of body of C3 Anterior side of body of C4	Flexion
Longus capitis	Transverse processes of C3, C4, C5, C6	Occipital bone	Flexion
Rectus capitis anterior	C1 transverse processes	Occipital bone	Flexion
Scalenus anterior, medius and posterior	Medial clavicle	C3, C4, C5, C6, C7 transverse processes	Flexion Lateral flexion

TABLE 6

COORDINATES OF MUSCLE ATTACHMENT SITES ON OCCIPITAL BONE

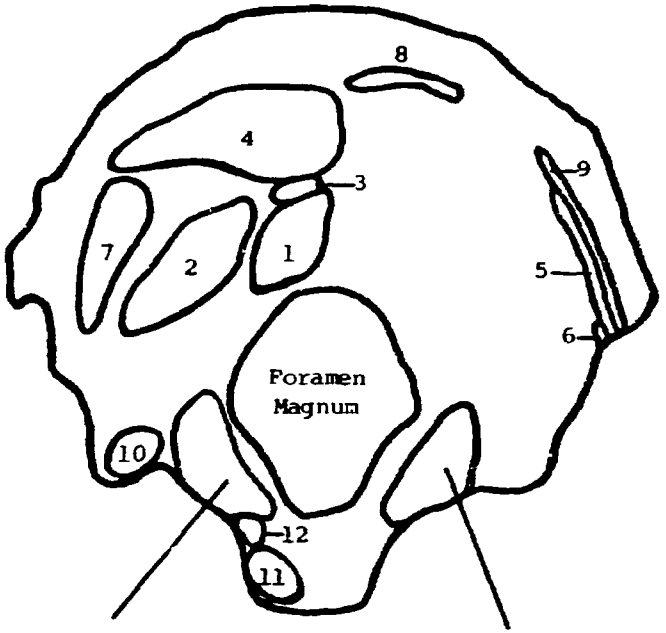

Inferior Aspect of Occipital Bone

Muscle	X (cm)	Y (cm)	Z (cm)
1 Rectus capitis posterior minor	-1.4	±0.8	14.8
2 Rectus capitis posterior major	-1.4	±2.4	15.2
3 Spinalis capitis	-2.2	±0.6	15.2
4 Semispinalis capitis	-3.6	±2.0	15.6
5 Splenius capitis	-1.0	±4.0	15.6
6 Longissimus capitis	0.2	±3.4	15.6
7 Obliquus capitis superior	-1.4	±3.5	15.6
8 Trapezius	-3.6	±1.0	15.8
9 Sternocleidomastoideus	-1.0	±4.0	15.6
10 Rectus capitis lateralis	2.2	±3.0	14.3
11 Longus capitis	3.9	±1.0	14.3
12 Rectus capitis anterior	3.2	±1.0	14.3

Notes: (1) Only the muscle attachment sites on one side of the occipital bone are drawn.
(2) Muscle attachment sites 5, 6, and 9 extend further anteriorly onto the temporal bones.
(3) The origin for the coordinate system is the center of T1.

element was taken to lie in the center of the area of bone to which the muscle is connected. Table 6 shows the coordinates for the various muscle attachment sites.

Inertial Properties of the Neck

The Liu and Wickstrom (1973) study on inertial property distribution does not include neck properties. Therefore, a simple approximate calculation had to be made to estimate the inertial properties for segments or slices of the neck. The physical dimensions of the neck used for this approximate calculation correspond with those of the average population. The shape of the neck was approximated by prismatic elliptical cylinders for the C1-C5 levels and by a flared elliptical continuation to the C7 level. The chin was not included with the neck but rather with the head. The thickness of each slice across the neck is the sum of the vertebral body height and half of each adjacent disc. Table 7 shows the dimensions used for the calculations. The formulas used to calculate the moments of inertia are:

$$I_{xx} = \frac{m}{12}\left(\frac{3}{4}a^2 + h^2\right)$$

$$I_{yy} = \frac{m}{12}\left(\frac{3}{4}b^2 + h^2\right)$$

$$I_{zz} = \frac{m}{16}\left(a^2 + b^2\right)$$

where a is the major diameter, b the minor diameter, h is the height and m is the mass of each slice with elliptical cross sections. The masses were

TABLE 7

DIMENSIONS OF ELLIPTICAL SLICES ACROSS THE NECK

Level of Slice	h, height (cm)	a, major diameter (cm)	b, minor diameter (cm)
C2	3.1	12	11
C3	1.69	12	11
C4	1.80	12	11
C5	1.49	12	11
C6	1.70	13.50	11
C7	1.93	21.66	11

estimated by consulting the results of Prasad and King (1974) who measured the combined mass of the head and neck to the C7 level for three cadavers to be 11.68 kg. A mass of 5.5 kg was taken for the head, which is the value used by McKenzie (1971), leaving about 6.2 kg for neck. By distributing the total neck mass to each slice according to the volume of the slice an approximate mass distribution was obtained: levels C1-C5 have a mass of 815 grams each, level C6 is 900 grams and level C7 is 1200 grams. Table 8 gives the overall results for the moments of inertia per segment. The head was treated as a spherical body.

TABLE 8

INERTIAL PROPERTIES FOR NECK AND HEAD

Level	Mass grams	$\bar{I}_{xx}$ gram-cm^2 x 10^4	$\bar{I}_{yy}$ gram-cm^2 x 10^4	$\bar{I}_{zz}$ gram-cm^2 x 10^4
Head	5500	17	17	17
C1	815	0.719	0.601	1.30
C2	815	0.719	0.601	1.30
C3	815	0.719	0.601	1.30
C4	815	0.719	0.601	1.30
C5	815	0.719	0.601	1.30
C6	900	1.054	0.656	1.71
C7	1200	3.518	0.775	4.39
T1*	1209	5.18	0.745	5.93

*T1 is from Liu and Wickstrom (1973) except for $\bar{I}_{zz}$ which was incorrectly listed as 17.16 x 10^4 gram-cm^2.

APPENDIX B

MATERIAL PROPERTY DATA

Most of the information available on the material properties of discs, facets, ligaments and motion segments is limited to the lumbar and thoracic region of the spine. Even in these regions the information is scarce and incomplete. Thus, before any modeling could be done, reasonable estimates of stiffnesses had to be obtained for the various components in the cervical region. Liu et al. (1981) have reported the only data available on stiffness properties of the cervical motion segments. A review of their data (Table 9) for static tests show inconsistencies between the two spines, designated EJ41 and PW35, that were tested. Figure 20 shows the terminology used in describing motion segment tests.

Spine EJ41 is stiffer in most tests, some stiffness values being more than twice the corresponding values for spine PW35. Also there is a lack of smoothness in the data which cannot be easily ascribed to natural causes. Furthermore, the atlanto-axial motion segment stiffnesses were only measured for one of the two specimens and the bending stiffnesses of the C5-C6 motion segment were also obtained for only one specimen. These problems and the fact that the motion segment studies had to skip every other motion segment in the stiffness tests indicated the need for providing a smooth transition in the stiffnesses from joint to joint until discontinuities in the motion segment properties can be verified. This smooth transition was obtained by using the geometry of the joints and estimates of the disc stiffnesses and facet stiffnesses, which were extracted from the work of Liu et al. (1981).

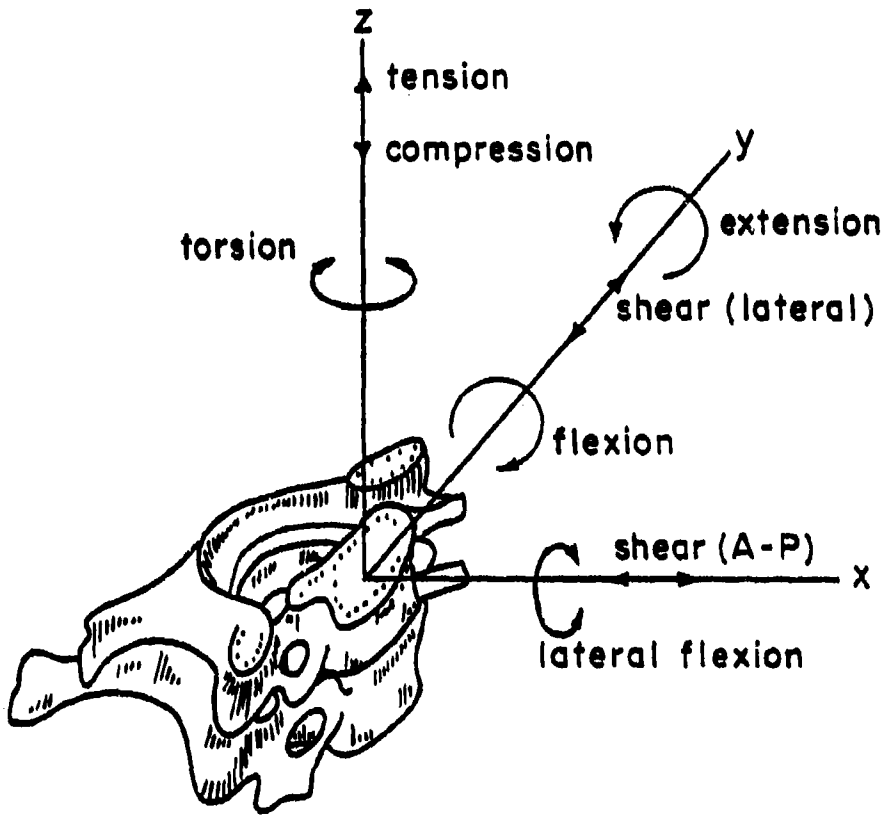

FIGURE 20. Terminology used to describe the stiffness tests of motion segments.

TABLE 9

STATIC STIFFNESSES OF CERVICAL MOTION SEGMENTS

FROM TWO SPINES (LIU ET AL., 1981)

(Stiffness units: $\times 10^8$ dynes/cm for tension, compression and shear; $\times 10^8$ dyne-cm/rad for bending and torsion)

Motion Segment	Cadaver Number		Motion Segment	Cadaver Number	
	PW35	EJ41		PW35	EJ41
	Stiffness in Tension			Stiffness in Compression	
C1C2	---	0.88	C1C2	---	21.27
C3C4	4.38	7.51	C3C4	29.88	43.78
C5C6	3.70	6.25	C5C6	14.73	46.41
C7T1	6.42	6.69	C7T1	28.46	75.30
	Stiffness in Shear (+X) (A-P shear, facets compressed)			Stiffness in Shear (-X) (A-P shear, facets pulled apart)	
C1C2	---	2.38	C1C2	---	3.19
C3C4	1.91	2.41	C3C4	1.21	1.53
C5C6	1.74	4.01	C5C6	0.74	1.12
C7T1	4.31	7.32	C7T1	1.25	2.03
	Stiffness in Shear (+Y) (lateral shear)			Stiffness in Shear (-Y) (lateral shear)	
C1C2	---	3.46	C1C2	---	2.62
C3C4	1.55	2.50	C3C4	1.65	2.10
C5C6	2.01	2.58	C5C6	1.87	2.53
C7T1	2.28	3.57	C7T1	1.99	5.18

TABLE 9 - continued

(Stiffness units: $\times 10^8$ dynes/cm for tension, compression and shear; $\times 10^8$ dyne-cm/rad for bending and torsion)

Motion Segment	Cadaver Number		Motion Segment	Cadaver Number	
	PW35	EJ41		PW35	EJ41
Stiffness in Lateral Bending ($+\theta_X$)			**Stiffness in Lateral Bending ($-\theta_X$)**		
C1C2	---	9.0	C1C2	---	17.8
C3C4	0.5	18.8	C3C4	24.3	19.4
C5C6	---	20.7	C5C6	---	27.2
C7T1	6.8	38.8	C7T1	13.9	19.4
Stiffness in Flexion ($+\theta_Y$)			**Stiffnesses in Extension ($-\theta_Y$)**		
C1C2	---	12.9	C1C2	---	3.6
C3C4	3.4	2.4	C3C4	7.1	7.1
C5C6	---	16.5	C5C6	---	18.4
C7T1	8.7	25.9	C7T1	9.4	13.0
Stiffness in Axial Torsion ($+\theta_Z$)			**Stiffness in Axial Torsion ($-\theta_Z$)**		
C1C2	---	1.9	C1C2	---	3.9
C3C4	14.9	21.0	C3C4	14.9	19.7
C5C6	11.0	27.8	C5C6	15.5	21.0
C7T1	19.1	32.4	C7T1	20.7	32.4

This appendix describes the stiffness data used in the model and the means by which the data were obtained. The complicated atlanto-axial and atlanto-occipital joints are described in detail because their unusual features required special consideration in the model. Also described are the articular facets, which are extremely important in the cervical spine and had to be modeled so as to include the compressive as well as tensile and shearing stiffness offered by these synovial joints. Finally, the muscles are described. A modified version of the mathematical model proposed by Apter and Graessley (1970) was incorporated into the neck model, allowing for a realistic muscle response. Although little is known about the material properties of the neck muscles in particular, reasonable estimates can be made on the basis of cross-sectional measurements of the muscles.

Discs and Facets

The method for estimating disc stiffness is essentially the same as that summarized by Belytschko et al. (1976). Geometric measurements of the discs were used with strength of materials formulas to predict the variation in stiffness from level to level. Using the experimentally measured stiffnesses of thoracic discs obtained by Markolf (1972) the scaling factor could be found, which was then used to estimate cervical disc stiffnesses. The details of this process are not repeated here as they can be found in Schultz et al. (1973) and Belytschko et al. (1976). Many of the same assumptions were made about the disc properties as in the previous studies. For example, the interior diameters of the annulus

fibrosis rings were assumed to be three-quarters of the outer diameters. Also, the force deflection relations were assumed to be linear for bending, torsion and shear. However, for axial loading a different assumption was made: the relation is linear for compression and linear for tension, but the stiffnesses are different. This nonlinearity in axial loading is more realistic since experimental work by Markolf (1972) on the thoracic and lumbar spine showed that compressive stiffnesses were 1.5 to 3.0 times greater than tensile stiffnesses.

The experimental study by Markolf (1972) provided important reference data. He conducted axial compression and tension tests on vertebra-disc-vertebra specimens with the posterior structures (i.e. articular facets and posterior ligaments) removed. Thus, the properties measured were essentially those of the discs themselves, if end plate deformation and cancellous bone deformation are neglected. Similarly for the anterior-to-posterior shear and medial-to-lateral shear tests, the posterior structures were removed so that the shear stiffnesses of the disc were measured. The remaining tests included the posterior structures. For thoracic vertebrae, Markolf concluded, on the basis of tests on one of the motion segments, that although removal of the posterior structures substantially decreased the stiffness in extension, it had little effect on lateral bending and on flexion. His results for flexion and lateral bending can therefore be directly applied to the discs. By assuming that the bending stiffness of a disc is the same for backward bending as it is for forward bending, all experimentally measured disc stiffnesses can then be used for scaling purposes. The relative stiffness values calculated on the basis of Schultz's formulas for the thoracic region provided the scaling factor needed to

TABLE 10

ESTIMATED DISC STIFFNESSES

Disc	Compression	Tension	Shear	Lateral Bending	Flexion and Extension	Axial Torsion
	units are: $\times 10^8$ dynes/cm			units are: $\times 10^8$ dyne-cm rad.		
C2C3	10.50	3.50	0.19	3.9	3.9	0.9
C3C4	11.40	3.80	0.20	4.3	4.3	1.2
C4C5	11.90	3.97	0.22	4.8	4.8	1.4
C5C6	14.50	4.83	0.26	5.8	5.8	1.8
C6C7	15.20	5.07	0.27	6.1	6.1	2.0
C7T1	20.00	6.67	0.36	8.4	8.4	2.9

estimate the stiffnesses of the cervical discs. Markolf's (1972) data indicates that the bending stiffnesses of the thoracic and lumbar discs are approximately equal in flexion and lateral bending. The stiffnesses in flexion and extension for the cervical discs are therefore assumed to be equal to the estimated lateral bending stiffnesses. Table 10 summarizes these results.

The next step in constructing a complete motion segment model was to estimate the contribution of the facets to the motion segment stiffnesses. This was accomplished by comparing stiffness calculations for a simple model of the motion segment to the stiffness data of Liu et al. (1981). This simple model consists of one spring for the disc with stiffness K_d and two springs representing the facets each with stiffness K_f, and arranged as shown in Figure 21. It is necessary to know the instantaneous axes of rotation for the motion segments, but these have not yet been determined for cervical spine motion. Although the instantaneous axes of rotation would depend on the type of force applied, they are here assumed to lie in the center of the disc for all types of loading. The purpose of this model is just to indicate the relative action of the facets. The moment arms, or distances of the facets from the disc center were acquired from Liu et al. (1981).

The formulas for motion segment stiffnesses are listed in Table 11 and are described in relation to the diagrams in Figure 22. The springs modeling the facets are aligned to resist the movement to which the motion segment is subjected. This alignment of the facet springs changes with each test and serves as a rough approximation of the line of resistance to the imposed forces.

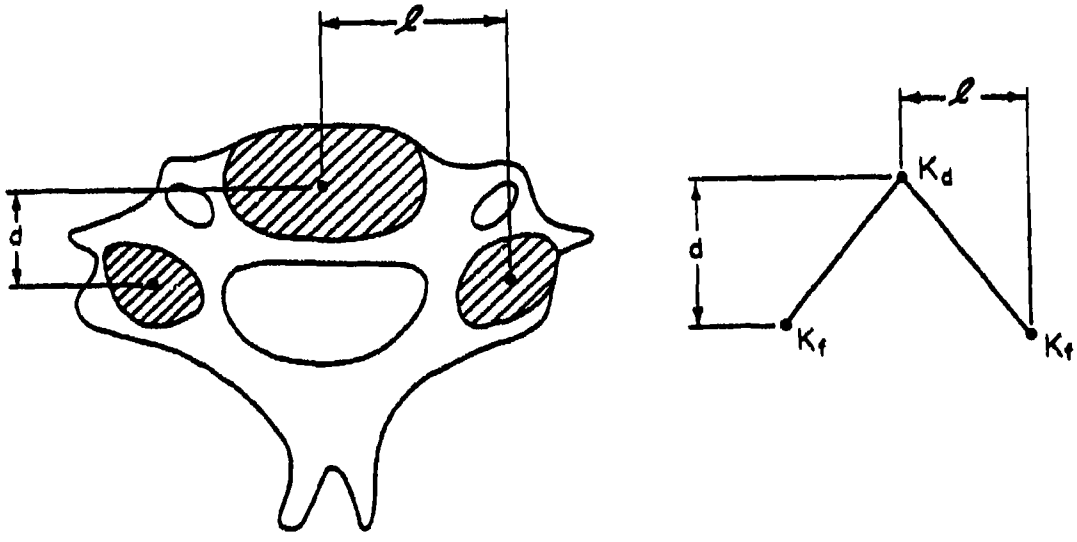

FIGURE 21. Simple three-spring motion segment model for estimating articular facet stiffness.

TABLE 11

STIFFNESS FORMULAS FOR THREE-SPRING SIMPLE MODEL OF MOTION SEGMENT

Tension	$k_d^t + (2)k_f^t$
Compression	$k_d^c + (2)k_f^c$
A-P shear (+X), facets pressed together	$k_d^s + (2)k_f^{+x}$
A-P shear (-X), facets pulled apart	$k_d^s + (2)k_f^{-x}$
Lateral shear ($\pm Y$)	$k_d^s + [k_{fl}^y + k_{fr}^y]$
Lateral bending ($\pm\theta_x$)	$k_d^b + (l^2)[k_{fl}^{l.b.} + k_{fr}^{l.b.}]$
Flexion ($+\theta_y$)	$k_d^b + (2d^2)k_f^f$
Extension ($-\theta_y$)	$k_d^b + (2d^2)k_f^e$
Axial torsion ($\pm\theta_z$)	$k_d^a + (l^2 + d^2)[k_{fl}^a + k_{fr}^a]$

Abreviations:

k_d^t = disc stiffness in tension

k_d^c = disc stiffness in compression

k_d^s = disc stiffness in shear

k_d^b = disc stiffness in bending

k_d^a = disc stiffness in axial torsion

k_{fl} = left facet stiffness

k_{fr} = right facet stiffness (see text and Figure 22)

k_f^t = facet stiffness in tension

k_f^c = facet stiffness in compression

k_f^{+x} = facet stiffness in (+X) shear

k_f^{-x} = facet stiffness in (-X) shear

k_f^y = facet stiffness in lateral shear

$k_f^{l.b.}$ = facet stiffness in lateral bending

k_f^f = facet stiffness in flexion

k_f^e = facet stiffness in extension

k_f^a = facet stiffness in axial torsion

Figure 22 shows the diagrams used to obtain the relations in Table 11. Lever arms d and l and disc stiffness, K_d, vary with the level in the spine. The values used for K_d and K_f differ for each test. For example, the tensile values differ from the compressive values. These formulas are explained below, with frequent reference to Figure 22 and Table 11. In Figure 22 diagrams are drawn to show the motion segment in front, top and side views. (All springs in the diagrams lie in the plane of the paper). The bottom vertebra of the motion segment is fixed. The top vertebra is subjected to the forces indicated by the arrows. The top and bottom vertebrae are not drawn in the diagrams but are indicated by using squares for the spring connection points on the top (movable) vertebra and circles for the connection points on the bottom (fixed) vertebra.

The compression and tension formulas are obtained from the diagram in Figure 22a. Although some sliding is expected to take place at the facets during compression, these formulas ignore the angle of inclination of the facet planes during compression.

Formulas for shear are obtained from the diagram in Figure 22b for A-P shear (forward-backward shear). When the top vertebra is moved forward with respect to the bottom vertebra (+X), the facets go into compression because of the 45° inclination of the facet planes. Actually, the facets do slide over each other to some extent. When the top vertebra is sheared backward with respect to the bottom vertebra (-X), the facet joints separate and the capsular ligaments holding the facets together are subjected to tension. We would expect the stiffness of the facet spring in compression (K_f^{+x}) to be greater than in tension (K_f^{-x}). The stiffness of the facet springs in the backward (-X) shear test should equal the stiff-

a. Front view
Tension and compression
($k_{fl} = k_{fr}$)

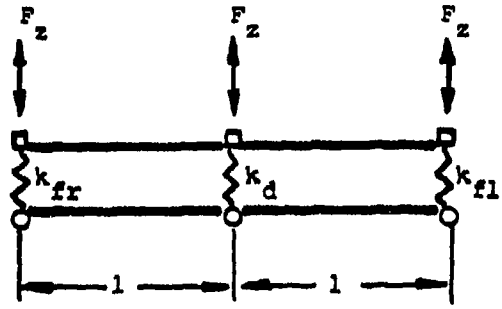

b. Top view
A-P shear
($k_{fl} = k_{fr}$)

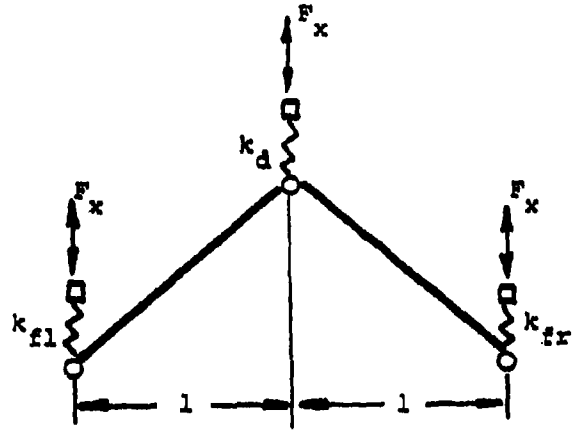

c. Top view
Lateral shear

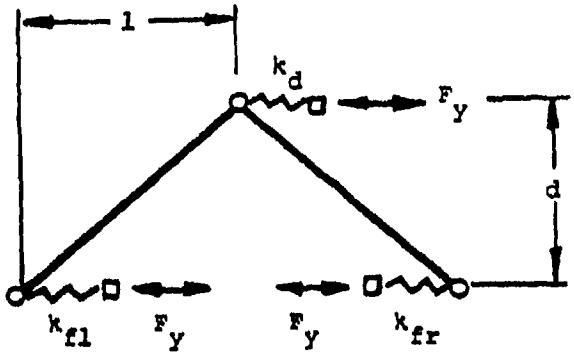

k_{fr} = right facet stiffness
k_{fl} = left facet stiffness
□ = attachment site of spring to movable vertebra
○ = attachment site of spring to fixed vertebra
~~ = axial spring

FIGURE 22. Diagrams for three-spring simple model of motion segment.

d. Front view
Lateral bending

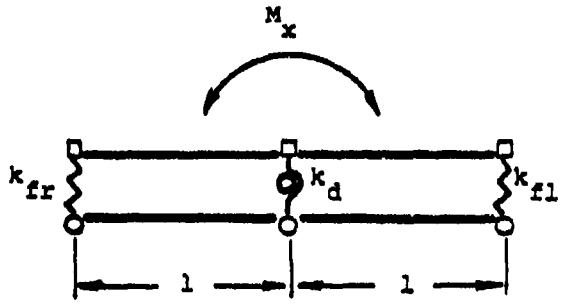

e. Side view
Flexion and extension
($k_{fl} = k_{fr}$)

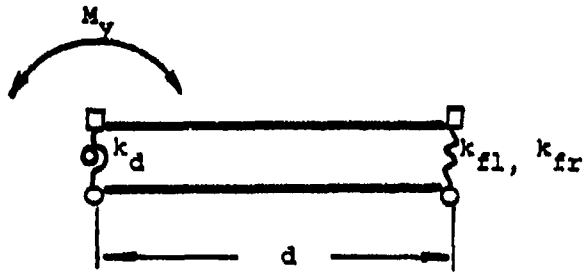

f. Top view
Torsion

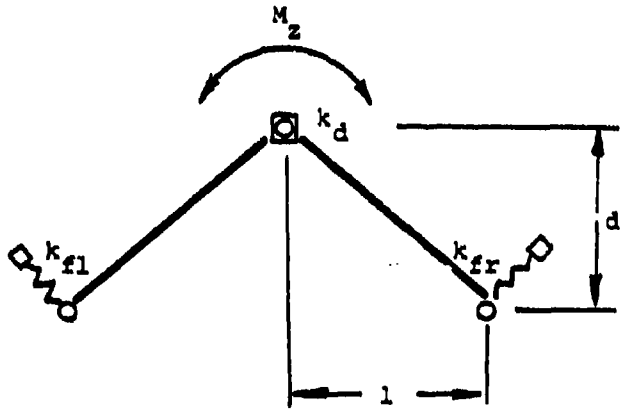

ϕ = torsional spring (also hidden from view under ⊡)

$\sim$ = axial spring

FIGURE 22 - continued

ness of the facets in the tension test. In sideways shearing the facets on one side are placed in tension and the facets on the other side in compression, because lateral shearing is accompanied by lateral bending. In the simple motion segment model in Figure 22c one facet spring is compressed while the other is placed in tension. It seems reasonable to expect that the stiffness of the compressed spring in sideways shear will equal the stiffness of the facet spring in +X forward shear; similarly, the stiffness of the facet spring that is placed in tension during sideways shear should equal the stiffness of the facet in -X backward shear. Using the formulas, this is expressed as:

$$K_d^s + [K_{f\ell}^y + K_{fr}^y] = K_d^s + [K_f^{+x} + K_f^{-x}]$$

In lateral bending the facets on one side are compressed while those on the other are placed in tension. Figure 22d shows the model in front view with moment arms ℓ from disc center to facets. The stiffness of the facet springs which are compressed in lateral bending is probably roughly equal to the stiffness of the facet springs in forward (+X) shear. The facet springs which are in tension during lateral bending are probably equal in stiffness to the facet springs in backward (-X) shear. For small angles of lateral bending (θ_x), the motion segment stiffness can be expressed as:

$$K_d^b + (\ell^2)[K_{f\ell}^{\ell\, b} + K_{fr}^{\ell b}] = K_d^b + (\ell^2)[K_f^{+x} + K_f^{-x}]$$

In flexion and extension, the moment arm from the fact spring to the disc spring is d. It is seen from Figure 22e that the facet springs are placed in tension during flexion and in compression during extension. Since both the left and the right facets are subjected to the same forces during each of these tests there is no need to distinguish the left from the right facet. It follows then that the motion segment stiffness is roughly equal to:

$$K_{MS} = K_d^b + (2d^2)K^{-x} \quad \text{for flexion}$$

$$K_{MS} = K_d^b + (2d^2)K^{+x} \quad \text{for extension.}$$

In torsion the moment arm in Figure 22f is seen to be of length $\sqrt{\ell^2 + d^2}$. Again, one facet spring is expected to be compressed while the other is put in tension. Thus from Table 11 using the same reasoning as before we can expect the motion segment stiffness to be approximately given by

$$K_{MS} = K_d^a + (\ell^2 + d^2)[K_f^{+x} + K_f^{-x}]$$

Using the formulas it is possible to estimate stiffness values for the facet springs by considering the static stiffnesses measured by Liu et al. and shown in Table 9. Static values are used because the dynamic tests show more scatter and seem less reliable. The moment arms d and ℓ used in the formulas in Table 11 were taken from data provided by Liu et al. and vary from level to level as follows:

Motion Segment	ℓ (cm)	d (cm)
C3C4	1.92	1.21
C5C6	2.08	1.23
C7T1	1.90	1.50

The only unknown left in the stiffness formulas in Table 11 is the stiffness of the facet spring. Table 12 shows motion segment stiffness that are calculated using the above described assumptions, i.e. assuming that the following relations are approximately true (see Table 11):

$$K_f^{-x} = K_f^t$$

$$(K_{f\ell}^y + K_{fr}^y) = (K_f^{-x} + K_f^{+x})$$

$$(K_{f\ell}^{\ell b} + K_{fr}^{\ell b}) = (K_f^{-x} + K_f^{+x})$$

$$K_f^f = K_f^{-x}$$

$$K_f^e = K_f^{+x}$$

$$(K_{f\ell}^a + K_{fr}^a) = (K_f^{-x} + K_f^{+x})$$

Using these assumptions there remain only three unknowns: K_f^c, K_f^{-x} and K_f^{+x}. Rather than calculating the exact facet stiffnesses for each test by equating the stiffness formulas in Table 11 to the measured stiffnesses of Liu et al., we will choose one value for each of the three unknowns that provides the best match to all of the tests of Liu et al. Good correspondence with the data is obtained by using the following stiffnesses: $K_f^c = 10.0 \times 10^8$ dynes/cm, $K_f^{-x} = 0.50 \times 10^8$ dynes/cm and $K_f^{+x} = 1.25 \times 10^8$

TABLE 12

ESTIMATED ARTICULAR FACET STIFFNESSES USING SIMPLE

THREE-SPRING MOTION SEGMENT MODEL

Motion Segment	Experimental Motion Segment Stiffnesses		Estimated Stiffness per Facet		Calculated Motion Segment Stiffnesses Using Simple Model
	PW35	EJ41	Facet on Left or Right	Facet on Right or Left	
	Stiffness in Tension				
	($\times 10^8$ dynes/cm)		($\times 10^8$ dynes/cm)		($\times 10^8$ dynes/cm)
C3C4	4.38	7.51	0.50	0.50	4.80
C5C6	3.70	6.25	0.50	0.50	5.83
C7T1	6.42	6.69	0.50	0.50	7.67
	Stiffness in Compression				
	($\times 10^8$ dynes/cm)		($\times 10^8$ dynes/cm)		($\times 10^8$ dynes/cm)
C3C4	29.88	43.78	10.00	10.00	31.40
C5C6	14.73	46.41	10.00	10.00	34.50
C7T1	28.46	75.30	10.00	10.00	40.00
	Stiffness in A-P Shear (+X), Facets Pressed Together				
	($\times 10^8$ dynes/cm)		($\times 10^8$ dynes/cm)		($\times 10^8$ dynes/cm)
C3C4	1.91	2.41	1.25	1.25	2.70
C5C6	1.74	4.01	1.25	1.25	2.76
C7T1	4.31	7.32	1.25	1.25	2.86
	Stiffness in A-P Shear (-X), Facets Pulled Apart				
	($\times 10^8$ dynes/cm)		($\times 10^8$ dynes/cm)		($\times 10^8$ dynes/cm)
C3C4	1.21	1.53	0.50	0.50	1.20
C5C6	0.74	1.12	0.50	0.50	1.26
C7T1	1.25	2.03	0.50	0.50	1.36

TABLE 12 - continued

Motion Segment	Experimental Motion Segment Stiffnesses		Estimated Stiffness per Facet		Calculated Motion Segment Stiffnesses Using Simple Model
	PW35	EJ41	Facet on Left or Right	Facet on Right or Left	
	Stiffness in Lateral Shear ($\pm Y$)				
	($\times 10^8$ dynes/cm)		($\times 10^8$ dynes/cm)		($\times 10^8$ dynes/cm)
C3C4	1.60	2.30	0.50	1.25	1.95
C5C6	1.94	2.55	0.50	1.25	2.00
C7T1	2.13	4.37	0.50	1.25	2.11
	Stiffness in Lateral Bending ($\pm\theta_x$)				
	($\times 10^8$ dyne-cm/rad)		($\times 10^8$ dynes/cm)		($\times 10^8$ dyne-cm/rad)
C3C4	12.4	19.1	0.50	1.25	10.8
C5C6	---	24.0	0.50	1.25	13.4
C7T1	10.3	29.1	0.50	1.25	14.7
	Stiffness in Flexion ($+\theta_Y$)				
	($\times 10^8$ dyne-cm/rad)		($\times 10^8$ dynes/cm)		($\times 10^8$ dyne-cm/rad)
C3C4	3.4	2.4	0.50	0.50	5.76
C5C6	---	16.5	0.50	0.50	7.31
C7T1	8.7	25.9	0.50	0.50	10.65
	Stiffness in Extension ($-\theta_Y$)				
	($\times 10^8$ dyne-cm/rad)		($\times 10^8$ dynes/cm)		($\times 10^8$ dyne-cm/rad)
C3C4	7.1	7.1	1.25	1.25	7.96
C5C6	---	18.4	1.25	1.25	9.58
C7T1	9.4	13.0	1.25	1.25	14.02
	Stiffness in Axial Torsion ($\pm\theta_Z$)				
	($\times 10^8$ dyne-cm/rad)		($\times 10^8$ dynes/cm)		($\times 10^8$ dyne-cm/rad)
C3C4	14.9	20.3	0.50	1.25	10.2
C5C6	13.2	24.4	0.50	1.25	12.0
C7T1	19.9	32.4	0.50	1.25	13.2

dynes/cm. Table 12 shows the motion segment stiffnesses that are calculated using these values and, for comparison, the experimental data is shown as well. Consider, for comparison of these values, some previous stiffnesses used in models: Schultz et al. (1973) assumed a stiffness of 0.50×10^8 dynes/cm in compression and tension for the facets and Prasad et al. (1974) used springs with compressive and shear stiffnesses of 2.1×10^8 dynes/cm each in the cervical region.

Ligaments

The ligaments of the spine have a number of different functions among which are the protection of the spinal cord from shear and impingment under static as well as dynamic loads. The ligaments must also allow for adequate movements of the head and neck with the least expenditure of muscular energy and at the same time they must guide the head and neck motion to maintain overall posture and equilibrium between the bones. The stiffness properties of the ligaments have to be estimated because of an almost total lack of direct measurements. Most ligament studies have dealt with the issue of strength rather than stiffness. It is well known though, that the load deformation curves for all ligaments are quite non-linear with the shapes of the curves probably being similar for each ligament. Another property that many spinal ligaments share in the lumbar region, at least, is pre-tension or resting tension, the tension present when the spine is in the neutral position. Pre-tension is ignored in the present model as it is not thought to contribute much to motion segment stiffness.

Tkaczuk (1968) studied the human lumbar longitudinal ligaments of about thirty-five specimens. The ultimate tensile stresses of the anterior and posterior longitudinal ligaments were almost the same, but the anterior longitudinal ligaments were stronger because their average widths and thicknesses were greater than those of the posterior longitudinal ligaments. From the data provided by Tkaczuk the average stiffness for a longitudinal ligament is estimated to be about 6.0×10^7 dynes/cm for the anterior ligament and 4.0×10^7 dynes/cm for the posterior ligament. The properties of the ligamenta flava of ten subjects were studied by Nachemson and Evans (1967). The ultimate tensile stress was about one-half and the load at failure about the same as that of the longitudinal ligaments. The strain at rupture was reported to be 70% in the young (< 20 years) with a modulus of elasticity at rupture of 10^8 dynes/cm^2. The ligamenta flava are the most purely elastic tissue in the human body, allowing large changes in length without much folding or slack. Unfortunately the dimensions of the ligaments were not provided in that study so the stiffness constant cannot be calculated. The physical properties of the other ligaments have not been reported in the literature.

The stiffness values that were assigned to ligaments in the model of Schultz et al. (1973) ranged from 5.0×10^6 to 5.0×10^7 dynes/cm. It is clear that assigning average stiffness values to linear springs will only roughly approximate ligament behavior. In addition, some ligaments like the capsular ligaments are quite lax, and allow about 2 to 3 mm of motion of the articular facets from the neutral position, according to Johnson et al. (1975). These are not only nonlinear in their material

response, but since they do not come into action until they are stretched, additional nonlinearity is introduced in the force-deflection relation.

For the neck model, linear springs are used with conservative estimates for the stiffnesses. Table 13 summarizes the stiffness data. The average stiffnesses that were used are considered to be conservative because the model is to be used for impact studies where the ligament deflections will probably be large enough for the force-deflection relation to be in the upper range of the curve, where stiffnesses could be as much as 10 times the average value seen in the curves of Tkaczuk (1968) and of Nachemson et al. (1967).

As a final note on ligaments, Allen (1948) and Portnoy et al. (1956) observed that vertebral balance in the neutral position is maintained by a delicate interplay of the muscles on the one hand and the ligaments on the other. Although the ligamentous spine without musculature was shown by Lucas and Bresler (1961) to be unable to support more than a 20 N load before buckling, this does not signify the relative unimportance of the ligaments. Interestingly, there are motions during which the muscles relax and the total load is borne by the ligaments and the muscles which are passive. For example, during flexion of the upper trunk in the standing position, progressively greater activity is registered in the erector spinae muscles and the superficial muscles of the back. However, Floyd and Silver (1951) showed that when flexion is extreme, the muscles relax and the ligaments and passive muscles support the load of the trunk. The neuromuscular control of these phenomena is beyond anything the present neck model is equipped to handle but is mentioned here to indicate the importance of including the ligaments in the model.

TABLE 13

STIFFNESSES OF LIGAMENT SPRINGS IN THE MODEL

Ligament Spring	Stiffness Value ($\times 10^8$ dynes/cm)
Anterior longitudinal ligament	0.50
Posterior longitudinal ligament	0.50
Ligamentum flavum	0.15
Interspinous ligament	0.25
Intertransverse ligament	0.05
Capsular ligament (two per facet)	0.25
Alar ligament	0.50
C1 - head nuchal ligament	0.25
Tectorial membrane	0.50
Posterior atlanto-occipital ligament	0.15
Cruciform ligament	0.50

Motion Segments in the Neck Model

An essential feature in the development of the neck model is the construction of a model of the motion segment which replicates the test results of Liu et al. (1981) under various loads. Several models were tried before the current one, but it was found to be quite difficult, if not impossible, to match the behavior of the motion segments accurately under all loads. Liu et al. used the stiffness approach in their testing program, i.e. they caused a specified motion of their motion segment and measured the forces and moments required to produce that motion. In the simulations of the motion segment, a specified force or moment was imposed on one of the vertebrae of the motion segment while the other one was fixed. Since the program is dynamic these tests were performed with a step-function load; half the value of the first peak in the displacement was used to calculate the overall motion segment stiffness. In the model, coupling of the motion is permitted, whereas it is not in the Liu et al. tests. These differences as well as others described next may account for the difficulty in matching the experimental results.

A sagittal view of the motion segment model is shown in Figure 23 with one of the facets and with the interspinous ligament in place. Two of the facet springs are arranged perpendicularly to the plane of contact of the facet joint. One of these springs (spring a) only acts when it is shortened and thus models the bony contact forces when the facets are pressed together. The other spring (spring e) acts only when lengthened and represents the capsular ligaments surrounding the facets and binding them together. While spring e helps limit motion perpendicular to the plane of

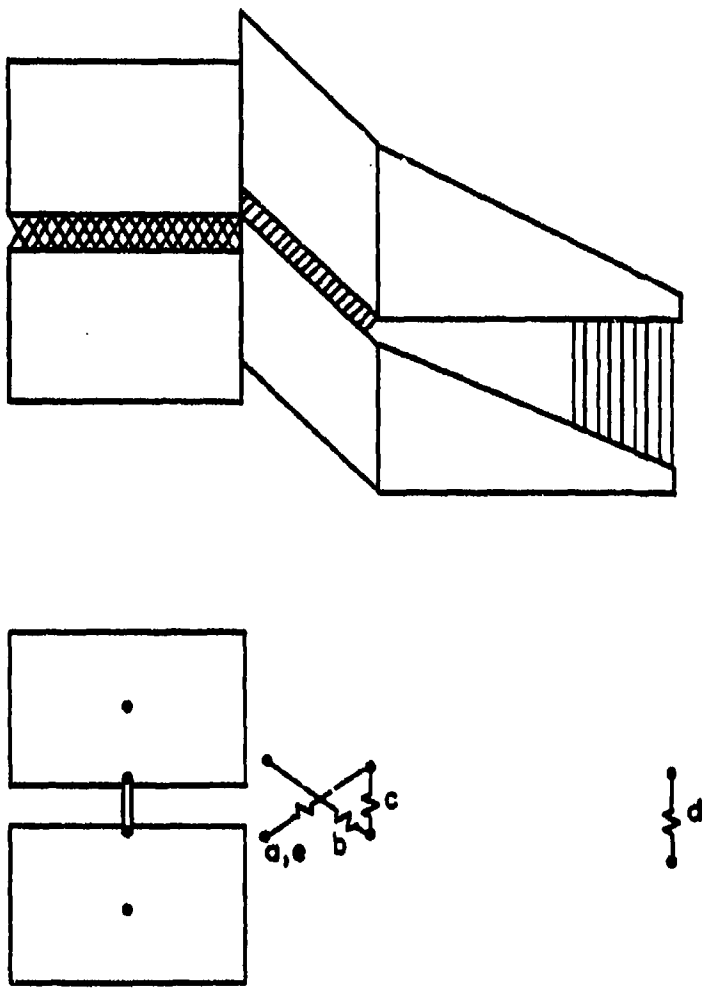

FIGURE 23. Motion segment model.

facet joint, spring b with compressive as well as tensile stiffness helps limit sliding motion of the facets. The vertical spring (spring c) was needed to model the resistance to vertical compression. These four springs all lie in a plane in joints C7-T1 up through C2-C3. In C1-C2 a different arrangement is used which is described below. The remaining spring in Figure 28 represents the posterior ligaments such as the ligamenta flava, interspinous ligament and supraspinous ligament.

With the facet stiffness estimates arrived at previously as a guide line, the following spring stiffnesses were chosen for use in the motion segment model:

spring	stiffness in motion segment model ($\times 10^8$ dynes/cm)	stiffness in neck model ($\times 10^8$ dynes/cm
a, compressive only	6.00	6.00
b, compressive and tensile	0.50	0.25
c, compressive only	6.00	6.00
d, tensile only	1.00	0.50
e, tensile only	0.50	0.25

Some of the spring stiffnesses in the neck model differ from those in the motion segment model because other springs were added to the neck model to represent the ligamenta flava, interspinous ligament and supraspinous ligament that were not included in the motion segment model. The springs representing ligaments in the motion segment model are therefore stiffer because not all ligaments are included.

The results of tests with the model are summarized in Table 14. The geometry for this motion segment was that of C3-C4; the results are therefore compared to the Liu et al. experimental data for the C3-C4 motion segment. The stiffness properties for the disc element used in this motion segment were the same as those used in the spine model for C3-C4 with two exceptions: The axial stiffness is the same in tension and compression because bilinear disc beam stiffness was not yet available when the motion segment was tested; the bending stiffness in flexion and extension was only about one-third of the value used in the spine model. This lower bending stiffness was the value used initially in the neck model, but was found to cause an instability in the solution due to excessive rotation of the beam elements during the $-G_x$ simulation. When the stiffness was increased to match the lateral bending stiffness, the instability problem disappeared. The reason for using a lower stiffness in the first place, was that the strength-of-materials formulas of Schultz et al. (1973) predicted a lower disc stiffness in flexion and extension than in lateral bending. Experimentally, however, the disc bending stiffnesses in flexion, extension and lateral bending are almost equal, so using equal bending stiffnesses in the neck model seems justifiable.

Because of the necessity of using only primary nodes as loading points in the program, simulation of vertical loading was carried out by a combination of a moment and a vertical load at the primary node. It was assumed that Liu et al. loaded their specimens along a vertical line about 2/3 of the distance from the primary node to the facets. The compressive stiffnesses obtained this way are significantly greater than those obtained by

TABLE 14

MOTION SEGMENT TEST RESULTS FOR C3-C4 MODEL

(units are x 10^8 dynes/cm or x 10^8 dyne-cm/rad)

Test	Model Stiffness	Experimental Stiffness	
		PW35	EJ41
Compression	34.40	29.88	43.78
Anterior-Posterior Shear (facets compressed)	1.20**	1.91	2.41
Anterior-Posterior Shear (facets pulled apart)	1.51	1.21	1.53
Lateral Shear	4.52	1.60	2.30
Lateral Bending	19.6 - 31.8*	12.4	19.1
Flexion	3.8 - 18.2*	3.4	2.4
Extension	15.9	7.1	7.1
Axial Torsion	6.5 - 8.0*	14.9	20.0

*Lower value is for test without interspinous ligament; higher value is for test with interspinous ligament.

**The interspinous ligament was not included in this test.

using only a vertical load. The loads for the other tests were applied without modification to the primary node of the upper rigid body while the lower was held fixed. For example, to test the motion segment in extension the appropriate moment was applied at the primary node. The rigid body was free to move in any direction, unlike the tests of Liu et al. where only extension was permitted for this test.

Table 14 shows some disconcerting discrepancies between the model stiffness and the experimental stiffness. These can be explained as resulting from differences in the methods of testing as well as to special features of the motion segment which the model does not include. Some of the differences in testing have already been mentioned. Another difference is that in the model much smaller loads and moments were used, often less than one-tenth those used by Liu et al. Since the experimental load-deflection curves obtained by Liu et al. were reasonably linear, one may assume that these differences in load magnitudes should not greatly affect the results. Probably the main cause of the discrepancies is the coupling which is allowed to take place in the model but was prevented from occurring in the Liu et al. tests. Panjabi et al. (1975) and Lysell (1969) studied the coupling effects in the lower cervical spine and found the facet orientation to be the cause of this important phenomenon. Lateral bending is coupled with axial rotation and vice versa. The coupling is such that in bending to the left the spinous process goes to the right, and in bending to the right it goes to the left. The amount of axial rotation that is coupled with lateral bending is about 2 degrees of rotation for every 3 degrees of lateral bending for the upper cervical spine according to Lysell (1969). This coupling decreases caudally until at C7 there is only 1 degree of coupled rotation per 7.5

degrees lateral bending. Another form of coupling was described by Panjabi et al. (1975) for the forward shearing (facets compressed) of a cervical motion segment which produced not only horizontal motion but also flexion.

Coupling was observed to a significant degree in the tests of the motion segment model and probably accounts directly or indirectly for the discrepancies. But, there are certain peculiarities of the joints, which have not been included in the model and may affect the mechanics of the joints. One is the locking mechanism described by Veleanu (1975), which protects the spinal canal and the cervical vascular system from damage. This locking mechanism becomes active during extension, lateral flexion and rotation. It results from the engagement of the transverse processes of the upper vertebra with the articular processes of the lower vertebrae. It is not always present at every level and its contribution to motion segment stiffness is unknown. Another characteristic anatomical feature of the cervical spine are the uncovertebral joints. These joints are formed by the upright lateral margins of the cranial end plates. They function as a guiding mechanism for flexion-extension movements and may prevent lateral sliding movement (Braakman and Penning, 1971). Their role in the stiffness properties of the motin segment has not been investigated.

Occipital - Atlanto - Axial Complex

A motion segment model was also developed for the atlanto-axial joint and was tested in the same way as the previously described model. The results were again compared with those of Liu et al. (1981) who provide the only quantitative stiffness information available for this joint. Since no

quantitative studies have been made on the atlanto-occipital joint, no simulated tests were performed on this joint and the approach used to model this region remains unverified.

The upper region of the cervical spine is extremely complex in its mechanical behavior. The range of motion has been estimated by White and Panjabi (1978) on the basis of some tests and a literature survey. The atlanto-occipital joint allows moderate flexion and extension (13°), moderate lateral bending (8°) and no axial rotation. The atlanto-axial joint permits moderate flexion and extension (10°), no lateral bending, but considerable axial rotation (47°). In fact, 50% or more of the axial rotation in the neck occurs at C1-C2. Translatory movements in any of these joints are small. According to White and Panjabi (1978) it is generally accepted that the rotation of C1 is coupled with vertical translation, in spite of some controversy in the literature. The instantaneous axes of rotation for the C1-C2 joint can be estimated from Werne's data (1957). For flexion and extension the instantaneous axis of rotation lies in the odontoid process of the axis about two-thirds from the bottom. For axial rotation, the axis lies in the center of C2.

Figure 24 shows the kind of modeling used. For the C1-C2 motion segment a disc beam is located along the position of the odontoid process. It replaces the joint between the odontoid process and the atlas, and the transverse ligament. The laterally outward orientation of the inferior articular facets of C2 is modeled by placing springs b and e along the normal to the articular surface; one of these acts only in tension, the other only in compression. The vertical facet springs a and d provide another compression-only and tension-only pair. The interspinous ligament is represented by

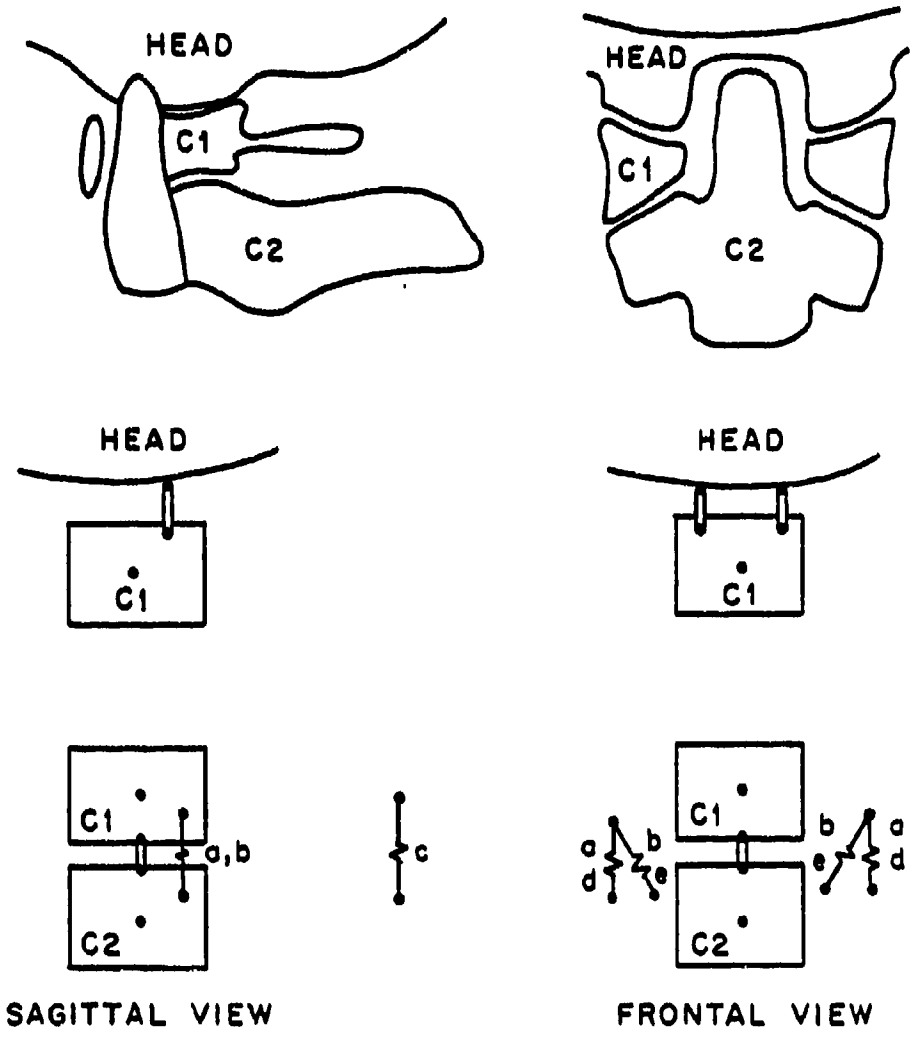

FIGURE 24. Occipital-atlanto-axial complex and models

TABLE 15

MOTION SEGMENT RESULTS FOR C1-C2 MODEL

(units are $\times 10^8$ dynes/cm or $\times 10^8$ dyne-cm/rad)

Test	Model Stiffness	Experimental Stiffness EJ41
Compression	32.42	21.27
Anterior-Posterior Shear (Atlas ring pulled anteriorly)	9.10	2.38
Anterior-Posterior Shear (Atlas ring compressed onto odontoid process)	6.30	3.19
Lateral Shear	5.40	3.04
Lateral Bending	35.1	9.0 - 17.8**
Flexion	12.3 - 39.0*	12.9
Extension	15.0	3.60
Axial Torsion	1.00	2.90

*Lower value is for test without interspinous ligament; higher value is for test with interspinous ligament.

**Left and right lateral bending stiffnesses.

spring c. The following stiffnesses were used to simulate the tests of Liu et al.

Spring	Stiffness in motion segment model ($\times 10^8$ dynes/cm)	Stiffness in Neck Model ($\times 10^8$ dynes/cm)
a, compressive only	6.00	6.00
b, compressive only	6.00	6.00
c, tensile only	1.00	0.25
d, tensile only	0.50	0.50
e, tensile only	0.50	0.50

The results of the tests are listed in Table 15. The previous comments regarding the lack of correspondence of some values with experimental data apply here as well. In the neck model, the C1-C2 disc beam element has a tensile stiffness which is 20% of the compressive stiffness, rather than 33% as in the other disc beam elements (5×10^8 dynes/cm for the compressive, and 1.0×10^8 dynes/cm for the tensile stiffness). In the motion segment model, a compressive and tensile stiffness of 10^9 dynes/cm was used. Spring c in the motion segment model represents all of the ligaments of the posterior part of the motion segment. When these ligaments are added in the neck model, the stiffness of spring c is reduced to a level that is expected for the ligament it represents in the neck model.

Finally, the C1-head joint was modeled without any consideration for the inclination of the facet planes. Because this joint permits very little rotation about the vertical axis or relative translation in the vertical

TABLE 16

STIFFNESS PROPERTIES OF DISC BEAM ELEMENTS USED IN THE MODEL

Joint Level	Axial Stiffness Dyne/cm x 10^9		Torsional Stiffness Dyne-cm/rad x 10^9	Bending Stiffness Dyne-cm/rad x 10^9		Shear Deformation Parameter, Φ	
	Compression	Tension		Sagittal Plane	Frontal Plane	Anterior-Posterior Shear	Lateral Shear
C1-head	1.00	0.10	0.05	0.40	0.40	28.5	7.0
C1-C2	0.50	0.10	0.05	0.90	0.40	17.7	13.4
C2-C3	1.05	0.35	0.09	0.08	0.39	30.5	47.6
C3-C4	1.14	0.38	0.12	0.10	0.43	32.1	52.7
C4-C5	1.19	0.40	0.14	0.12	0.48	33.0	57.8
C5-C6	1.45	0.48	0.18	0.16	0.58	34.5	63.0
C6-C7	1.52	0.51	0.20	0.22	0.61	34.3	86.6
C7-T1	2.00	0.67	0.29	0.37	0.84	40.2	107.0

Note: All disc elements are axially damped using 0.2% stiffness proportional damping.

direction, it was deemed appropriate to represent the facets - occiput joints by beam elements 0.6 cm in length oriented vertically. (The length of these beam elements was taken to equal the length used for the beam elements representing the cervical intervertebral discs.) This still permits flexion and extension. The stiffness properties of these disc beam elements and of those of the other joints are summarized in Table 16 along with the shear deformation parameters which were calculated in the same fashion as in previous work. (Belytschko et al., 1976)

Muscles

The mechanical behavior of skeletal muscle has been extensively studied in the past, and although the molecular basis for muscle contraction is not yet clearly understood, the overall physical response of muscle both active and passive is now well defined for isolated muscle. A model for muscle behavior to be used for studying the response of the head and spine to impact should include both the passive response of the muscle, a viscoelastic phenomenon, and the active response involving muscular contraction. Such a model was already available from the work of Apter and Graessley (1970) although their studies concentrated more on the mechanics of smooth muscle than on skeletal muscle. By modifying their constants to fit the model's response to experimental data in the literature, a useful muscle element was obtained which was tested under various conditions expected during impact of the head and spine.

Before describing the development of the muscle model, a short summary of some pertinent muscle mechanics is in order. There are basically two types of experiments that physiologists use to study muscle behavior. In

one, the muscle is stimulated to contract without being permitted to shorten. This is called isometric contraction. In the other type, a muscle is caused to contract and is allowed to shorten while in the contracted state. This is referred to as isotonic contraction. Intact muscle, when it is *in situ* consists of contractile muscle tissue made up of muscle fibers, and elastic tissue made up of connective tissue. Like most soft tissue in the human body, the force-displacement relation of passive muscle is quite nonlinear. This is shown by the dashed line in Figure 25a. When a muscle, isolated from the body, is stretched and released, it returns to its so-called rest length. If a muscle is held at this rest length and is stimulated to contract isometrically, the tension developed will depend on the muscle's length. If the same muscle is allowed to shorten and is again stimulated to contract at shorter fixed lengths, the tension developed at each fixed length will be different. This is shown in Figure 25a by that portion of the solid curve which is to the left of the rest length. At shorter lengths, progressively lower tensions are supported. If the same muscle is held at fixed lengths greater than the rest length and stimulated to contract isometrically, the solid curve to the right of the rest length in Figure 25a is obtained. The shape of this part of the curve varies from muscle to muscle. In this part of the curve, the total tension in the muscle arises both from the passive tension required to stretch the muscle beyond its rest length and the tension developed by the contractile process. If the passive tension is subtracted from the total tension, the dotted curve is obtained, which is the tension developed by contraction alone. The maximum contractile tension is developed at rest length, which is the length at which the muscle operates, for the most part, in the human body.

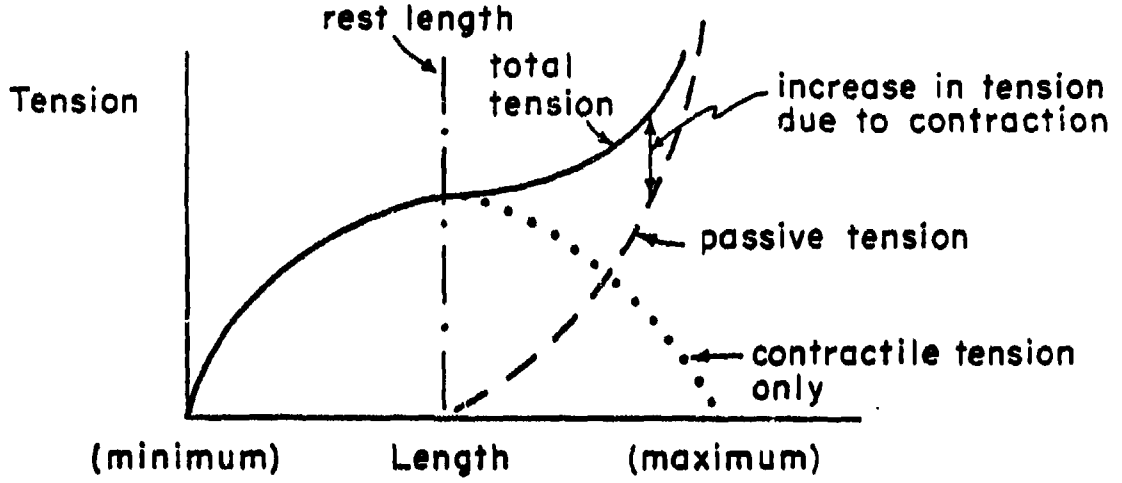

a.

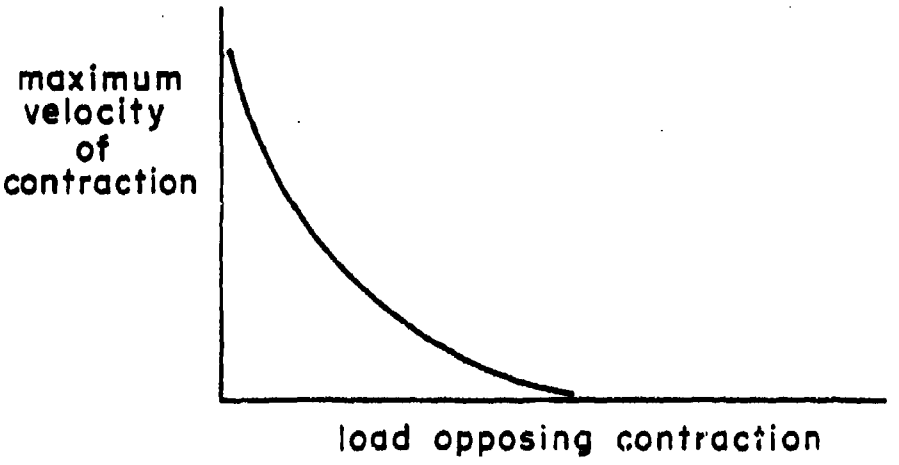

b.

FIGURE 25 a. Length tension diagram of muscle.
b. Maximum velocity of shortening versus load.

Another fundamental relationship of muscle mechanics is the force-velocity relationship. A muscle that contracts freely against no load reaches a state of full contraction in about one-twentieth of a second for the average muscle. However, as load is applied to the muscle, the velocity of contraction decreases as the load increases until the load equals the maximum force that the muscle can sustain. At that point, the velocity of contraction becomes zero and no contraction occurs. This relationship is shown in Figure 25b.

Skeletal muscles are normally activated only upon receiving impulses from the motor nerves. The events involved in activating a skeletal muscle are generally all-or-none, meaning that if an adequate impulse arrives from a motor nerve the contraction follows automatically. This event is rapid, allowing fast muscle to twitch 80 to 100 times per second in complete contraction cycles until the muscle can no longer relax before the next contraction cycle hits. The muscle then remains contracted and is said to be in a state of tetany. Once this state is reached, further increases in the rate of stimulation only increase the force of contraction by a few percent.

Each motor nerve sends signals to literally thousands of muscle fibers which all contract each time the motor nerve sends a spike. The motor nerve and its associated muscle fibers is called a motor unit. A major muscle is composed of thousands of muscle fibers which are controlled by a few hundred motor nerves. These motor neurons are associated with each other and are under control of the central nervous system. Precise control over the muscles is achieved by nervous integration and by the grading of contraction. The latter occurs in two ways: first, by selecting the number of motor units contracting simultaneously, and second by changing the frequency of contrac-

tion of the active motor units. The precise control of the muscles is a matter still under active investigation by physiologists and is certainly beyond the scope of the present study.

The muscle model used for this study appears to be the only one in the literature that matches both the velocity-time relation for contraction and the tension-time relation for a stimulated muscle quite well. It is based on the simplest description of muscle, a three parameter viscoelastic model (Apter et al., 1966), for which the mechanical response is given by

$$\sigma + \frac{\eta}{E_2}\dot{\sigma} = E_1 \varepsilon + (E_1 + E_2)\frac{\eta}{E_2}\dot{\varepsilon} \quad ,$$

in which σ is the stress and ε is the strain. The strain is defined as

$$\varepsilon = \frac{\ell - \ell_o}{\ell_o} \quad ,$$

where ℓ is the existing length and ℓ_o is the instantaneous unstretched length of the muscle which varies with the level of contraction. Inertial terms have not been included.

The elastic moduli, E_1 and E_2, the viscosity coefficient, η and the instantaneous length of muscle are assumed to depend on some molecular activity within the muscle. The state of contraction is assumed to depend on the concentration of some molecule within the cell which varies with time as

$$\dot{n} = k_2\varepsilon - k_3 n + S(t) \quad ,$$

where n is the concentration of the molecule, k_2 and k_3 are rate constants, and S(t) is the influx of the molecule due to membrane depolarization as a result of stimulation to the muscle cell. The function S(t) has the form of a pulse in Apter and Graessley's model but for our purposes it may be taken to be a step function since this was found to give good results under a variety of tests.

The variables in the equation for the muscle reponse are functions of the concentration n:

$$\ell_o = \ell_o^\infty + \frac{\ell_o^o - \ell_o^\infty}{1 + k_1 n}$$

$$E_1 = E_1^\infty - \frac{E_1^\infty - E_1^o}{1 + k_4 n}$$

$$E_2 = E_2^\infty - \frac{E_2^\infty - E_2^o}{1 + k_5 n}$$

$$\eta = \eta^\infty - \frac{\eta^\infty - \eta^o}{1 + k_6 n}$$

where superscript o and ∞ refer to completely relaxed and completely contracted states, respectively, and where k_1, k_4, k_5 and k_6 are constants determined from experimental data. The stress-strain relations were programmed by writing backward differences for the time derivatives:

$$\sigma_i = \frac{1}{E_2 \Delta t + \eta} \left[\eta\, \sigma_{i-1} + E_2 \Delta t E_1\, \varepsilon_i + (E_1 + E_2)\, \eta\, (\varepsilon_i - \varepsilon_{i-1})\right]$$

and

$$n_i = \frac{\Delta t}{1 + \Delta t k_3} \left[\frac{n_{i-1} - l}{\Delta t} + k_2 \varepsilon_i + S(t) \right]$$

The constants were chosen so the results would match experimental data on human muscle.

Figure 26 shows the results of the model using the biceps brachii muscle in comparison with the in vivo data provided by Inman and Ralston (1964) in their study on human amputees. Muscle constants used for these tests are listed in Table 17. The results show that the model accurately predicts the muscular response during stretch reflex, isometric contraction, passive stretching and various combinations of stretching and contraction. These results have been verified by consulting the work of Hill (1970) as well. The stretch reflex is modeled by letting S(t) become a nonzero constant after the reflex time has expired. For passive muscles S(t) is always zero. The stress relaxation and creep response of the model were not tested since these events have a time scale which is far greater than the duration of impact.

The maximum stress a human muscle can develop on tetanic stimulation has been estimated to lie between 4×10^6 and 10×10^6 dynes per square centimeter of muscle cross section. (Fick, 1910; Haxton, 1944; Morris, 1948). The force which a muscle can exert may be estimated by multiplying the maximum stress by the cross section of the muscle. The cross-sectional area should reflect the internal arrangement of muscle fibers. In some muscles, the fibers may be arranged diagonally to the length of the muscle, in others they may be parallel to the lengths. One way of measuring cross-

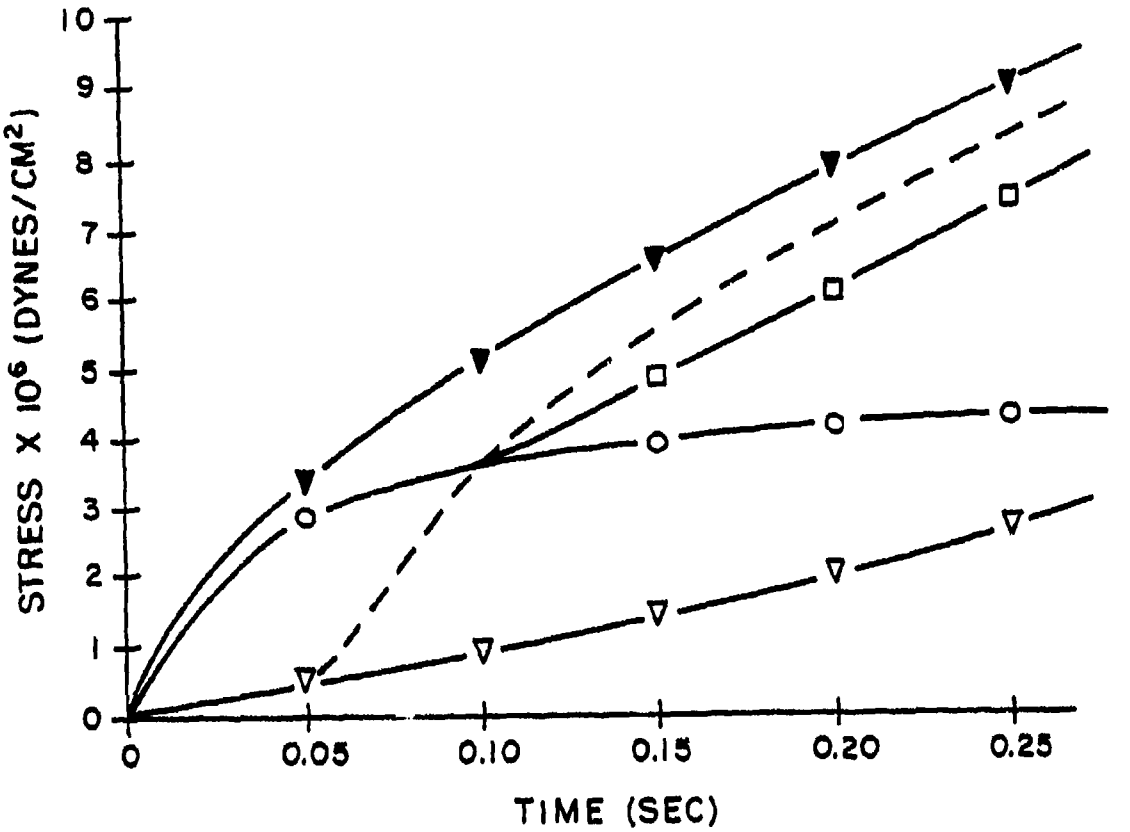

▽ Stretching of passive muscle to twice its original length

○ Isometric contraction

□ Isometric contraction until t = 0.10 sec, then muscle is stretched while contraction continues

▼ Muscle is stretched while being stimulated to contract

--- Muscle is stretched, at first passively until t = 0.05 sec, then muscle is stimulated to contract while being stretched further

FIGURE 26. Stress-time relation for various combinations of stimulation and stretching of muscle.

TABLE 17

CONSTANTS USED IN MUSCLE ELEMENT TEST

$S(t) = \begin{cases} 0 \text{ cm}^3/\text{g} & 0 < t < t_o \\ 100 \text{ cm}^3/\text{g} & t_o \leq t < \infty \end{cases}$	(t_o is the time, in seconds, at which contraction begins)
$E_1^\infty = 5 \times 10^6$ dynes/cm^2	
$E_1^0 = 1 \times 10^6$ dynes/cm^2	(for all tests except for passive stretching)
$E_1^0 = 2.5 \times 10^6$ dynes/cm^2	(for passive stretching test)
$\eta^\infty = 1.6 \times 10^5$ poise/cm^2	
$\eta^0 = 1.0 \times 10^4$ poise/cm^2	
$E_2^\infty = 7 \times 10^5$ dynes/cm^2	
$E_2^0 = 1 \times 10^5$ dynes/cm^2	
$k_1 = 0.75$ cm^3/g	
$k_2 = 1.8$ g/cm^3 sec	
$k_3 = 0.15$ sec^{-1}	
$k_4 = 1.0$ cm^3/g	
$k_5 = 1.0$ cm^3/g	
$k_6 = 1.0$ cm^3/g	
$l^0 = 12.8$ cm	

TABLE 18

MUSCLE CROSS-SECTIONAL AREAS USED IN THE MODEL

Muscle Group	Physiological Cross-Section cm^2	Anatomical Cross-Section cm^2	Cross-Sectional Area in Model cm^2	Elements per Muscle
Rectus Capitis Posterior Minor	0.385	1.00	1.00	1
Rectus Capitis Posterior Major	0.50	1.25	1.25	1
Spinalis Cervicis	---	1.25	1.25	1
Spinalis Capitis	---	0.50	0.50	2
Semispinalis Cervicis	---	2.00	2.00	4
Semispinalis Capitis	2.38	---	2.40	2
Multifidus	---	1.25	1.25	1
Interspinalis	---	---	0.50	1
Obliquus Capitis Superior	---	1.00	1.00	1
Splenius Capitis	1.22	1.70	1.70	2
Splenius Cervicis	0.70	1.00	1.00	3
Longissimus Cervicis	---	0.60	0.60	2
Longissimus Capitis	---	0.50	0.50	3
Trapezius	10.60	9.60	10.00	2
Sternocleidomastoideus	1.60	3.00	3.00	2
Rectus Capitis Lateralis	---	0.25	0.25	1
Intertransversarii	---	0.25	0.25	1
Levator Scapulae	17.75	3.50	3.50	2

TABLE 18- continued

Muscle Group	Physiological Cross-Section cm^2	Anatomical Cross-Section cm^2	Cross-Sectional Area in Model cm^2	Elements per Muscle
Longus Colli	---	0,75	0,75	3
Longus Capitis	---	0,75	0,75	4
Rectus Capitis Anterior	---	0,25	0,25	1
Scalenus Anterior, Medius and Posterior	1,65	4,00	4,00	5

Note: The physiological cross sections were obtained from Schumacher and Wolff (1966). The anatomical cross sections were measured from the drawings of Eycleshymer and Shoemaker (1911) by taking the largest cross-section for each muscle.

sectional area is to divide the volume of the muscle by its length. This figure is called the physiological cross-section. Since the internal arrangement of the fibers was not determined for the neck muscles, the cross-sectional area used in the model was obtained from the maximum cross-section, perpendicular to the muscle at the belly of the muscle. This was measured from the drawings of Eycleshymer and Shoemaker (1911). These values may therefore underestimate the total cross-sectional area of the fibers. Table 18 lists the cross-sectional areas obtained in this way, and for comparison lists the physiological cross-sections measured for some of the muscles by Schumacher and Wolff (1966).

APPENDIX C

NECK DATA

This appendix provides a listing of:

(1) Material property data cards for 37 different material types including 8 different disc beam element types, 8 different spring element types and 21 different muscle element types.

(2) Nodal data cards for primary and secondary nodes in global coordinates for 198 nodes. There is one card per node.

(3) Element data cards for 255 elements. There is one card per element.

```
C C1-HEAD DISC BEAM ELEMENTS REPRESENTING THE ATLANTO-OCCIPITAL JOINTS
    1    3
   1.00E09   5.00E07   4.00E08   4.00E08
   1.00E08             2.85E01   7.00E00   .002      .002
C C1-C2 DISC BEAM ELEMENT REPRESENTING THE ATLANTO-AXIAL JOINT WITHOUT THE FACET
    2    3
   5.00E08   5.00E07   4.00E08   9.00E08
   1.00E08             1.77E01   1.34E01   .002      .002
C C2-C3 DISC BEAM ELEMENT REPRESENTING THE C2-C3 DISC
    3    3
   1.05E09   9.00E07   3.90E08   8.00E07
   3.50E08             3.05E01   4.76E01   .002      .002
C C3-C4 DISC BEAM ELEMENT REPRESENTING THE C3-C4 DISC
    4    3
   1.14E09   1.20E08   4.30E08   1.00E08
   3.80E08             3.21E01   5.27E01   .002      .002
C C4-C5 DISC BEAM ELEMENT REPRESENTING THE C4-C5 DISC
    5    3
   1.19E09   1.40E08   4.80E08   1.20E08
   3.97E08             3.30E01   5.78E01   .002      .002
C C5-C6 DISC BEAM ELEMENT REPRESENTING THE C5-C6 DISC
    6    3
   1.45E09   1.80E08   5.80E08   1.60E08
   4.83E08             3.45E01   6.30E01   .002      .002
C C6-C7 DISC BEAM ELEMENT REPRESENTING THE C6-C7 DISC
    7    3
   1.52E09   2.00E08   6.10E08   2.20E08
   5.07E08             3.43E01   8.66E01   .002      .002
C C7-T1 DISC BEAM ELEMENT REPRESENTING THE C7-T1 DISC
    8    3
   2.00E09   2.90E08   8.40E08   3.70E08
   6.67E08             4.02E01   1.07E02   .002      .002
C COMPRESSIVE SPRING ELEMENT USED FOR FACETS
    9    1
    -1.0     6.00E08
    -1.0
C COMPRESSIVE AND TENSILE SPRING ELEMENT USED FOR FACETS
   10    1
             2.50E07
    -1.0
C TENSILE SPRING ELEMENT USED FOR LIGAMENTS
   11    1
     1.0     5.00E07
    -1.0
C TENSILE SPRING ELEMENT USED FOR LIGAMENTS
   12    1
     1.0     1.00E08
    -1.0
C ZERO STIFFNESS ELEMENT
   13    1


C TENSILE SPRING ELEMENT USED FOR LIGAMENTS
   14    1
     1.0     2.50E07
```

```
   -1.0
C TENSILE SPRING ELEMENT USED FOR LIGAMENTS
   15    1
    1.        1.5E07
   -1.
C TENSILE SPRING ELEMENT USED FOR LIGAMENTS
   16    1
    1.        5.0E06
   -1.
C RECTUS CAPITIS POSTERIOR MINOR MUSCLE ELEMENT
   17    1
                          1.
    1.
C RECTUS CAPITIS POSTERIOR MAJOR MUSCLE ELEMENT
   18    1
                          1.
    1.25
C SPINALIS CERVICIS MUSCLE ELEMENT
   19    1
                          1.
    1.25
C SPINALIS CAPITIS MUSCLE ELEMENT
   20    1
                          1.
    .25
C SEMISPINALIS CERVICIS MUSCLE ELEMENT
   21    1
                          1.
    .5
C SEMISPINALIS CAPITIS MUSCLE ELEMENT
   22    1
                          1.
    1.2
C MULTIFIDUS MUSCLE ELEMENT
   23    1
                          1.
    1.25
C INTERSPINALIS MUSCLE ELEMENT
   24    1
                          1.
    .5
C OBLIQUUS CAPITIS SUPERIOR MUSCLE ELEMENT
   25    1
                          1.
    1.
C SPLENIUS CAPITIS MUSCLE ELEMENT
   26    1
                          1.
    .85
C SPLENIUS CERVICIS MUSCLE ELEMENT
   27    1
                          1.
    .33
C LONGISSIMUS CERVICIS MUSCLE ELEMENT
   28    1
```

```
                        1.
    .3
C LONGISSIMUS CAPITIS MUSCLE ELEMENT
   29    1
                        1.
    .17
C TRAPEZIUS MUSCLE ELEMENT
   30    1
                        1.
    5.
C STERNOCLEIDOMASTOIDEUS MUSCLE ELEMENT
   31    1
                        1.
    1.0
C RECTUS CAPITIS LATERALIS MUSCLE ELEMENT
   32    1
                        1.
    .25
C INTERTRANSVERSARIUS MUSCLE ELEMENT
   33    1
                        1.
    .25
C LEVATOR SCAPULAE MUSCLE ELEMENT
   34    1
                        1.
    1.75
C LONGUS COLLI MUSCLE ELEMENT
   35    1
                        1.
    .25
C LONGUS CAPITIS MUSCLE ELEMENT
   36    1
                        1.
    .2
C RECTUS CAPITIS ANTERIOR MUSCLE ELEMENT
   37    1
                        1.
    .25
C CENTER OF LOWER END PLATE OF T1
    1       -.270E+00           -.690E+00
C PRIMARY NODE OF T1
    2    P     0                          .121E+04  .518E+05  .745E+04  .593E+05
C LOWER NODE OF T1-C7 DISC BEAM ELEMENT
    3         .270E+00           .790E+00
C UPPER NODE OF T1-C7 DISC BEAM ELEMENT
    4         .470E+00           .136E+01
C PRIMARY NODE OF C7
    5    P   .750E+00           .211E+01  .120E+04  .352E+05  .775E+04  .439E+05
C LOWER NODE OF C7-C6 DISC BEAM ELEMENT
    6           .95                2.8
C UPPER NODE OF C7-C6 DISC BEAM ELEMENT
    7           1.1                3.38
C PRIMARY NODE OF C6
    8    P   .132E+01           .405E+01  .900E+03  .105E+05  .656E+04  .171E+05
C LOWER NODE OF C6-C5 DISC BEAM ELEMENT
```

```
    9        .150E+01                .471E+01
C UPPER NODE OF C6-C5 DISC BEAM ELEMENT
   10          1.69                   5.29
C PRIMARY NODE OF C5
   11     P  .185E+01                .591E+01  .815E+03  .719E+04  .601E+04  .130E+05
C LOWER NODE OF C5-C4 DISC BEAM ELEMENT
   12        .197E+01                .657E+01
C UPPER NODE OF C5-C4 DISC BEAM ELEMENT
   13          2.07                   7.16
C PRIMARY NODE OF C4
   14     P  .217E+01                .785E+01  .815E+03  .719E+04  .601E+04  .130E+05
C LOWER NODE OF C4-C3 DISC BEAM ELEMENT
   15        .224E+01                .847E+01
C UPPER NODE OF C4-C3 DISC BEAM ELEMENT
   16        .232E+01                .908E+01
C PRIMARY NODE OF C3
   17     P  .240E+01                .967E+01  .815E+03  .719E+04  .601E+04  .130E+05
C LOWER NODE OF C3-C2 DISC BEAM ELEMENT
   18        .244E+01                .103E+02
C UPPER NODE OF C3-C2 DISC BEAM ELEMENT
   19          2.48                   10.91
C PRIMARY NODE OF C2
   20     P  .252E+01                .116E+02  .815E+03  .719E+04  .601E+04  .130E+05
C LOWER NODE OF C2-C1 DISC BEAM ELEMENT
   21        .260E+01                .123E+02
C UPPER NODE OF C2-C1 DISC BEAM ELEMENT
   22        .264E+01                .129E+02
C PRIMARY NODE OF C1
   23     P  .272E+01                .136E+02  .815E+03  .719E+04  .601E+04  .130E+05
C C1 RIGHT SUPERIOR FACET
   24          2.2        -2.         14.2
C RIGHT OCCIPITAL CONDYLE (MEDIAL ASPECT)
   25          2.2        -2.         14.8
C PRIMARY NODE OF HEAD
   26     P  .400E+01                .200E+02  .550E+04  .170E+06  .170E+06  .170E+05
C RIGHT OCCIPITAL CONDYLE (ANTERIOR ASPECT)
   27          3.         -1.5        14.8
C EXTERNAL OCCIPITAL PROTUBERANCE
   28       -.400E+01                .154E+02
C C1 SPINOUS PROCESS TIP
   29       -.140E+01                .132E+02
C C2 SPINOUS PROCESS TIP
   30       -.195E+01                .110E+02
C C3 SPINOUS PROCESS TIP
   31       -.165E+01                .890E+01
C C4 SPINOUS PROCESS TIP
   32       -.205E+01                .690E+01
C C5 SPINOUS PROCESS TIP
   33       -.240E+01                .490E+01
C C6 SPINOUS PROCESS TIP
   34          -3.4                    3.4
C C7 SPINOUS PROCESS TIP
   35       -.460E+01                .200E+01
C T1 SPINOUS PROCESS TIP
   36       -.560E+01
```

```
C T1 RIGHT SUPERIOR FACET
   37      -.114E+01 -.190E+01  .173E+01
C C7 RIGHT INFERIOR FACET
   38      -.790E+00 -.190E+01  .191E+01
C T1 RIGHT SUPERIOR FACET
   39      -.870E+00 -.190E+01  .165E+01
C C7 RIGHT INFERIOR FACET
   40      -.106E+01 -.190E+01  .201E+01
C C7 RIGHT SUPERIOR FACET
   41      -.100E+00 -.214E+01  .363E+01
C C6 RIGHT INFERIOR FACET
   42       .240E+00 -.214E+01  .389E+01
C C7 RIGHT SUPERIOR FACET
   43       .180E+00 -.214E+01  .360E+01
C C6 RIGHT INFERIOR FACET
   44      -.400E-01 -.214E+01  .392E+01
C C6 RIGHT SUPERIOR FACET
   45       .370E+00 -.207E+01  .543E+01
C C5 RIGHT INFERIOR FACET
   46       .670E+00 -.207E+01  .569E+01
C C6 RIGHT SUPERIOR FACET
   47       .670E+00 -.207E+01  .540E+01
C C5 RIGHT INFERIOR FACET
   48       .400E+00 -.207E+01  .571E+01
C C5 RIGHT SUPERIOR FACET
   49       .610E+00 -.190E+01  .718E+01
C C4 RIGHT INFERIOR FACET
   50       .910E+00 -.190E+01  .743E+01
C C5 RIGHT SUPERIOR FACET
   51       .910E+00 -.190E+01  .714E+01
C C4 RIGHT INFERIOR FACET
   52       .630E+00 -.190E+01  .745E+01
C C4 RIGHT SUPERIOR FACET
   53       .910E+00 -.190E+01  .890E+01
C C3 RIGHT INFERIOR FACET
   54       .124E+01 -.190E+01  .914E+01
C C4 RIGHT SUPERIOR FACET
   55       .118E+01 -.190E+01  .885E+01
C C3 RIGHT INFERIOR FACET
   56       .940E+00 -.190E+01  .918E+01
C C3 RIGHT SUPERIOR FACET
   57       .930E+00 -.197E+01  .104E+02
C C2 RIGHT INFERIOR FACET
   58       .116E+01 -.197E+01  .108E+02
C C3 RIGHT SUPERIOR FACET
   59       .122E+01 -.197E+01  .105E+02
C C2 RIGHT INFERIOR FACET
   60       .910E+00 -.197E+01  .108E+02
C C2 RIGHT SUPERIOR FACET
   61       .201E+01 -.180E+01  .121E+02
C C1 RIGHT INFERIOR FACET
   62       .203E+01 -.180E+01  .126E+02
C C2 RIGHT SUPERIOR FACET
   63       .201E+01 -.160E+01  .121E+02
C T1 LEFT SUPERIOR FACET
```

```
   64      -.114E+01  .190E+01  .173E+01
C C7 LEFT INFERIOR FACET
   65      -.790E+00  .190E+01  .191E+01
C T1 LEFT SUPERIOR FACET
   66      -.870E+00  .190E+01  .165E+01
C C7 LEFT INFERIOR FACET
   67      -.106E+01  .190E+01  .201E+01
C C7 LEFT SUPERIOR FACET
   68      -.100E+00  .214E+01  .363E+01
C C6 LEFT INFERIOR FACET
   69       .240E+00  .214E+01  .389E+01
C C7 LEFT SUPERIOR FACET
   70       .180E+00  .214E+01  .360E+01
C C6 LEFT INFERIOR FACET
   71      -.400E-01  .214E+01  .392E+01
C C6 LEFT SUPERIOR FACET
   72       .370E+00  .207E+01  .543E+01
C C5 LEFT INFERIOR FACET
   73       .670E+00  .207E+01  .569E+01
C C6 LEFT SUPERIOR FACET
   74       .670E+00  .207E+01  .540E+01
C C5 LEFT INFERIOR FACET
   75       .400E+00  .207E+01  .571E+01
C C5 LEFT SUPERIOR FACET
   76       .610E+00  .190E+01  .718E+01
C C4 LEFT INFERIOR FACET
   77       .910E+00  .190E+01  .743E+01
C C5 LEFT SUPERIOR FACET
   78       .910E+00  .190E+01  .714E+01
C C4 LEFT INFERIOR FACET
   79       .630E+00  .190E+01  .745E+01
C C4 LEFT SUPERIOR FACET
   80       .910E+00  .190E+01  .890E+01
C C3 LEFT INFERIOR FACET
   81       .124E+01  .190E+01  .914E+01
C C4 LEFT SUPERIOR FACET
   82       .118E+01  .190E+01  .885E+01
C C3 LEFT INFERIOR FACET
   83       .940E+00  .190E+01  .918E+01
C C3 LEFT SUPERIOR FACET
   84       .930E+00  .197E+01  .104E+02
C C2 LEFT INFERIOR FACET
   85       .116E+01  .197E+01  .108E+02
C C3 LEFT SUPERIOR FACET
   86       .122E+01  .197E+01  .105E+02
C C2 LEFT INFERIOR FACET
   87       .910E+00  .197E+01  .108E+02
C C1 LEFT INFRIOR FACET
   88       .201E+01  .180E+01  .121E+02
C C2 LEFT SUPERIOR FACET
   89       .203E+01  .180E+01  .126E+02
C C2 LEFT SUPERIOR FACET
   90       .201E+01  .160E+01  .121E+02
C NOT IN USE
   91       .930E+00 -.183E+01  .104E+02
```

```
C NOT IN USE
   92        .930E+00  .183E+01  .104E+02
C C1 LEFT SUPERIOR FACET
   93          2.2       2.        14.2
C LEFT OCCIPITAL CONDYLE (MEDIAL ASPECT)
   94          2.2       2.        14.8
C TIP OF ODONTOID PROCESS
   95        .300E+01    -0       .138E+02
C CENTER OF LOWER END PLATE OF T1
   96       -.270E+00    -0      -.690E+00
C CENTER OF UPPER END PLATE OF T1
   97        .310E+00    -0       .690E+00
C CENTER OF LOWER END PLATE OF C7
   98        .470E+00    -0       .144E+01
C CENTER OF UPPER END PLATE OF C7
   99        .104E+01    -0       .277E+01
C CENTER OF LOWER END PLATE OF C6
  100        .112E+01    -0       .340E+01
C CENTER OF UPPER END PLATE OF C6
  101        .160E+01    -0       .471E+01
C CENTER OF LOWER END PLATE OF C5
  102        .165E+01    -0       .524E+01
C CENTER OF UPPER END PLATE OF C5
  103        .207E+01    -0       .653E+01
C CENTER OF LOWER END PLATE OF C4
  104        .207E+01    -0       .712E+01
C CENTER OF UPPER END PLATE OF C4
  105        .234E+01    -0       .853E+01
C CENTER OF LOWER END PLATE OF C3
  106        .228E+01    -0       .896E+01
C CENTER OF UPPER END PLATE OF C3
  107        .252E+01    -0       .104E+02
C CENTER OF LOWER END PLATE OF C2
  108        .248E+01    -0       .108E+02
C CENTER OF UPPER SURFACE OF C2 CYLINDER
  109        .264E+01    -0       .124E+02
C CENTER OF LOWER SURFACE OF C1 CYLINDER
  110        .276E+01    -0       .129E+02
C CENTER OF UPPER SURFACE OF C1 CYLINDER
  111        .276E+01    -0       .143E+02
C T1 ATTACHMENT SITE FOR POSTERIOR LONGITUDINAL LIGAMENT
  112       -.870E+00    -0       .400E+00
C C7 ATTACHMENT SITE FOR POSTERIOR LONGITUDINAL LIGAMENT
  113       -.100E+00    -0       .243E+01
C C6 ATTACHMENT SITE FOR POSTERIOR LONGITUDINAL LIGAMENT
  114        .490E+00    -0       .435E+01
C C5 ATTACHMENT SITE FOR POSTERIOR LONGITUDINAL LIGAMENT
  115        .100E+01    -0       .618E+01
C C4 ATTACHMENT SITE FOR POSTERIOR LONGITUDINAL LIGAMENT
  116        .132E+01    -0       .804E+01
C C3 ATTACHMENT SITE FOR POSTERIOR LONGITUDINAL LIGAMENT
  117        .156E+01    -0       .980E+01
C C2 ATTACHMENT SITE FOR POSTERIOR LONGITUDINAL LIGAMENT
  118        .171E+01    -0       .116E+02
C C1 ATTACHMENT SITE FOR POSTERIOR LONGITUDINAL LIGAMENT
```

```
  119       .189E+01    -0       .136E+02
C HEAD ATTACHMENT SITE FOR TECTORIAL MEMBRANE
  120         1.9                  14.6
C T1 ATTACHMENT SITE FOR ANTERIOR LONGITUDINAL LIGAMENT
  121         .8                   -.3
C C7 ATTACHMENT SITE FOR ANTERIOR LONGITUDINAL LIGAMENT
  122         1.6                  1.8
C C6 ATTACHMENT SITE FOR ANTERIOR LONGITUDINAL LIGAMENT
  123         2.2                  3.8
C C5 ATTACHMENT SITE FOR ANTERIOR LONGITUDINAL LIGAMENT
  124         2.65                 5.65
C C4 ATTACHMENT SITE FOR ANTERIOR LONGITUDINAL LIGAMENT
  125         3.                   7.7
C C3 ATTACHMENT SITE FOR ANTERIOR LONGITUDINAL LIGAMENT
  126         3.25                 9.6
C C2 ATTACHMENT SITE FOR ANTERIOR LONGITUDINAL LIGAMENT
  127         3.4                  11.55
C C1 ATTACHMENT SITE FOR ANTERIOR LONGITUDINAL LIGAMENT
  128         3.5                  13.6
C MIDPOINT OF THE ANTERIOR MARGIN OF THE FORAMEN MAGNUM
  129         3.5                  14.6
C LEFT OCCIPITAL CONDYLE (ANTERIOR ASPECT)
  130         3.0        1.5       14.8
C T1 RIGHT LIGAMENTUM FLAVUM ATTACHMENT POINT
  131         -2.3       -.58      .9
C C7 RIGHT LIGAMENTUM FLAVUM ATTACHMENT POINT
  132         -1.45      -.64      3.
C C6 RIGHT LIGAMENTUM FLAVUM ATTACHMENT POINT
  133         -.8        -.7       4.8
C C5 RIGHT LIGAMENTUM FLAVUM ATTACHMENT POINT
  134         -.2        -.74      6.55
C C4 RIGHT LIGAMENTUM FLAVUM ATTACHMENT POINT
  135         .1         -.72      8.3
C C3 RIGHT LIGAMENTUM FLAVUM ATTACHMENT POINT
  136         .2         -.7       9.9
C C2 RIGHT LIGAMENTUM FLAVUM ATTACHMENT POINT
  137         .5         -.73      11.8
C C1 RIGHT LIGAMENTUM FLAVUM ATTACHMENT POINT
  138         .7         -.75      13.6
C HEAD ATTACHMENT SITE FOR RIGHT SIDE OF POSTERIOR ATLANTO-OCCIPITAL LIGAMENT
  139         .8         -.75      14.8
C T1 LEFT LIGAMENTUM FLAVUM ATTACHMENT POINT
  140         -2.3       .58       .9
C C7 LEFT LIGAMENTUM FLAVUM ATTACHMENT POINT
  141         -1.45      .64       3.
C C6 LEFT LIGAMENTUM FLAVUM ATTACHMENT POINT
  142         -.8        .7        4.8
C C5 LEFT LIGAMENTUM FLAVUM ATTACHMENT POINT
  143         -.2        .74       6.55
C C4 LEFT LIGAMENTUM FLAVUM ATTACHMENT POINT
  144         .1         .72       8.3
C C3 LEFT LIGAMENTUM FLAVUM ATTACHMENT POINT
  145         .2         .7        9.9
C C2 LEFT LIGAMENTUM FLAVUM ATTACHMENT POINT
  146         .5         .73       11.8
```

```
C C1 LEFT LIGAMENTUM FLAVUM ATTACHMENT POINT
  147          .7          .75         13.6
C HEAD ATTACHMENT SITE FOR LEFT SIDE OF POSTERIOR ATLANTO-OCCIPITAL LIGAMENT
  148          .8          .75         14.8
C T1 RIGHT TRANSVERSE PROCESS TIP
  149         -1.5        -4.2          .6
C C7 RIGHT TRANSVERSE PROCESS TIP
  150          .1         -3.6         2.35
C C6 RIGHT TRANSVERSE PROCESS TIP
  151          1.         -3.          4.2
C C5 RIGHT TRANSVERSE PROCESS TIP
  152          1.6        -3.1         6.
C C4 RIGHT TRANSVERSE PROCESS TIP
  153          2.         -2.8         7.9
C C3 RIGHT TRANSVERSE PROCESS TIP
  154          2.3        -2.74        9.7
C C2 RIGHT TRANSVERSE PROCESS TIP
  155          1.95       -2.9        11.6
C C1 RIGHT TRANSVERSE PROCESS TIP
  156          2.2        -3.8        13.6
C T1 LEFT TRANSVERSE PROCESS TIP
  157         -1.5         4.2          .6
C C7 LEFT TRANSVERSE PROCESS TIP
  158          .1          3.6         2.35
C C6 LEFT TRANSVERSE PROCESS TIP
  159          1.          3.          4 2
C C5 LEFT TRANSVERSE PROCESS TIP
  160          1.6         3.1         6.
C C4 LEFT TRANSVERSE PROCESS TIP
  161          2.          2.8         7.9
C C3 LEFT TRANSVERSE PROCESS TIP
  162          2.3         2.74         9.7
C C2 LEFT TRANSVERSE PROCESS TIP
  163          1.95        2.9         11.6
C C1 LEFT TRANSVERSE PROCESS TIP
  164          2.2         3.8         13.6
C RECTUS CAPITIS POSTERIOR MINOR MUSCLE ATTACHMENT POINT ON RIGHT SIDE OF SKULL
  165         -1.4         -.8         14.8
C RECTUS CAPITIS POSTERIOR MAJOR MUSCLE ATTACHMENT POINT ON RIGHT SIDE OF SKULL
  166         -1.4        -2.4         15.2
C SPINALIS CAPITIS MUSCLE ATTACHMENT POINT ON RIGHT SIDE OF SKULL
  167         -2.2         -.6         15.2
C SEMISPINALIS CAPITIS MUSCLE ATTACHMENT POINT ON RIGHT SIDE OF SKULL
  168         -3.6        -2.          15.6
C SPLENIUS CAPITIS MUSCLE ATTACHMENT POINT ON RIGHT SIDE OF SKULL
  169         -1.         -4.          15.6
C LONGISSIMUS CAPITIS MUSCLE ATTACHMENT POINT ON RIGHT SIDE OF SKULL
  170          0.2        -3.4         15.6
C RECTUS CAPITIS POSTERIOR MINOR MUSCLE ATTACHMENT POINT ON LEFT SIDE OF SKULL
  171         -1.4          .8         14.8
C RECTUS CAPITIS POSTERIOR MAJOR MUSCLE ATTACHMENT POINT ON LEFT SIDE OF SKULL
  172         -1.4         2.4         15.2
C SPINALIS CAPITIS MUSCLE ATTACHMENT POINT ON LEFT SIDE OF SKULL
  173         -2.2          .6         15.2
C SEMISPINALIS CAPITIS MUSCLE ATTACHMENT POINT ON LEFT SIDE OF SKULL
```

```
  174         -3.6        2.          15.6
C SPLENIUS CAPITIS MUSCLE ATTACHMENT POINT ON LEFT SIDE OF SKULL
  175         -1.         4.          15.6
C LONGISSIMUS CAPITIS MUSCLE ATTACHMENT POINT ON LEFT SIDE OF SKULL
  176          0.2        3.4         15.6
C OBLIQUUS CAPITIS SUPERIOR MUSCLE ATTACHMENT POINT ON RIGHT SIDE OF SKULL
  177         -1.4       -3.5         15.6
C OBLIQUUS CAPITIS SUPERIOR MUSCLE ATTACHMENT POINT ON LEFT SIDE OF SKULL
  178         -1.4        3.5         15.6
C AXIS ORIENTATION NODE FOR ELEMENTS 1 THROUGH 7
  179          1.                      1.
C AXIS ORIENTATION NODE FOR ELEMENT 8
  180          1.         -2.          1.
C AXIS ORIENTATION NODE FOR ELEMENT 78
  181          1.          2.          1.
C MEDIAL SECTION OF RIGHT CLAVICLE
  182          4.5        -7.
C MEDIAL SECTION OF LEFT CLAVICLE
  183          4.5         7.
C STERNAL HEAD
  184          6.                     -5.
C RIGHT CLAVICLE LATERAL END
  185                     -9.          4.
C LEFT CLAVICLE LATERAL END
  186                      9.          4.
C RIGHT SPINE OF SCAPULA
  187         -3.        -13.          2.
C LEFT SPINE OF SCAPULA
  188         -3.         13.          2.
C TRAPEZIUS MUSCLE ATTACHMENT POINT ON RIGHT SIDE OF SKULL
  189         -3.6        -1.         15.8
C TRAPEZIUS MUSCLE ATTACHMENT POINT ON LEFT SIDE OF SKULL
  190         -3.6         1.         15.8
C RECTUS CAPITIS LATERALIS MUSCLE ATTACHMENT POINT ON RIGHT SIDE OF SKULL
  191          2.2        -3.         14.3
C RECTUS CAPITIS LATERALIS MUSCLE ATTACHMENT POINT ON LEFT SIDE OF SKULL
  192          2.2         3.0        14.3
C LONGUS CAPITIS MUSCLE ATTACHMENT POINT ON RIGHT SIDE OF SKULL
  193          3.9        -1.         14.3
C LONGUS CAPITIS MUSCLE ATTACHMENT POINT ON LEFT SIDE OF SKULL
  194          3.9         1.         14.3
C RECTUS CAPITIS ANTERIOR MUSCLE ATTACHMENT POINT ON RIGHT SIDE OF SKULL
  195          3.2        -1.         14.3
C RECTUS CAPITIS ANTERIOR MUSCLE ATTACHMENT POINT ON LEFT SIDE OF SKULL
  196          3.2         1.         14.3
C RIGHT MEDIAL SECTION OF SCAPULA
  197         -3.         -9.          2.
C LEFT MEDIAL SECTION OF SCAPULA
  198         -3.          9.          2.
C T1-C7 DISC BEAM ELEMENT
    1    3    4    2    5                    179    8    3
C C7-C6 DISC BEAM ELEMENT
    2    6    7    5    8                    179    7    3
C C6-C5 DISC BEAM ELEMENT
    3    9   10    8   11                    179    6    3
```

```
C C5-C4 DISC BEAM ELEMENT
    4   12   13   11   14                    179    5    3
C C4-C3 DISC BEAM ELEMENT
    5   15   16   14   17                    179    4    3
C C3-C2 DISC BEAM ELEMENT
    6   18   19   17   20                    179    3    3
C C2-C1 DISC BEAM ELEMENT
    7   21   22   20   23                    179    2    3
C RIGHT C1-HEAD DISC BEAM ELEMENT REPRESENTING RIGHT ATLANTO-OCCIPITAL JOINT
    8   24   25   23   26                    180    1    3
C RIGHT LATERAL ALAR ODONTOID (CHECK) LIGAMENT
    9   95   27   20   26                     12    1
C C1-HEAD NUCHAL LIGAMENT
   10   29   28   23   26                     14    1
C C2-C1 INTERSPINOUS AND NUCHAL LIGAMENT
   11   30   29   20   23                     14    1
C C3-C2 INTERSPINOUS AND NUCHAL LIGAMENT
   12   31   30   17   20                     14    1
C C4-C3 INTERSPINOUS AND NUCHAL LIGAMENT
   13   32   31   14   17                     14    1
C C5-C4 INTERSPINOUS AND NUCHAL LIGAMENT
   14   33   32   11   14                     14    1
C C6-C5 INTERSPINOUS AND NUCHAL LIGAMENT
   15   34   33    8   11                     14    1
C C7-C6 INTERSPINOUS AND NUCHAL LIGAMENT
   16   35   34    5    8                     14    1
C T1-C7 INTERSPINOUS AND NUCHAL LIGAMENT
   17   36   35    2    5                     14    1
C RIGHT T1-C7 VERTICAL COMPRESSIVE FACET SPRING
   18   37   40    2    5                      9    1
C RIGHT T1-C7 TANGENT FACET SPRING
   19   37   38    2    5                     10    1
C RIGHT T1-C7 NORMAL COMPRESSIVE FACET SPRING
   20   39   40    2    5                      9    1
C RIGHT T1-C7 NORMAL TENSILE FACET SPRING
   21   39   40    2    5                     10    1
C RIGHT C7-C6 VERTICAL COMPRESSIVE FACET SPRING
   22   41   44    5    8                      9    1
C RIGHT C7-C6 TANGENT FACET SPRING
   23   41   42    5    8                     10    1
C RIGHT C7-C6 NORMAL COMPRESSIVE FACET SPRING
   24   43   44    5    8                      9    1
C RIGHT C7-C6 NORMAL TENSILE FACET SPRING
   25   43   44    5    8                     10    1
C RIGHT C6-C5 VERTICAL COMPRESSIVE FACET SPRING
   26   45   48    8   11                      9    1
C RIGHT C6-C5 TANGENT FACET SPRING
   27   45   46    8   11                     10    1
C RIGHT C6-C5 NORMAL COMPRESSIVE FACET SPRING
   28   47   48    8   11                      9    1
C RIGHT C6-C5 NORMAL TENSILE FACET SPRING
   29   47   48    8   11                     10    1
C RIGHT C5-C4 VERTICAL COMPRESSIVE FACET SPRING
   30   49   52   11   14                      9    1
C RIGHT C5-C4 TANGENT FACET SPRING
```

```
   31   49   50   11   14                          10    1
C RIGHT C5-C4 NORMAL COMPRESSIVE FACET SPRING
   32   51   52   11   14                           9    1
C RIGHT C5-C4 NORMAL TENSILE FACET SPRING
   33   51   52   11   14                          10    1
C RIGHT C4-C3 VERTICAL COMPRESSIVE FACET SPRING
   34   53   56   14   17                           9    1
C RIGHT C4-C3 TANGENT FACET SPRING
   35   53   54   14   17                          10    1
C RIGHT C4-C3 NORMAL COMPRESSIVE FACET SPRING
   36   55   56   14   17                           9    1
C RIGHT C4-C3 NORMAL TENSILE FACET SPRING
   37   55   56   14   17                          10    1
C RIGHT C3-C2 VERTICAL COMPRESSIVE FACET SPRING
   38   57   60   17   20                           9    1
C RIGHT C3-C2 TANGENT FACET SPRING
   39   57   58   17   20                          10    1
C RIGHT C3-C2 NORMAL COMPRESSIVE FACET SPRING
   40   59   60   17   20                           9    1
C RIGHT C3-C2 NORMAL TENSILE FACET SPRING
   41   59   60   17   20                          10    1
C NOT IN USE
   42   91   60   17   20                          13    1
C NOT IN USE
   43   91   60   17   20                          13    1
C RIGHT C2-C1 NORMAL COMPRESSIVE FACET SPRING (45 DEGREE LATERAL INCLINATION)
   44   63   62   20   23                           9    1
C RIGHT C2-C1 NORMAL TENSILE FACET SPRING (45 DEGREE LATERAL INCLINATION)
   45   63   62   20   23                          10    1
C RIGHT C2-C1 VERTICAL COMPRESSIVE FACET SPRING
   46   61   62   20   23                           9    1
C RIGHT C2-C1 VERTICAL TENSILE FACET SPRING
   47   61   62   20   23                          10    1
C LEFT T1-C7 VERTICAL COMPRESSIVE FACET SPRING
   48   64   67    2    5                           9    1
C LEFT T1-C7 TANGENT FACET SPRING
   49   64   65    2    5                          10    1
C LEFT T1-C7 NORMAL COMPRESSIVE FACET SPRING
   50   66   67    2    5                           9    1
C LEFT T1-C7 NORMAL TENSILE FACET SPRING
   51   66   67    2    5                          10    1
C LEFT C7-C6 VERTICAL COMPRESSIVE FACET SPRING
   52   68   71    5    8                           9    1
C LEFT C7-C6 TANGENT FACET SPRING
   53   68   69    5    8                          10    1
C LEFT C7-C6 NORMAL COMPRESSIVE FACET SPRING
   54   70   71    5    8                           9    1
C LEFT C7-C6 NORMAL TENSILE FACET SPRING
   55   70   71    5    8                          10    1
C LEFT C6-C5 VERTICAL COMPRESSIVE FACET SPRING
   56   72   75    8   11                           9    1
C LEFT C6-C5 TANGENT FACET SPRING
   57   72   73    8   11                          10    1
C LEFT C6-C5 NORMAL COMPRESSIVE FACET SPRING
   58   74   75    8   11                           9    1
```

```
C LEFT C6-C5 NORMAL TENSILE FACET SPRING
   59   74   75    8   11                          10    1
C LEFT C5-C4 VERTICAL COMPRESSIVE FACET SPRING
   60   76   79   11   14                           9    1
C LEFT C5-C4 TANGENT FACET SPRING
   61   76   77   11   14                          10    1
C LEFT C5-C4 NORMAL COMPRESSIVE FACET SPRING
   62   78   79   11   14                           9    1
C LEFT C5-C4 NORMAL TENSILE FACET SPRING
   63   78   79   11   14                          10    1
C LEFT C4-C3 VERTICAL COMPRESSIVE FACET SPRING
   64   80   83   14   17                           9    1
C LEFT C4-C3 TANGENT FACET SPRING
   65   80   81   14   17                          10    1
C LEFT C4-C3 NORMAL COMPRESSIVE FACET SPRING
   66   82   83   14   17                           9    1
C LEFT C4-C3 NORMAL TENSILE FACET SPRING
   67   82   83   14   17                          10    1
C LEFT C3-C2 VERTICAL COMPRESSIVE FACET SPRING
   68   84   87   17   20                           9    1
C LEFT C3-C2 TANGENT FACET SPRING
   69   84   85   17   20                          10    1
C LEFT C3-C2 NORMAL COMPRESSIVE FACET SPRING
   70   86   87   17   20                           9    1
C LEFT C3-C2 NORMAL TENSILE FACET SPRING
   71   86   87   17   20                          10    1
C NOT IN USE
   72   92   87   17   20                          13    1
C NOT IN USE
   73   92   87   17   20                          13    1
C LEFT C2-C1 NORMAL COMPRESSIVE FACET SPRING (45 DEGREE LATERAL INCLINATION)
   74   90   89   20   23                           9    1
C LEFT C2-C1 NORMAL TENSILE FACET SPRING (45 DEGREE LATERAL INCLINATION)
   75   90   89   20   23                          10    1
C LEFT C2-C1 VERTICAL COMPRESSIVE FACET SPRING
   76   88   89   20   23                           9    1
C LEFT C2-C1 VERTICAL TENSILE FACET SPRING
   77   88   89   20   23                          10    1
C LEFT C1-HEAD DISC BEAM ELEMENT REPRESENTING THE LEFT ATLANTO-OCCIPITAL JOINT
   78   93   94   23   26                     181    1    3
C NONACTIVE ELEMENT USED TO CONNECT A SECONDARY NODE TO A PRIMARY NODE
   79   96    2    2                          13    1
C NONACTIVE ELEMENT USED TO CONNECT A SECONDARY NODE TO A PRIMARY NODE
   80   97    2    2                          13    1
C NONACTIVE ELEMENT USED TO CONNECT A SECONDARY NODE TO A PRIMARY NODE
   81   98    5    5                          13    1
C NONACTIVE ELEMENT USED TO CONNECT A SECONDARY NODE TO A PRIMARY NODE
   82   99    5    5                          13    1
C NONACTIVE ELEMENT USED TO CONNECT A SECONDARY NODE TO A PRIMARY NODE
   83  100    8    8                          13    1
C NONACTIVE ELEMENT USED TO CONNECT A SECONDARY NODE TO A PRIMARY NODE
   84  101    8    8                          13    1
C NONACTIVE ELEMENT USED TO CONNECT A SECONDARY NODE TO A PRIMARY NODE
   85  102   11   11                          13    1
C NONACTIVE ELEMENT USED TO CONNECT A SECONDARY NODE TO A PRIMARY NODE
```

```
   86  103   11   11                                  13    1
C NONACTIVE ELEMENT USED TO CONNECT A SECONDARY NODE TO A PRIMARY NODE
   87  104   14   14                                  13    1
C NONACTIVE ELEMENT USED TO CONNECT A SECONDARY NODE TO A PRIMARY NODE
   88  105   14   14                                  13    1
C NONACTIVE ELEMENT USED TO CONNECT A SECONDARY NODE TO A PRIMARY NODE
   89  106   17   17                                  13    1
C NONACTIVE ELEMENT USED TO CONNECT A SECONDARY NODE TO A PRIMARY NODE
   90  107   17   17                                  13    1
C NONACTIVE ELEMENT USED TO CONNECT A SECONDARY NODE TO A PRIMARY NODE
   91  108   20   20                                  13    1
C NONACTIVE ELEMENT USED TO CONNECT A SECONDARY NODE TO A PRIMARY NODE
   92  109   20   20                                  13    1
C NONACTIVE ELEMENT USED TO CONNECT A SECONDARY NODE TO A PRIMARY NODE
   93  110   23   23                                  13    1
C NONACTIVE ELEMENT USED TO CONNECT A SECONDARY NODE TO A PRIMARY NODE
   94  111   23   23                                  13    1
C POSTERIOR LONGITUDINAL LIGAMENT BETWEEN T1 AND C7
   95  112  113    2    5                            12    1
C POSTERIOR LONGITUDINAL LIGAMENT BETWEEN C7 AND C6
   96  113  114    5    8                            12    1
C POSTERIOR LONGITUDINAL LIGAMENT BETWEEN C6 AND C5
   97  114  115    8   11                            12    1
C POSTERIOR LONGITUDINAL LIGAMENT BETWEEN C5 AND C4
   98  115  116   11   14                            12    1
C POSTERIOR LONGITUDINAL LIGAMENT BETWEEN C4 AND C3
   99  116  117   14   17                            12    1
C POSTERIOR LONGITUDINAL LIGAMENT BETWEEN C3 AND C2
  100  117  118   17   20                            12    1
C POSTERIOR LONGITUDINAL LIGAMENT BETWEEN C2 AND C1
  101  118  119   20   23                            12    1
C TECTORIAL MEMBRANE
  102  119  120   23   26                            12    1
C NOT USED
  103  119  120   23   26                            13    1
C ANTERIOR LONGITUDINAL LIGAMENT BETWEEN T1 AND C7
  104  121  122    2    5                            11    1
C ANTERIOR LONGITUDINAL LIGAMENT BETWEEN C7 AND C6
  105  122  123    5    8                            11    1
C ANTERIOR LONGITUDINAL LIGAMENT BETWEEN C6 AND C5
  106  123  124    8   11                            11    1
C ANTERIOR LONGITUDINAL LIGAMENT BETWEEN C5 AND C4
  107  124  125   11   14                            11    1
C ANTERIOR LONGITUDINAL LIGAMENT BETWEEN C4 AND C3
  108  125  126   14   17                            11    1
C ANTERIOR LONGITUDINAL LIGAMENT BETWEEN C3 AND C2
  109  126  127   17   20                            11    1
C ANTERIOR LONGITUDINAL LIGAMENT BETWEEN C2 AND C1
  110  127  128   20   23                            11    1
C ANTERIOR LONGITUDINAL LIGAMENT BETWEEN C1 AND BASE OF SKULL
  111  128  129   23   26                            11    1
C RIGHT TECTORIAL LIGAMENT (DEEP PORTION)
  112  127   27   20   26                            12    1
C LEFT TECTORIAL LIGAMENT (DEEP PORTION)
  113  127  130   20   26                            12    1
```

```
C LEFT LATERAL ALAR ODONTOID (CHECK) LIGAMENT
  114   95  130   20   26                          12    1
C VERTICAL LIMB OF CRUCIFORM LIGAMENT
  115   95  129   20   26                          12    1
C RIGHT T1-C7 LIGAMENTUM FLAVUM
  116  131  132    2    5                          15    1
C RIGHT C7-C6 LIGAMENTUM FLAVUM
  117  132  133    5    8                          15    1
C RIGHT C6-C5 LIGAMENTUM FLAVUM
  118  133  134    8   11                          15    1
C RIGHT C5-C4 LIGAMENTUM FLAVUM
  119  134  135   11   14                          15    1
C RIGHT C4-C3 LIGAMENTUM FLAVUM
  120  135  136   14   17                          15    1
C RIGHT C3-C2 LIGAMENTUM FLAVUM
  121  136  137   17   20                          15    1
C RIGHT C2-C1 LIGAMENTUM FLAVUM
  122  137  138   20   23                          15    1
C RIGHT SIDE OF POSTERIOR ATLANTO-OCCIPITAL LIGAMENT
  123  138  139   23   26                          15    1
C LEFT T1-C7 LIGAMENTUM FLAVUM
  124  140  141    2    5                          15    1
C LEFT C7-C6 LIGAMENTUM FLAVUM
  125  141  142    5    8                          15    1
C LEFT C6-C5 LIGAMENTUM FLAVUM
  126  142  143    8   11                          15    1
C LEFT C5-C4 LIGAMENTUM FLAVUM
  127  143  144   11   14                          15    1
C LEFT C4-C3 LIGAMENTUM FLAVUM
  128  144  145   14   17                          15    1
C LEFT C3-C2 LIGAMENTUM FLAVUM
  129  145  146   17   20                          15    1
C LEFT C2-C1 LIGAMENTUM FLAVUM
  130  146  147   20   23                          15    1
C LEFT SIDE OF POSTERIOR ATLANTO-OCCIPITAL LIGAMENT
  131  147  148   23   26                          15    1
C RIGHT T1-C7 INTER-TRANSVERSE LIGAMENT
  132  149  150    2    5                          16    1
C RIGHT C7-C6 INTER-TRANSVERSE LIGAMENT
  133  150  151    5    8                          16    1
C RIGHT C6-C5 INTER-TRANSVERSE LIGAMENT
  134  151  152    8   11                          16    1
C RIGHT C5-C4 INTER-TRANSVERSE LIGAMENT
  135  152  153   11   14                          16    1
C RIGHT C4-C3 INTER-TRANSVERSE LIGAMENT
  136  153  154   14   17                          16    1
C RIGHT C3-C2 INTER-TRANSVERSE LIGAMENT
  137  154  155   17   20                          16    1
C RIGHT C2-C1 INTER-TRANSVERSE LIGAMENT
  138  155  156   20   23                          16    1
C LEFT T1-C7 INTER-TRANSVERSE LIGAMENT
  139  157  158    2    5                          16    1
C LEFT C7-C6 INTER-TRANSVERSE LIGAMENT
  140  158  159    5    8                          16    1
C LEFT C6-C5 INTER-TRANSVERSE LIGAMENT
```

```
  141  159  160    8   11                          16    1
C LEFT C5-C4 INTER-TRANSVERSE LIGAMENT
  142  160  161   11   14                          16    1
C LEFT C4-C3 INTER-TRANSVERSE LIGAMENT
  143  161  162   14   17                          16    1
C LEFT C3-C2 INTER-TRANSVERSE LIGAMENT
  144  162  163   17   20                          16    1
C LEFT C2-C1 INTER-TRANSVERSE LIGAMENT
  145  163  164   20   23                          16    1
C NONACTIVE ELEMENT USED TO CONNECT A SECONDARY NODE TO A PRIMARY NODE
  146    1    2    2                              13    1
C RIGHT RECTUS CAPITIS POSTERIOR MAJOR MUSCLE
  147   30  166   20   26                          18    1
C RIGHT RECTUS CAPITIS POSTERIOR MINOR MUSCLE
  148   29  165   23   26                          17    1
C LEFT RECTUS CAPITIS POSTERIOR MAJOR MUSCLE
  149   30  172   20   26                          18    1
C LEFT RECTUS CAPITIS POSTERIOR MINOR MUSCLE
  150   29  171   23   26                          17    1
C SPINALIS CERVICIS MUSCLE BETWEEN T1 AND C2
  151   36   30    2   20                          19    1
C SPINALIS CERVICIS MUSCLE BETWEEN C7 AND C2
  152   35   30    5   20                          19    1
C RIGHT SPINALIS CAPITIS MUSCLE BETWEEN T1 AND HEAD
  153  149  167    2   26                          20    1
C RIGHT SPINALIS CAPITIS MUSCLE BETWEEN C7 AND HEAD
  154  150  167    5   26                          20    1
C LEFT SPINALIS CAPITIS MUSCLE BETWEEN T1 AND HEAD
  155  157  173    2   26                          20    1
C LEFT SPINALIS CAPITIS MUSCLE BETWEEN C7 AND HEAD
  156  158  173    5   26                          20    1
C LEFT SEMISPINALIS CERVICIS MUSCLE BETWEEN C7 AND C2
  157  158   30    5   20                          21    1
C LEFT SEMISPINALIS CERVICIS MUSCLE BETWEEN T1 AND C3
  158  157   31    2   17                          21    1
C LEFT SEMISPINALIS CERVICIS MUSCLE BETWEEN T1 AND C4
  159  157   32    2   14                          21    1
C LEFT SEMISPINALIS CERVICIS MUSCLE BETWEEN T1 AND C5
  160  157   33    2   11                          21    1
C RIGHT SEMISPINALIS CAPITIS MUSCLE BETWEEN T1 AND HEAD
  161  149  168    2   26                          22    1
C RIGHT SEMISPINALIS CAPITIS MUSCLE BETWEEN C7 AND HEAD
  162  150  168    5   26                          22    1
C LEFT SEMISPINALIS CAPITIS MUSCLE BETWEEN T1 AND HEAD
  163  157  174    2   26                          22    1
C LEFT SEMISPINALIS CAPITIS MUSCLE BETWEEN C7 AND HEAD
  164  158  174    5   26                          22    1
C LEFT MULTIFIDUS MUSCLE BETWEEN T1 AND C7
  165  157   35    2    5                          23    1
C LEFT MULTIFIDUS MUSCLE BETWEEN C7 AND C6
  166  158   34    5    8                          23    1
C LEFT MULTIFIDUS MUSCLE BETWEEN C6 AND C5
  167  159   33    8   11                          23    1
C LEFT MULTIFIDUS MUSCLE BETWEEN C5 AND C4
  168  160   32   11   14                          23    1
```

```
C LEFT MULTIFIDUS MUSCLE BETWEEN C4 AND C3
  169  161   31   14   17                          23    1
C T1-C7 INTERSPINALIS MUSCLE
  170   36   35    2    5                          24    1
C C7-C6 INTERSPINALIS MUSCLE
  171   35   34    5    8                          24    1
C C6-C5 INTERSPINALIS MUSCLE
  172   34   33    8   11                          24    1
C C5-C4 INTERSPINALIS MUSCLE.
  173   33   32   11   14                          24    1
C C4-C3 INTERSPINALIS MUSCLE
  174   32   31   14   17                          24    1
C C3-C2 INTERSPINALIS MUSCLE
  175   31   30   17   20                          24    1
C RIGHT OBLIQUUS CAPITIS SUPERIOR MUSCLE
  176   29  177   23   26                          25    1
C LEFT OBLIQUUS CAPITIS SUPERIOR MUSCLE
  177   29  178   23   26                          25    1
C RIGHT SPLENIUS CAPITIS MUSCLE BETWEEN C7 AND HEAD
  178   35  169    5   26                          26    1
C RIGHT SPLENIUS CAPITIS MUSCLE BETWEEN T1 AND HEAD
  179   36  169    2   26                          26    1
C LEFT SPLENIUS CAPITIS MUSCLE BETWEEN C7 AND HEAD
  180   35  175    5   26                          26    1
C LEFT SPLENIUS CAPITIS MUSCLE BETWEEN T1 AND HEAD
  181   36  175    2   26                          26    1
C RIGHT SPLENIUS CERVICIS MUSCLE BETWEEN T1 AND C1
  182   36  156    2   23                          27    1
C RIGHT SPLENIUS CERVICIS MUSCLE BETWEEN T1 AND C2
  183   36  155    2   20                          27    1
C RIGHT SPLENIUS CERVICIS MUSCLE BETWEEN T1 AND C3
  184   36  154    2   17                          27    1
C LEFT LONGISSIMUS CERVICIS MUSCLE BETWEEN T1 AND C2
  185  157  163    2   20                          28    1
C LEFT LONGISSIMUS CERVICIS MUSCLE BETWEEN T1 AND C3
  186  157  162    2   17                          28    1
C LEFT LONGISSIMUS CERVICIS MUSCLE BETWEEN T1 AND C4
  187  157  161    2   14                          28    1
C LEFT LONGISSIMUS CERVICIS MUSCLE BETWEEN T1 AND C5
  188  157  160    2   11                          28    1
C LEFT LONGISSIMUS CERVICIS MUSCLE BETWEEN T1 AND C6
  189  157  159    2    8                          28    1
C RIGHT LONGISSIMUS CAPITIS MUSCLE BETWEEN C4 AND HEAD
  190  153  170   14   26                          29    1
C RIGHT LONGISSIMUS CAPITIS MUSCLE BETWEEN C6 AND HEAD
  191  151  170    8   26                          29    1
C RIGHT LONGISSIMUS CAPITIS MUSCLE BETWEEN T1 AND HEAD
  192  149  170    2   26                          29    1
C LEFT LONGISSIMUS CAPITIS MUSCLE BETWEEN C4 AND HEAD
  193  161  176   14   26                          29    1
C LEFT LONGISSIMUS CAPITIS MUSCLE BETWEEN C6 AND HEAD
  194  159  176    8   26                          29    1
C LEFT LONGISSIMUS CAPITIS MUSCLE BETWEEN T1 AND HEAD
  195  157  176    2   26                          29    1
C RIGHT SEMISPINALIS CERVICIS MUSCLE BETWEEN C7 AND C2
```

```
  196  150   30    5   20                          21    1
C RIGHT SEMISPINALIS CERVICIS MUSCLE BETWEEN T1 AND C3
  197  149   31    2   17                          21    1
C RIGHT SEMISPINALIS CERVICIS MUSCLE BETWEEN T1 AND C4
  198  149   32    2   14                          21    1
C RIGHT SEMISPINALIS CERVICIS MUSCLE BETWEEN T1 AND C5
  199  149   33    2   11                          21    1
C RIGHT MULTIFIDUS MUSCLE BETWEEN T1 AND C7
  200  149   35    2    5                          23    1
C RIGHT MULTIFIDUS MUSCLE BETWEEN C7 AND C6
  201  150   34    5    8                          23    1
C RIGHT MULTIFIDUS MUSCLE BETWEEN C6 AND C5
  202  151   33    8   11                          23    1
C RIGHT MULTIFIDUS MUSCLE BETWEEN C5 AND C4
  203  152   32   11   14                          23    1
C RIGHT MULTIFIDUS MUSCLE BETWEEN C4 AND C3
  204  153   31   14   17                          23    1
C LEFT SPLENIUS CERVICIS MUSCLE BETWEEN T1 AND C1
  205   36  164    2   23                          27    1
C LEFT SPLENIUS CERVICIS MUSCLE BETWEEN T1 AND C2
  206   36  163    2   20                          27    1
C LEFT SPLENIUS CERVICIS MUSCLE BETWEEN T1 AND C3
  207   36  162    2   17                          27    1
C RIGHT LONGISSIMUS CERVICIS MUSCLE BETWEEN T1 AND C2
  208  149  155    2   20                          28    1
C RIGHT LONGISSIMUS CERVICIS MUSCLE BETWEEN T1 AND C3
  209  149  154    2   17                          28    1
C RIGHT LONGISSIMUS CERVICIS MUSCLE BETWEEN T1 AND C4
  210  149  153    2   14                          28    1
C RIGHT LONGISSIMUS CERVICIS MUSCLE BETWEEN T1 AND C5
  211  149  152    2   11                          28    1
C RIGHT LONGISSIMUS CERVICIS MUSCLE BETWEEN T1 AND C6
  212  149  151    2    8                          28    1
C RIGHT TRAPEZIUS MUSCLE BETWEEN RIGHT CLAVICLE AND HEAD
  213  185  189    2   26                          30    1
C LEFT TRAPEZIUS MUSCLE BETWEEN LEFT CLAVICLE AND HEAD
  214  186  190    2   26                          30    1
C RIGHT TRAPEZIUS MUSCLE BETWEEN RIGHT SCAPULA AND HEAD
  215  187  189    2   26                          30    1
C LEFT TRAPEZIUS MUSCLE BETWEEN LEFT SCAPULA AND HEAD
  216  188  190    2   26                          30    1
C RIGHT STERNOCLEIDOMASTOIDEUS MUSCLE BETWEEN STERNUM AND HEAD
  217  184  169    2   26                          31    1
C RIGHT STERNOCLEIDOMASTOIDEUS MUSCLE BETWEEN MEDIAL SECTION OF RIGHT CLAVICLE
C   AND HEAD
  218  182  169    2   26                          31    1
C LEFT STERNOCLEIDOMASTOIDEUS MUSCLE BETWEEN MEDIAL SECTION OF LEFT CLAVICLE
C   AND HEAD
  219  183  175    2   26                          31    1
C RIGHT STERNOCLEIDOMASTOIDEUS MUSCLE BETWEEN LATERAL SECTION OF RIGHT CLAVICLE
C   AND HEAD
  220  182  169    2   26                          31    1
C LEFT STERNOCLEIDOMASTOIDEUS MUSCLE BETWEEN LATERAL SECTION OF LEFT CLAVICLE
C   AND HEAD
  221  183  175    2   26                          31    1
```

```
C RIGHT RECTUS CAPITIS LATERALIS MUSCLE
  222  156  191   23   26                          32    1
C LEFT RECTUS CAPITIS LATERALIS MUSCLE
  223  164  192   23   26                          32    1
C LEFT T1-C7 INTERTRANSVERSARIUS MUSCLE
  224  149  150    2    5                          33    1
C LEFT C7-C6 INTERTRANSVERSARIUS MUSCLE
  225  150  151    5    8                          33    1
C LEFT C6-C5 INTERTRANSVERSARIUS MUSCLE
  226  151  152    8   11                          33    1
C LEFT C5-C4 INTERTRANSVERSARIUS MUSCLE
  227  152  153   11   14                          33    1
C LEFT C4-C3 INTERTRANSVERSARIUS MUSCLE
  228  153  154   14   17                          33    1
C LEFT C3-C2 INTERTRANSVERSARIUS MUSCLE
  229  154  155   17   20                          33    1
C LEFT C2-C1 INTERTRANSVERSARIUS MUSCLE
  230  155  156   20   23                          33    1
C RIGHT T1-C7 INTERTRANSVERSARIUS MUSCLE
  231  157  158    2    5                          33    1
C RIGHT C7-C6 INTERTRANSVERSARIUS MUSCLE
  232  158  159    5    8                          33    1
C RIGHT C6-C5 INTERTRANSVERSARIUS MUSCLE
  233  159  160    8   11                          33    1
C RIGHT C5-C4 INTERTRANSVERSARIUS MUSCLE
  234  160  161   11   14                          33    1
C RIGHT C4-C3 INTERTRANSVERSARIUS MUSCLE
  235  161  162   14   17                          33    1
C RIGHT C3-C2 INTERTRANSVERSARIUS MUSCLE
  236  162  163   17   20                          33    1
C RIGHT C2-C1 INTERTRANSVERSARIUS MUSCLE
  237  163  164   20   23                          33    1
C RIGHT LEVATOR SCAPULAE MUSCLE BETWEEN RIGHT SCAPULA AND C1
  238  197  156    2   23                          34    1
C RIGHT LEVATOR SCAPULAE MUSCLE BETWEEN RIGHT SCAPULA AND C3
  239  197  154    2   17                          34    1
C LEFT LEVATOR SCAPULAE MUSCLE BETWEEN LEFT SCAPULA AND C1
  240  198  164    2   23                          34    1
C LEFT LEVATOR SCAPULAE MUSCLE BETWEEN LEFT SCAPULA AND C3
  241  198  162    2   17                          34    1
C LONGUS COLLI MUSCLE BETWEEN C5 AND C4
  242  124  125   11   14                          35    1
C LONGUS COLLI MUSCLE BETWEEN C6 AND C3
  243  123  126    8   17                          35    1
C LONGUS COLLI MUSCLE BETWEEN T1 AND C4
  244  121  125    2   14                          35    1
C RIGHT LONGUS CAPITIS MUSCLE BETWEEN C6 AND HEAD
  245  151  193    8   26                          36    1
C RIGHT LONGUS CAPITIS MUSCLE BETWEEN C5 AND HEAD
  246  152  193   11   26                          36    1
C RIGHT LONGUS CAPITIS MUSCLE BETWEEN C4 AND HEAD
  247  153  193   14   26                          36    1
C RIGHT LONGUS CAPITIS MUSCLE BETWEEN C3 AND HEAD
  248  154  193   17   26                          36    1
C LEFT LONGUS CAPITIS MUSCLE BETWEEN C6 AND HEAD
```

```
  249  159  194    8   26
C LEFT LONGUS CAPITIS MUSCLE BETWEEN C5 AND HEAD                36    1
  250  160  194   11   26
C LEFT LONGUS CAPITIS MUSCLE BETWEEN C4 AND HEAD                36    1
  251  161  194   14   26
C LEFT LONGUS CAPITIS MUSCLE BETWEEN C3 AND HEAD                36    1
  252  162  194   17   26
C RIGHT RECTUS CAPITIS MUSCLE BETWEEN C1 AND HEAD               36    1
  253  156  195   23   26
C LEFT RECTUS CAPITIS MUSCLE BETWEEN C1 AND HEAD                37    1
  254  164  196   23   26
C LEFT STERNOCLEIDOMASTOIDEUS MUSCLE BETWEEN STERNUM AND HEAD
  255  184  175    2   26                                       31    1
```

References

Allen, C.E.L., "Muscle Action Potentials Used in the Study of Dynamic Anatomy," Brit. J. Phys. Med. 11: 66-73, (1948).

Apter, J.T. and Graessley, W.W., "A Physical Model for Muscular Behavior," Biophys. J. 10: 539-55, (1970).

Apter, J.T., Robinowitz, M., Cummings, D.H., Circ. Res., 19: 104, (1966).

Becker, E.B., "Preliminary Discussion of an Approach to Modeling Living Human Head and Neck to $-G_x$ Impact Acceleration," Human Impact Response, W.F. King and H.J. Mertz (Eds.) New York: 321-329, (1972).

Belytschko, T., Schwer, L., and Schultz, A., A Model for Analytic Investigation of Three-Dimensional Head-Spine Dynamics AMRL-TR-76-10 (ADA025911) Aerospace Medical Research Laboratory, Wright-Patterson AFB, Ohio (1976).

Belytschko, T., Schwer, L., Klein, M.J., "Large Displacement, Transient Analysis of Space Frames," International Journal for Numerical Methods in Engineering, 11: 65-84, (1977).

Belytschko, T., Schwer, L., and Privitzer, E., "Theory and Application of a Three-Dimensional Model of the Human Spine," Aviat. Space Environ. Med. 49: 158-165, (1978).

Belytschko, T. and Privitzer, E., Refinement and Validation of a Three-Dimensional Head-Spine Model, AMRL-TR-78-7 (ADA062592) Aerospace Medical Research Laboratory Wright-Patterson AFB, Ohio (1978).

Bowman, B.M., et al., MVMA Two-Dimensional Crash Victim Simulation Version 3, (NTIS Nos. PB 235 753, PB 236 908) UM-HSRI-BI-74-1, Highway Safety Research Institute, University of Michigan, Ann Arbor, (1974).

Bowman, B.M., Schneider, L.W. and Foust, D.R., "Simulated Occupant Response to Side Impact Collisions," Proceedings of the 19th Stapp Car Crash Conference, pp 429-454, (1975).

Braakman, R. and Penning, L., Injuries of the Cervical Spine, Amsterdam, Excerpta Medica, 53-62, (1971).

Crouch, J.E., Functional Human Anatomy, Second Edition, Lea & Febiger, Philadelphia, (1973).

Culver, C.C., Neathery, R.F., Mertz, H.J., "Mechanical Necks with Humanlike Responses," 16th Stapp Car Crash and Field Demonstration Conference Proceedings, SAE Paper No. 720959, (1972).

Ewing, C.L. and Thomas, D.J., Human Head and Neck Response to Impact Acceleration, NAMRL Monograph 21, August 1972.

Ewing, C.L. and Thomas, D.J., "Torque versus Angular Displacement Response of Human Head to $-G_x$ Impact Acceleration," Proceedings 17th Stapp Car Crash Conference, Paper #730976, 309-343, (1973).

Ewing, C.L., Thomas, D.J., Lustik, L., Muzzy III, W.H., Willems, G.C. and Majewski, P., "Dynamic Response of the Human Head and Neck to G_y Impact Acceleration," Proceedings 21st Stapp Car Crash Conference, Paper # 770928, 549-586, (1977).

Ewing, C.L., Thomas, D.J., Lustik, L., Willems, G.C., Muzzy III, W.H., Becker, E.B., and Jessop, M.E., "Dynamic Response of Human and Primate Head and Neck to G_y Impact Acceleration," Final Report, Naval Aerospace Medical Research Laboratory Detachment DOT HS-803-058, January, 1978.

Eycleshymer, A.C. and Shoemaker, D.M., A Cross-Section Anatomy, D. Appleton C., New York, (1911).

Feuer, H., "Management of Acute Spine and Spinal Cord Injuries, Old and New Concepts," Arch. Surg. III: 638-645. (1976).

Fick, R., Handbuck der Anatomie und Mechanik der Gelenke, Jena, G. Fischer, Chapter 17, (1910).

Floyd, W.F., and Silver, P.H.S., "Function of Erector Spinae in Flexion of of the Trunk," Lancet, 133-8, January 20, 1951.

Foust, D.R., Chaffin, D.B., Snyder, R.G. and Baum, J.K., "Cervical Range of Motion and Dynamic Response and Strength of Cervical Muscles," Proceedings of 17th Stapp Car Conference, Paper #730975, 285-309, (1973).

Francis, C.C., "Dimensions of the Cervical Vertebrae," Anat. Record 122: 603-609, (1955).

Frisch, C.D., D'Aulerio, L., O'Rourke, J., "Mechanism of Head and Neck Response to $-G_x$ Impact Acceleration: A Math Modeling Approach," Aviation Space and Environmental Medicine, 223-230, March 1977.

Haxton, H.A., "Absolute Muscle Force in Ankle Flexors of Man," J. Physiol. 103: 267, (1944).

Hill, A.V., First and Last Experiments in Muscle Mechanics, Cambridge University Press, (1970).

Huston, R.L., Huston, J.C., Harlow, M.W., "Comprehensive, Three-Dimensional Head-Neck Model for Impact and High-Acceleration Studies," Aviat. Space Environ. Med. 49(1): 205-10, (1978).

Inman, V.T. and Ralston, H.T., Human Limbs and Their Substitutes, Ed. by P.E. Klopsteg and P.D. Wilson, p. 296, McGraw-Hill, N.Y., (1964).

Jirout, J., "Patterns of Changes in the Cervical Spine on Lateroflexion," Neuroradiology: 2, 164-166, (1971).

Jirout, J., "Changes in the Atlas-Axis Relations on Lateral Flexion of the Head and Neck," Neuroradiology: 6, 215-218, (1973).

Jirout, J., "The Dynamic Dependence of the Lower Cervical Vertebrae on the Atlanto-Occipital Joints," Neuroradiology: 7. 249-252, (1974).

Johnson, R.W., Crelin, E.S., White III, A.A., Panjabi, M.M., and Southwick, W.O., "Some New Observations on the Functional Anatomy of the Lower Cervical Spine," Clin. Orthop.: 3, 192-200, (1975).

Katake, K., "Studies on the Strength of Human Skeletal Muscles," J. Kyoto Pref. Med. Univ. 69: 463-483, (1961).

King, A.I. and Chou, C.C., "Mathematical Modeling, Simulation, and Experimental Testing of Biomechanical System Crash Response," J. Biomechanics: 9, 301-317, (1976).

Lanier, R., "The Presacral Vertebrae of American White and Negro Males," Amer. J. Physical Anthro. XXV, 341-420, (1939).

Liu, Y. King, Krieger, K.W., Njus, G., Ueno, K. and Wakeno, K., Investigation of Cervical Spine Dynamics. AFAMRL-TR-80-138, Air Force Aerospace Medical Research Laboratory, Wright-Patterson AFB, Ohio (1981).

Liu, Y.K. and Wickstrom, J.K., "Estimation of the Inertial Property Distribution of the Human Torso from Segmented Cadaveric Data," Perspectives in Biomedical Engr., (1973).

Lucas, D. and Bresler, B., "Stability of the Ligamentous Spine," Biomechanics Laboratory Report, 40, University of California at San Francisco, (1961).

Lysell, E., "Motion in the Cervical Spine," Acta. Orthop. Scand. 123 (Suppl), (1969).

Markolf, K.L., "Deformation of the Thoracolumbar Intervertebral Joints in Response to External Loads," J.B.J.S.: 54-A, 511-533, (1972).

Martinez, J.L., and Garcia, D.J., "A Model for Whiplash," J. Biomechanics: 1, 23-32, (1968).

McKenzie, J.A., Williams, J.F., "The Dynamic Behavior of the Head and Cervical Spine During Whiplash," J. Biomechanics: 4, 477-490, (1971).

Mestdagh, H., "Morphological Aspects and Biomechanical Properties of the Vertebroaxial Joint (C2-C3)," Acta Morphol. Neerl.-Scand.: 14, 19-30, (1976).

Morris, C.B., "The Measurement of the Strength of Muscle Relative to the Cross-Section," Res. Quart. Am. Assn. Health, Phys. Ed. & Recrn.: 19, 295-303, (1948).

Nachemson, A.L., Evans, J.H., "Some Mechanical Properties of the Third Human Lumbar Interlaminar Ligament (Ligamentum Flavum)," J. Biomechanics: 1, 211-220. (1967).

Orne, D. and Liu, Y. King, "A Mathematical Model of Spinal Response to Impact," J. Biomechanics: 4, 49-71, (1969).

Panjabi, M.M., "Cervical Spine Mechanics as a Function of Transection of Components," J. Biomechanics: 8, 327-336, (1975).

Perry, J. and Nickel, V.L., "Total Cervical Spine Fusion for Neck Paralysis," J. Bone Jnt. Surgery: 41-A, 37, (1959).

Portnoy, H. and Morin, F., "Electromyographic Study of Postural Muscles in Various Positions and Movements," Am. J. Physiol.: 186, 122-6, (1956).

Prasad, P. and King, A.I., "An Experimentally Validated Dynamic Model of the Spine," Transaction of the ASME, J. Applied Mech., 546-550, (1974).

Quiring, D.P., The Head and Trunk Muscles and Motor Points, Lea and Febiger, Philadelphia, (1949).

Reber, J.A., and Goldsmith, W., "Analysis of Large Head-Neck Motion," J. Biomechanics: 12, 211-222, (1979).

Schultz, A., Belytschko, T., Andriacchi, T. and Galante, J., "Analog Studies of Forces in the Human Spine: Mechanical Properties and Motion Segment Behavior," J. Biomechanics: 6, 373-383, (1973).

Schumacher, G.H. and Wolff, E., "Trockenewicht und physiologischer Querschnitt der menschlichen Skelettmuskulatur II. Physiologische Querschnitte," Anat. Anz.: 19, 259-269, (1966).

Tkaczuk, H., "Tensile Properties of Human Lumbar Longitudinal Ligaments," Acta Orthop. Scand. Suppl. No. 115, (1968).

Veleanu, C., "Vertebral Structural Peculiarities with a Role in the Cervical Spine Mechanics," Folia Morph. Prague: 19, 388-396, (1971).

Veleanu, C., "The Cervical Locking Mechanism; Its Contribution to the Cervical Spine Stability and to the Vertebral Artery and Spinal Cord Safety, An Anatomical Study," Rev. Roum. Morphol. Embryol. Physiol., Morphol-Embryol.: 21, 3-7, (1975).

Von Gierke, H.E., "Biodynamic Models and Their Applications," J. Accoust. Soc. Am.: 50, 1397-1413, (1971).

Warwick, R. and Williams, P.L. (ed) Gray's Anatomy, Saunders, Philadephia, (1973).

Werne, S., "Studies in Spontaneous Atlas Dislocation," Acta Orthop. Scand.: 23 (Suppl.), (1957).

White III, A.A. and Panjabi, M.M., Clinical Biomechanics of the Spine, J.B. Lippincott, Philadelphia, (1978).

Yamada, H., Strength of Biological Materials, (Edited by Evans, F.G.), Williams & Wilkins, Baltimore, (1970).

*U.S.Government Printing Office: 1981 — 559-007/6009